Department of Earth Sciences
University College London (UCL)

The behaviour of the stable isotopes of nitrogen during diamond formation

Rebecca Elizabeth Southworth

Submitted in fulfilment of the requirements
for the degree of Doctor of Philosophy
at University College London

April 4, 2016

Declaration

I, Rebecca Southworth, confirm that the work presented in this thesis is my own. Where information has been derived from other sources, I confirm that this has been indicated in the thesis.

Abstract

The study of mantle diamonds offers the possibility to investigate the geodynamic carbon cycle with an unrivalled spatial and temporal scope. Impurities in diamond, of which nitrogen is the most common, provide a window into the cycling of mantle volatiles. The isotopic compositions of carbon and nitrogen for crustal and mantle derived samples are, on average, distinct, making the carbon and nitrogen isotopic systems potentially useful indicators of interactions between crustal and mantle volatiles. For peridotitic diamonds in particular there is a very large range in δ^{15}N (-40 to $+15$ ‰) with only a small range in δ^{13}C (-5 ± 3 ‰). These variations in diamonds can be attributed to multistage growth from isotopically distinct reservoirs or to fractionation processes operating during single growth steps, or perhaps both.

In this thesis, data from mixed-habit diamonds shows that large kinetic fractionations are unlikely to occur in nature. Data from sub-lithospheric diamonds from Juina, and diamondites from Orapa show evidence of recycling of crustal fluids as well as evidence of the involvement of primordial nitrogen during diamond formation. These data lead to the creation of a preliminary model for the deep nitrogen cycle.

Acknowledgements

I would like to thank my supervisor, Dr Adrian Jones, for giving me this opportunity and for help and ideas throughout my project. Thanks to EPSRC and De Beers Technologies for funding this project. I would also like to thank Dr Sami Mikhail for the provision of samples and help with data analysis, and Dr Dan Howell for the provision of samples and for involving me in his study. Huge thanks to Dr Sasha Verchovsky and Dr Feargus Abernethy at the Open University for their help with the Finesse equipment, without which, this project would not have been possible. Additionally, I would like to thank Dr Dan Frost, Dr Robert Myhill and Esther Posner from the Bayerisches Geoinstitüt (BGI) for their assistance with the multi-anvil HPHT experiments, and Dr Ed Bailey from UCL for help with the piston-cylinder experiments. Thanks also to Professor Sara Russell and Dr Mahesh Anand for an enjoyable and thought-provoking viva. Their insights and suggestions helped me to make considerable improvements to this thesis.

Finally, I would like to thank my family for their support over the years, and their absolute belief in my ability to succeed. None of my achievements would have been possible without them.

Contents

List of Figures

List of Tables

Chapter 1

An introduction to diamond formation and the role of mantle nitrogen

1.1 Diamonds

The study of mantle diamonds offers the possibility to investigate the geodynamic carbon cycle with an unrivalled spatial and temporal scope. Diamond-formation in the mantle is known to occur across at least $^{3}/_{4}$ of the history of the Earth (Gurney et al., 2010, and references therein), and the inclusions in diamond provide the deepest samples of the Earth (Pearson et al., 2014). Other impurities in diamond, of which nitrogen is the most common (Kaiser and Bond, 1959), provide a window into the cycling of mantle volatiles. Therefore, it could be said that diamond is a unique letter sent from the depths of the Earth (Sunagawa, 2005).

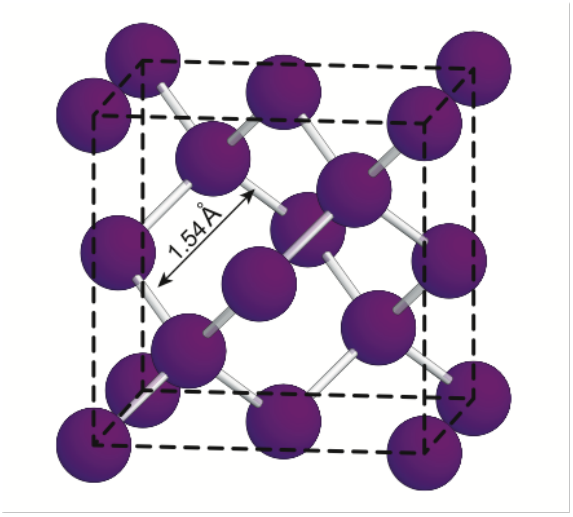

Figure 1.1: Ball and stick model of the diamond structure showing the unit cell with the C–C distance indicated. From Harlow and Davies (2005).

1.1.1 Morphology

Diamond is the high-pressure phase of carbon, which exists in a simple but elegant crystal structure where each carbon atom is bonded to four other atoms in a tetrahedral arrangement yielding a strong, rigid framework (Figure 1.1) (Harlow and Davies, 2005). The C–C bonding is of sp^3 pure covalent nature, which, combined with the structural arrangement, accounts for its unique physical properties, such as the highest hardness of any known material, small compressibility, large thermal conductivity and small thermal expansion, and the highest elasticity of any known material (Harlow and Davies, 2005; Sunagawa, 2005). Diamond occurs in nature in both single crystal and polycrystalline forms.

1.1.1.1 Monocrystalline diamonds

Growth forms are the morphologies of a crystal determined by the structural characteristics and the effects of environmental conditions (Sunagawa, 2005). Octahedral diamonds, or forms with curved faces originating from octahedral, are the most commonly found single crystal diamonds in nature (Boyd et al., 1987; Sunagawa, 2005). They are the

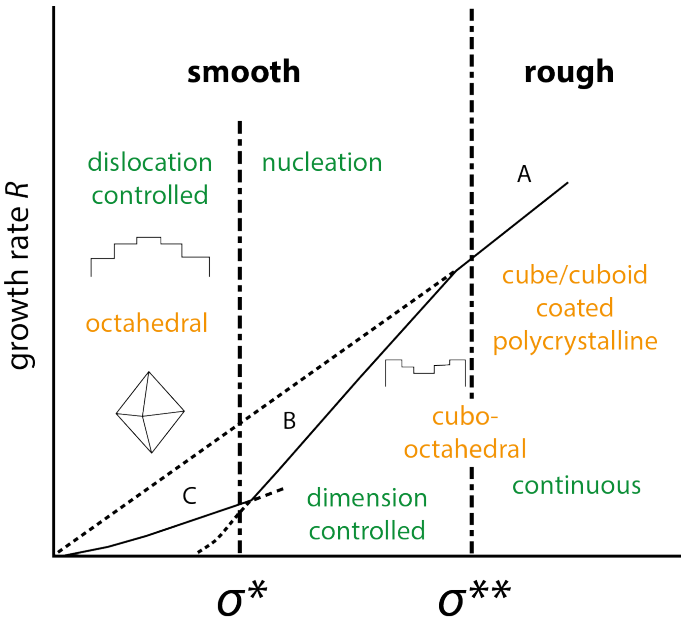

Figure 1.2: Morphology of natural diamond crystals expected in relation to the carbon supersaturation. At saturations below σ^* the growth rate is low and octahedral diamonds form. At increasing saturations to σ^{**} and greater, the growth rate increases and cubo-octahedral, cuboid, coated and polycrystalline diamonds form. Modified from Sunagawa (2005) and Bulanova (1995).

result of spiral growth controlled by dislocations on a {111}[1] face under low driving force conditions (Figure 1.2) – low supersaturation levels between solid-liquid interfaces (Boyd et al., 1987; Harris, 1992; Sunagawa, 2005). There is also a group of natural diamonds which exhibit cubic or cuboid morphology (Sunagawa, 2005). These cuboid diamonds show exclusively rugged surfaces with no crystallographically flat faces (Sunagawa, 2005). They are characterised by a thick fibrous texture in the <111> and <100> directions (Sunagawa, 2005). This fibrous growth occurs via an adhesive-type mechanism during periods of high supersaturation between solid-liquid interfaces with respect to the diamond phase (Figure 1.2) (Boyd et al., 1987; Harris, 1992) - higher driving force conditions (Sunagawa, 2005).

[1]There are three major crystallographic planes which can be used to describe the diamond structure: {111}, {110} and {100}. The family of equivalent planes is denoted by braces, '{}', and specific planes are denoted by brackets, '()' e.g. (100). Specific directions are denoted by square bracekts, "[]" e.g. [100], and the family of equivalent directions is denoted by arrow brackets, '<>' e.g. <100>. As diamond is cubic all planes are perpendicular to directions (ElementSix, 2015).

1.1.1.2 Coated diamonds

'Coated diamonds' consist of an octahedral, gem-quality core surrounded by a turbid, pseudo-cubic overgrowth – 'coat', where the coats have a fibrous internal structure and contain abundant sub-micrometre sized inclusions of fluid that became trapped during crystal growth (Boyd et al., 1992). The fibrous nature of the coats is formed by small particles within the fluid that adhered to the surfaces of the octahedral diamonds preventing continuous faceted growth, so growth continued as a series of independently nucleated fibres (Boyd et al., 1992). The distinctive composition of coat materials strongly suggests that these diamonds grew from an evolved fluid, rich in incompatible elements and volatiles (Harris, 1992). The determination of the K/Ar ages of cores and coats (Burgess et al., 2002), and also the differences in nitrogen content and aggregation (see Section 1.1.2) between cores and coats indicate that they grow during separate events (Tomlinson et al., 2006), with the cores being much older, and the coats possibly relating to the host kimberlite event (Boyd et al., 1992; Burgess et al., 2002).

1.1.1.3 Polycrystalline diamond

Polycrystalline diamonds are aggregates of minute crystals which grow under higher driving force conditions (Sunagawa, 2005) – growth in a highly supersaturated fluid (Figure 1.2; Bureau et al., 2012). Generally, they are classified based on qualitative external characteristics (ballas, bort, framesite, carbonado, etc. (Dobosi and Kurat, 2002; Heaney et al., 2005; Sunagawa, 2005)), as their names have a cultural rather than scientific origin (Heaney et al., 2005). Like their monocrystalline counterparts, polycrystalline diamonds occasionally bear silicates, oxides and sulphides (Dobosi and Kurat, 2002). Trace element data show that in some cases silicates and diamond likely grew from the same fluid, and thus these polycrystalline diamonds should be regarded as rocks in which diamond is the dominant mineral – diamondites (Kurat and Dobosi, 2000).

Table 1.1: Classification of diamonds (Boyd et al., 1987).

Spectral type	**Nitrogen aggregation state**	**Characteristic absorption (cm^{-1})**
IaA	Nitrogen as substitutional pairs	1282
IaB	Substitutional nitrogen within aggregates greater than two and possibly four	1175
Ib	Nitrogen as isolated substitutional atoms	1137
IIa	(Nitrogen low to absent)	
IIb	(Nitrogen low to absent: traces of boron present)	

1.1.2 Lattice bound impurities

Diamonds typically contain detectable and quantifiable amounts of nitrogen as a lattice bound impurity (Kaiser and Bond, 1959). Diamonds which contain detectable quantities of nitrogen, >20 ppm, are classified as Type I diamonds (Shirey et al., 2013). Nitrogen can be present in diamonds with a number of structures which give rise to characteristic absorption spectra in the infrared (Boyd et al., 1987). Type I diamonds can be further subdivided based on the structure of the nitrogen atoms within the lattice (Table 1.1). It is generally assumed that natural diamonds incorporate nitrogen as a simple 1:1 substitution for carbon in the 'Ib' structure (Boyd et al., 1992). The Ib structure is unstable and within a relatively short time the isolated atoms diffuse and combine to form pairs – the IaA structure – according to a second order kinetic law as a function of temperature (Taylor et al., 1996). The aggregation does not cease once most of the nitrogen is within IaA, but continues to form IaB centres, which are thought to consist of a group of four nitrogen atoms and a vacancy (Boyd et al., 1992).

Type II diamonds contain no detectable nitrogen. These are subdivided based on their electrical conductivity. Type IIa diamonds are non-conducting, whereas Type IIb dia-

monds have semiconducting properties. This is due to the presence of boron as a lattice bound impurity (Chrenko, 1973).

1.1.3 Formation in the Earth

1.1.3.1 Source rocks

In most instances, diamonds reach the Earth's surface through transport from depths of >150 km by two types of volcanic rock: kimberlite and lamproite (Harris, 1992; Stachel et al., 2005). The world-wide distribution of these mantle-derived magmas is typically confined to cratons (continents underlain by relatively immobile regions of crust) at least 1.0 Ga old (Harris, 1992). Within the igneous deposits, some diamonds occur within two types of xenolith: peridotite and, more commonly, eclogite (Nixon, 1987). These rocks are the remnants of the major primary source of diamonds within the Earth (Harris, 1992). Therefore, the principal source of diamonds in the Earth's mantle is the deep subcratonic lithosphere (Boyd and Gurney, 1986). Beneath the seismically stable, old portions of cratons, the lithospheric mantle extends down up to 300 km in depth, known as the 'mantle keel' (Shirey et al., 2013), where the mantle is significantly cooler than the convecting mantle at equivalent depth, which results in the temperature dependent graphite-diamond transition rising to shallower depth (Figures 1.3 and 1.4; Stachel and Harris, 2009). Lithospheric diamonds crystallise between 135 and 200 km depth (4.3–6.5 GPa) along model geothermal gradients consistent with a 36–43 mW m^{-2} surface heat flow (Gurney et al., 2010).

The crystal structure of diamond ensures slow diffusion so that inclusions in natural diamonds may be maintained as closed systems over extended periods of geological time (Gurney et al., 2010). The study of microscopic syngenetic inclusions in diamonds provides information about the mineralogy and chemistry of the Earth's interior (Harris, 1992; Harte et al., 1980), and the origins of diamond itself (Stachel et al., 2005). Based on the

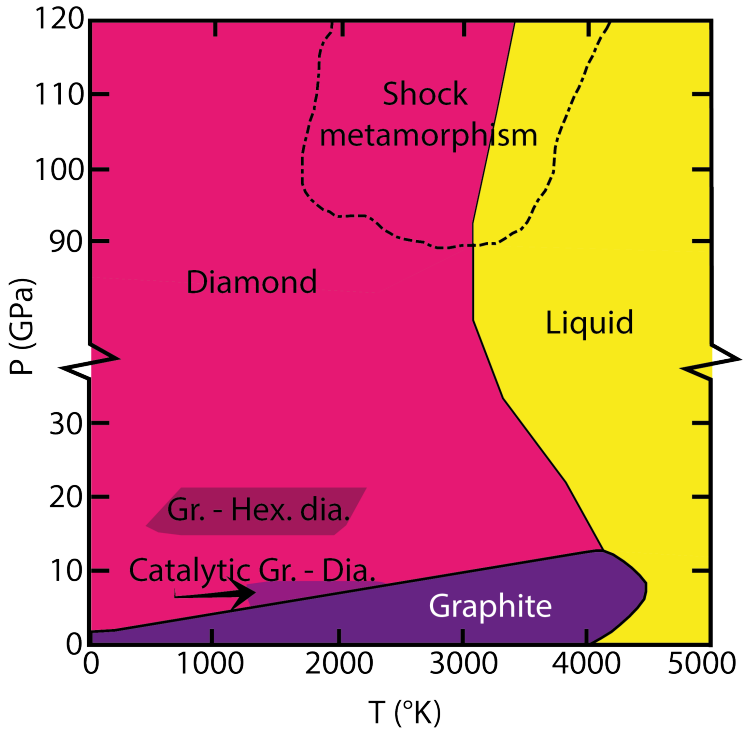

Figure 1.3: The phase diagram for carbon. The region labelled 'Catalytic Gr. – Dia.' is the region where most HPHT experimental diamond growth from graphite in the presence of a catalyst occurs. Modified from Bundy (1980).

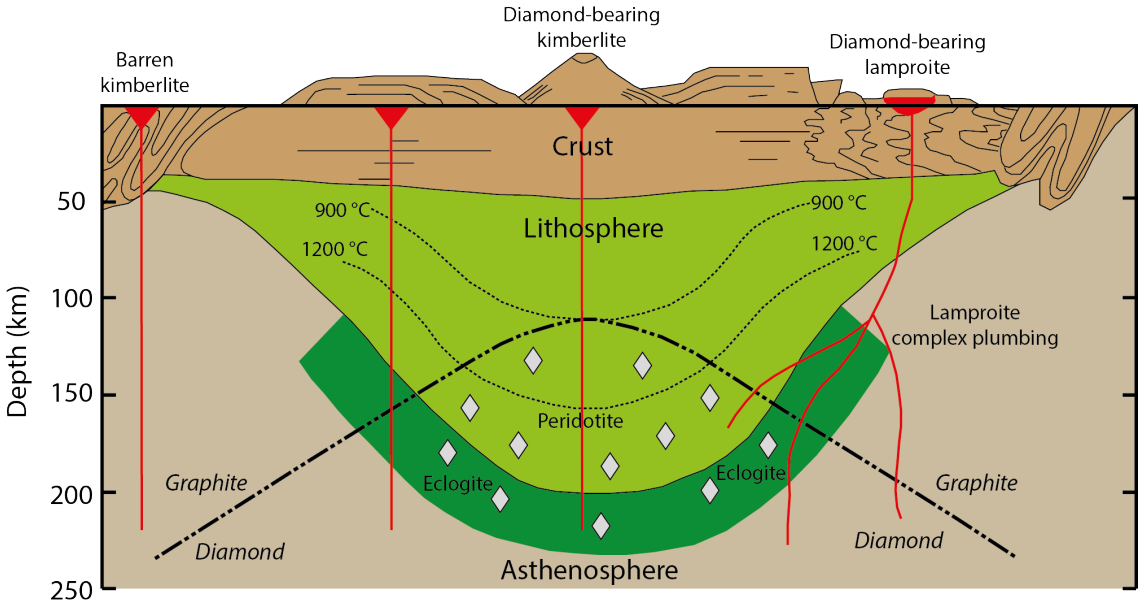

Figure 1.4: A schematic cross-section of a typical subcratonic lithosphere diamond-forming environment. The graphite–diamond phase boundary has been deflected to shallower depths relative to the ambient mantle, due to the lower temperatures in the subcratonic keel. Kimerberlite genesis occurs at ∼200–250 km depth. Modified from Haggerty (1986).

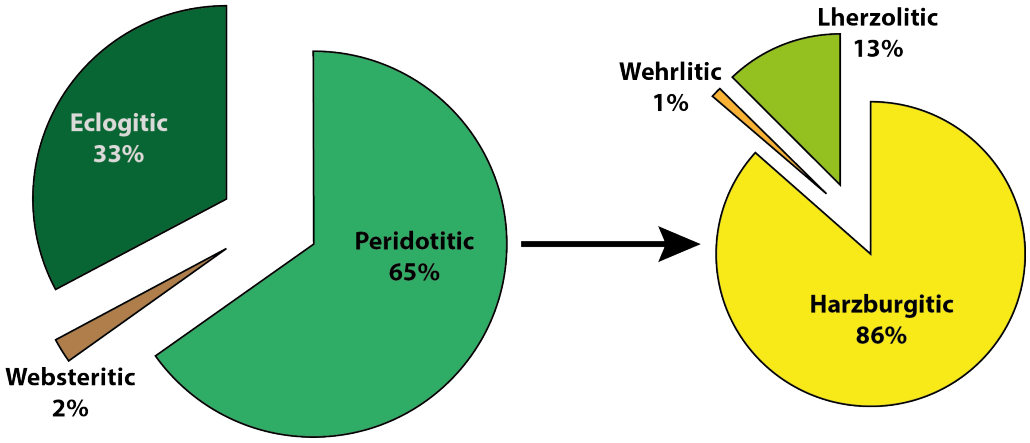

Figure 1.5: Left: the relative abundance of the peridotitic, eclogitic and websteritic suites based on 2844 inclusion bearing diamonds. Right: the relative proportions of the harzburgitic (dunitic), lherzolitic and wehrlitic parageneses derived from compositional classification of 685 peridotitic garnet inclusions. Modified from Stachel and Harris (2009).

study of inclusions in diamonds, three suites of rocks have been identified that may act as a substrate for diamond formation in the lithospheric mantle: peridotite, eclogite and websterite (Figure 1.5; Stachel and Harris, 2009), although inclusion-bearing diamonds are not necessarily xenocrysts derived directly from the rocks (Harte et al., 1980). Amongst the dominant lithospheric diamonds are samples derived from even greater depths, extending to at least 700 km (Stachel et al., 2005).

Peridotitic paragenesis Peridotitic diamonds are so-named based upon the mineralogical affinity of their inclusions with common peridotite (Harris, 1992). They can be further divided into lherzolitic (olivine, enstatite, chrome diopside, ± garnet, ± chromite), harzburgitic (olivine, enstatite, ± garnet, ± chromite) and wehrlitic (olivine, clinopyroxene, Ca- and Cr-rich garnets) subcategories (Figure 1.5) (Harris, 1992; Stachel and Harris, 2009). In harzburgitic inclusions, the olivines and enstatites usually contain more of the magnesium end-member than their lherzolitic equivalents: 94 % vs. 92 % for olivine, and 96 % vs. 94 % for enstatite (Harris, 1992). Wehrlites are rare and represent a type of peridotite with clinopyroxene but without orthopyroxene, likely due to overprint by infiltrating melts (Stachel and Harris, 2009). In the likely presence of hydrous volatiles during

diamond formation, the formation of lherzolitic diamonds will usually occur above the solidus temperature of the source rocks, whereas harzburgitic rocks have a higher solidus temperature, implying that formation of harzburgitic diamonds commonly occurs under subsolidus conditions (Stachel and Harris, 2009). The ages of peridotitic diamonds fall mainly within the range 3.0–3.3 Ga (Bulanova, 1995).

Eclogitic paragenesis Eclogite is the high pressure equivalent of basalt (Stachel and Harris, 2009), and is the original host rock from which diamond was first recovered (Jacob, 2004). In the lithospheric mantle, eclogite likely relates to the subduction of former oceanic crust (Jacob, 2004; Stachel and Harris, 2009). The prinicipal minerals occurring in eclogitic inclusions are garnet and clinopyroxene (Harris, 1992), with occurrences of coesite, ilmenite, corundum, kyanite, phlogopite, sanidine and rutile (Sobolev et al., 1999). The most significant compositional features of eclogitic paragenesis are the presence of Na in garnet and K in clinopyroxene, though there are wide compositional variations through all eclogitic type diamonds (Sobolev et al., 1999). In general terms, eclogitic diamonds have a less diverse inclusion chemistry, are younger (ages ranging from 990–1670 Ma, see Bulanova, 1995) and equilibrated at temperatures 200℃ more than peridotitic diamonds (Harris, 1992).

Websteritic paragenesis Websteritic inclusions are chemically transitional between the peridotitic and eclogitic reservoirs (Aulbach et al., 2002; Deines et al., 1993; Gurney et al., 1984; Sobolev et al., 1999). They are similar to eclogitic inclusions, but the websterite paragenesis was proposed for diamonds containing inclusions of Mg-Fe garnets with moderate CaO contents (similar to lherzolite), clinopyroxene with variable Na contents, and the rare occurrence of orthopyroxene (enstatite) (Harris, 1992; Sobolev et al., 1999). The websteritic source at Venetia was proposed to be the product of a reaction between slab-derived melts and peridotitic lithosphere resulting in an intermediate major element composition and a trace-element budget dominated by the melt (Aulbach et al., 2002).

Sulphide-bearing diamonds Diamonds containing sulphide inclusions are unlikely to form a distinct paragenesis, but form part of the peridotitic, eclogitic or websteritic assemblage (Harris, 1992). However, they are difficult to assign as they often do not coexist with definable silicates or oxides (Harris, 1992). In the diamond stability field, sulphides likely occur mostly as homogenous mono-sulphide solid solutions, but when extracted from their host diamonds, they appear as Cu-Fe-Ni-rich minerals which have exsolved during subsolidus re-equilibrations through cooling (Thomassot et al., 2009, and references therein).

'Super-deep' diamonds The terms 'super-deep' or 'ultra-deep' refer to any diamonds that were formed at depths below the subcontinental lithosphere. The possibility that diamonds could contain inclusions formed in the lower mantle was first recognised based on the observation of ferropericlase possibly associated with orthopyroxene (retrograde from the perovskite structure) (Scott Smith et al., 1984). However, the first clear evidence for the presence of such deep-seated samples was the discovery of associations of ferropericlase with $MgSiO_2$, $CaSiO_2$, SiO_2 and a tetragonal almandine pyrope phase (TAPP) in diamonds from São Luiz, Brazil (Stachel et al., 2000, and references therein). These rare super-deep diamonds may come from the deep upper mantle, where majorite garnet becomes stable; the transition zone, characterized by the stepwise conversion of olivine first to wadsleyite and then to ringwoodite; and the lower mantle where the dominant phases are CaSi- and MgSi-perovskites, ferropericlase and stishovite (Figure 1.6; Stachel et al., 2000, 2005). The trace element chemistry (high Sr and LREE in combination with positive and negative Eu anomalies) of lower mantle inclusions, composition of majorite garnet inclusions, and light $\delta^{13}C$ values (-10 to -27 ‰) of diamonds themselves, suggest a link with subducted oceanic crust (Stachel et al., 2000; Walter et al., 2011) consistent with the megalith model of Ringwood (1991) where subducting slabs may become buoyant at the top of the lower mantle, and the subsequent pile of subducted lithosphere may be the primary source of lower mantle diamonds (Figure 1.7). Further evidence of a subduction link is the presence of high-pressure carbonates as inclusions within super-deep diamonds,

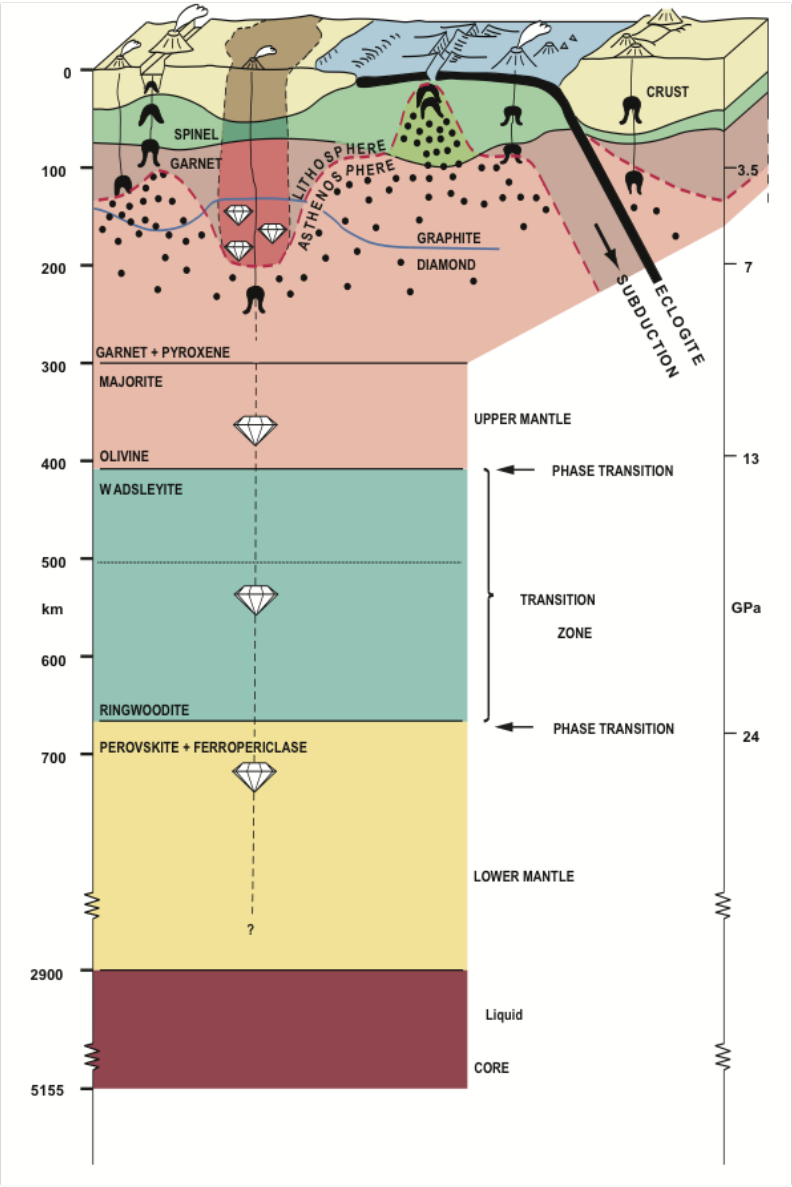

Figure 1.6: Vertical section through the Earth's crust, mantle and core. From Stachel et al. (2005).

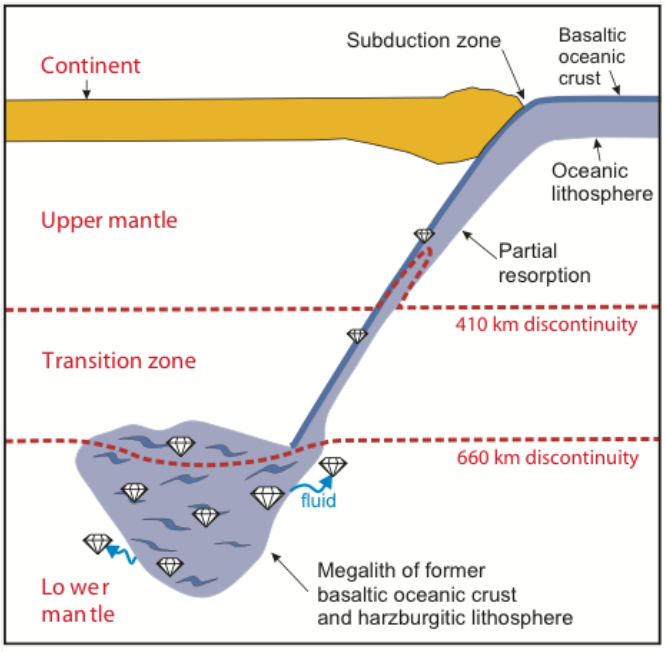

Figure 1.7: The megalith model of Ringwood (1991) suggests that subducting oceanic slabs may become buoyant at the top of the lower mantle. The resulting pile of subducted lithosphere is called a 'megalith'. The evidence for diamond formation at the top of the lower mantle, in combination with crustal signatures in lower-mantle diamonds containing CaSi-perovskite, suggests that megaliths may well be the primary source. From Stachel et al. (2005).

believed to have originated as carbonate sediments which were then subducted and eventually incorporated into diamond in the lowermost transition zone (>580 km depth) or even the lower mantle (Brenker et al., 2007).

1.1.3.2 Redox conditions

The phase boundary between graphite (low-P, high-T carbon phase) and diamond was determined experimentally to equate to depths of ∼150 km at lithospheric mantle temperatures (Bundy, 1980; Kennedy and Kennedy, 1976). In experiments, diamond is often grown by taking graphite, in the presence of a solvent catalyst, to within the diamond stability field (Figure 1.3) using high pressure apparatus (e.g. Akaishi et al., 1990, 2001; Pal'yanov et al., 1999; Sokol and Pal'yanov, 2008; Taniguchi et al., 1996; Tomlinson et al.,

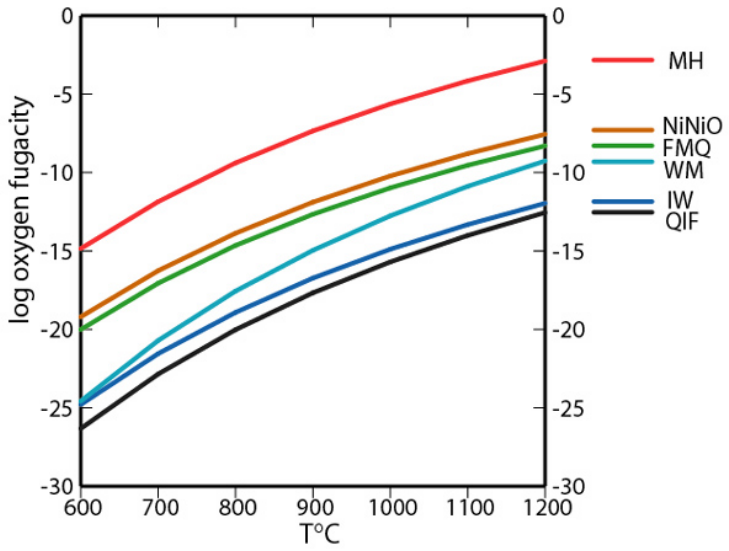

Figure 1.8: Log fO_2 vs. temperature at 1 Bar pressure for common buffer assemblages. Plotted using algorithms compiled by Frost (1991), where MH – magnetite–hematite, NiNiO – nickel–nickel oxide, FMQ – fayalite–magnetite–quartz, WM – wüstite–magnetite, IW – iron wüstite, and QIF – quartz–iron–fayalite.

2011). However, the direct conversion of graphite to diamond is not considered a relevant process for the formation of macroscopic octahedral diamonds in nature (Cartigny et al., 2014; Stachel and Harris, 2009). An alternative to graphite conversion is redox reactions, which depend on the oxidation state of the mantle.

The mantle redox state is expressed as *oxygen fugacity*, which is measured on a log scale relative to a buffer reaction describing the stable assemblage (Figure 1.8). Oxygen fugacity (fO_2) is a thermodynamic constraint that describes the amount of oxygen available to react in a given system (Frost and McCammon, 2008). It is of huge importance because it affects the speciation and mobility of volatile elements in the mantle, and controls the character of degassing species (Stagno et al., 2013). The oxidation state also has a major role in defining the stability of C-bearing phases in the Earth such as carbonates and diamonds (Frost and McCammon, 2008). Oxygen fugacity is dependent on the pressure controlled Fe^{3+}/Fe^{2+} equilibria, and therefore decreases with depth (Frost and McCammon, 2008).

The speciation of carbon in the Earth's mantle is largely governed by oxygen fugacity,

where graphite, diamond or CH_4 are stable under reducing conditions, and carbonate minerals or CO_2-bearing melts or fluids are stable under more oxidising conditions (Stagno and Frost, 2010). In the cratonic lithosphere, at depths where diamonds can form, the oxygen fugacity (ΔFMQ-1 to -3) is not compatible with the stability of either a carbonate or methane rich liquid, but is compatible with a metasomatic liquid dominated either by water or silicate melt (Stagno et al., 2013). Diamond and graphite should be the dominant host for carbon at depths >150 km, with carbonates only existing at these depths in highly oxidised regions, or as dilute melt species (Stagno and Frost, 2010). Reactions of these carbon bearing melts with the ambient mantle can precipitate diamond. There are two principle types or redox reaction relevant for natural diamond formation.

1. **Reduction of carbonate** The redox equilibria (Figure 1.9) governing carbonate reduction for eclogite (DCDD), harzburgite (EMOD) and lherzolite (EMFDD) are respectively: dolomite + coesite = diopside + diamond (Luth, 1993), enstatite + magnesite = olivine + diamond (Stachel and Harris, 2009, and references therein) and enstatite + magnesite = forsterite + diopside + diamond (Luth, 1993). CO_2 bearing fluids or melts (e.g. from a subducting slab) would reduce to form diamonds in the ambient mantle at any pressure >4 GPa (Frost and McCammon, 2008).

2. **Oxidation of a reduced carbon species** The reaction $CH_4 + O_2 = C + 2H_2O$ is thought to reflect the influx of reduced fluids from the convecting upper mantle into a more oxidised lithospheric mantle and will be associated with a reduction in solidus temperature (Stachel and Harris, 2009). CH_4-rich fluids rising from the deeper mantle would be oxidised at $\sim$6 GPa to produce diamond and H_2O (Frost and McCammon, 2008). However, the present day subcratonic lithosphere is generally too reduced for this process to occur (Stachel and Harris, 2009). Moreover, it is possible that the subcratonic lithospheric mantle is actually more reduced than the asthenospheric mantle (Haggerty, 1986).

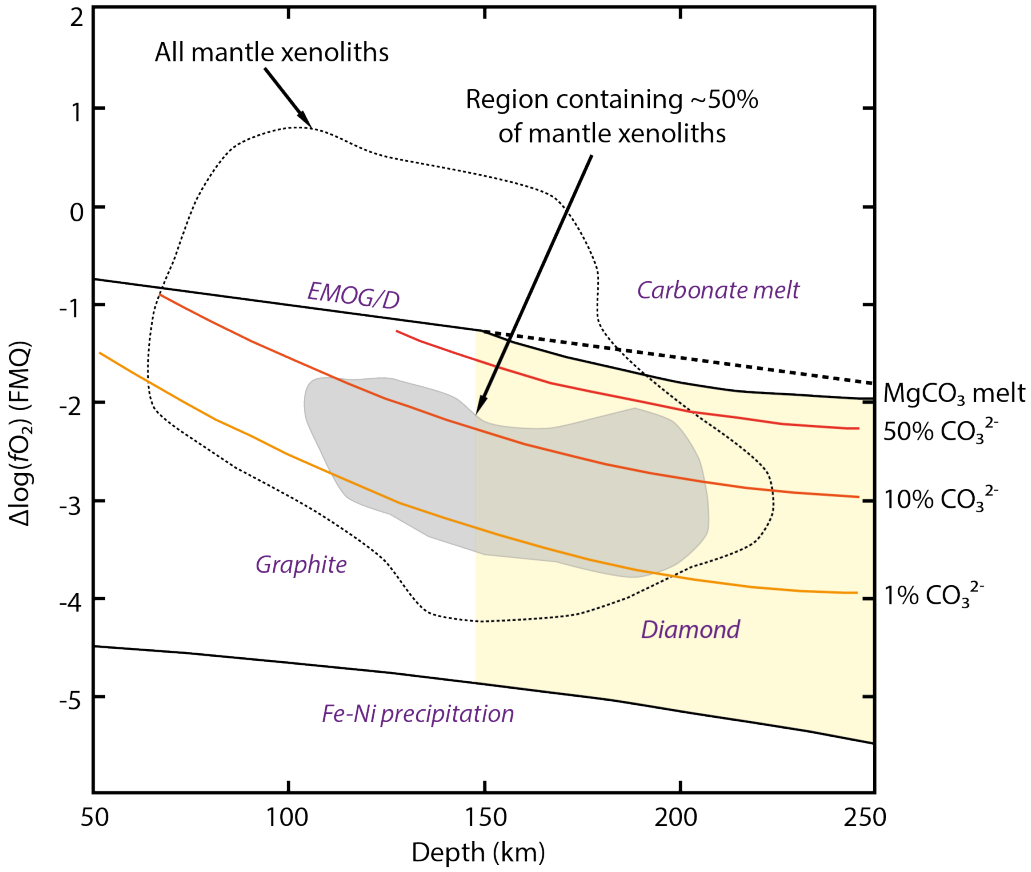

Figure 1.9: Log(fO_2)(normalised to FMQ) based on calculations for xenoliths from the cratonic lithosphere. The coloured region indicates the diamond stability field. The curve labelled EMOG/D is the oxygen fugacity calculated along a cratonic geotherm. It defines the stability field between diamond (or graphite) and magnesite ($MgCO_3$) in the mantle. At depths >150 km, this curve dips owing to carbonate melting. The curves plotted below EMOG/D indicate oxygen fugacities for melts in equilibrium with diamond or graphite, for different carbonate (CO_3^{2-}) contents (molar percentage of MCO_3 is indicated for each curve, where M is a divalent cation). Modified from Stagno et al. (2013).

1.1.3.3 Diamond growth from fluids

There is considerable evidence that diamond is a metasomatic mineral (Cartigny et al. (2014) and references therein). Evidence provided by S and O isotopes, along with the C and N isotope systems (discussed in detail in Section 1.3), suggests that diamonds grow from external carbon (and nitrogen) introduced to eclogites and peridotites through the percolation of a carbon/volatile rich fluid (Cartigny, 2005). The majority of xenoliths from the diamond stability field have oxygen fugacities that would not be in equilibrium with a pure carbonate melt (Figure 1.9), but only with melt phases in which the carbonate component (or CO_2 component in fluids) is relatively dilute at 1–10 % (Stagno et al., 2013). Experimental results have shown that multi-component fluids (aqueous, carbonate-enriched silicate melts) and a single supercritical fluid highly enriched in carbon and water, can be the parent of fibrous, cloudy, polycrystalline and coated diamonds, suggesting that these diamonds may form at locations where such fluids are abundant (Bureau et al., 2012) - subduction zones. Microinclusions in fibrous diamonds of carbonate-bearing fluids/melt indicates that these diamonds precipitated from oxidised fluids/melts known as high-density fluids (HDFs) (Weiss et al., 2014). Four different end members of fluid compositions have been identified in fibrous diamonds: saline (Izraeli et al., 2001), silicic and carbonatitic (Kopylova et al., 2010; Tomlinson et al., 2006) with high-Mg and low-Mg compositions (Klein-BenDavid et al., 2009). Changes in fluid composition have been shown to correlate with changes in carbon isotope ratios indicating that the carbon is carried within the fluid (Shiryaev et al., 2005). The presence of peridotitic and eclogitic suite minerals as inclusions within fibrous diamonds indicates that they share a growth environment with octahedral diamonds (Tomlinson et al., 2006), therefore, the fluids involved in the growth of fibrous diamonds should be comparable to the fluids involved in the growth of octahedral diamonds. Recently, HDF microinclusions have been found in octahedral diamonds, suggesting that HDFs are involved in the formation of many types of diamonds (Weiss et al., 2014). Additionally, the presence of water-saturated ringwoodite in an inclusion in a diamond from Juina, Brazil (Pearson et al., 2014), indicates that fluids play an important

role in diamond formation throughout the mantle. The abundance and oxygen fugacity of C-O-H-N fluids have a major effect on silicate mineralogy and melting as well as diamond crystallisation (Galimov, 1991; Haggerty, 1986; Harte et al., 1999), however it is possible that the physico-chemical circumstance controlling diamond crystallisation may not be closely linked in time to some circumstances controlling silicate mineral development (Deines, 1996).

1.2 Nitrogen in the mantle

Nitrogen is present in various geological reservoirs (mantle, crust, atmosphere and biosphere), but there are large differences in the nitrogen isotope composition and concentration (Figure 1.10) of the various reservoirs (Halama et al., 2010). It is these differences that make nitrogen potentially important as a geochemical tracer, but nitrogen behaviour in the various environments needs to be better understood before these data can be used effectively. Whilst nitrogen only occurs as a trace element in rocks, 97.98% of all terrestrial nitrogen is found in crystalline rocks (Sharp, 2007), making understanding the behaviour of nitrogen during crystallisation vitally important. The actual nitrogen content of the mantle is not well constrained and has been estimated to be anywhere from 2.8 ppm (Marty, 1995) to 36 ppm (Javoy, 1997).

1.2.1 Nitrogen speciation in the mantle

1.2.1.1 Nitrogen in subducting slabs

Nitrogen is incorporated into the mantle by the subduction of oceanic lithosphere and crust (Halama et al., 2012; Li et al., 2007; Marty and Dauphas, 2003). Nitrogen in oceanic sediments is initially fixed by organic matter (Busigny and Bebout, 2013). During diagenesis, nitrogen is speciated as ammonium (NH_4^+) which substitutes for K^+ in potassium-

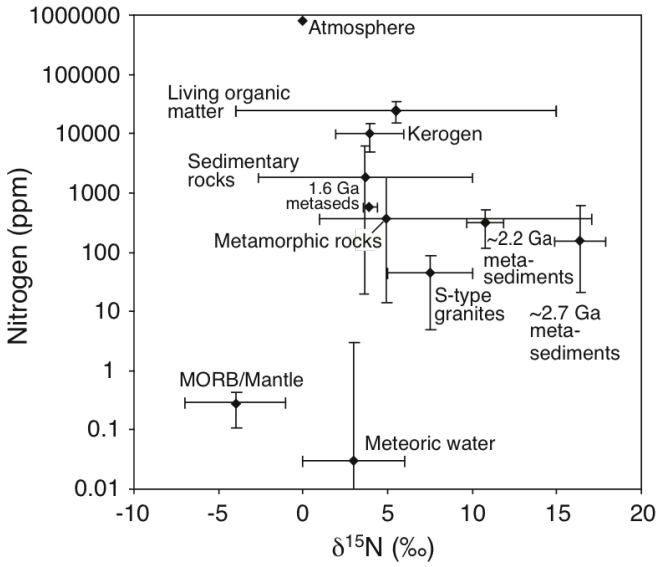

Figure 1.10: Ranges of δ^{15}N compositions and nitrogen concentrations for various geological environments. From Pitcairn et al. (2005).

bearing minerals, therefore nitrogen behaves as a lithophile element in the geochemical cycle (Yokochi et al., 2009). A considerable amount of nitrogen in metamorphic and granitic rocks is held as NH_4^+ ions within the crystal lattice of silicate minerals (Honma and Itihara, 1981), in particular, phengite, a high-pressure white mica in metamorphic rocks (Busigny et al., 2003). In addition to metasediments, altered oceanic crust has been shown to have a significant enrichment in nitrogen compared with concentrations in fresh mid-ocean ridge basalt (MORB) (Li et al., 2007). A study of ophiolitic metagabbros showed that the rocks contained a not-insignificant amount of nitrogen, 2.6–55 ppm, but K-bearing phases were almost completely absent, leading to the conclusion that nitrogen can also reside as NH_4^+ in Ca–Na bearing minerals (Busigny et al., 2011). Metamorphic devolatilisation dictates the amount of crustal N (^{15}N-enriched) that is conveyed into the mantle beyond sub-arc regions (Li et al., 2007). The release of NH_4^+ from rocks into fluids during subduction is controlled by the P–T path they follow, with warm P–T paths (e.g. >13 ℃/km) resulting in significant loss of nitrogen, and cold P–T paths (e.g. <10℃/km) not associated with significant nitrogen loss (Busigny and Bebout, 2013). This means that in regions where the subducting slab is cold, a significant amount of nitrogen may be

transported to the transition zone or even lower mantle within the slab.

1.2.1.2 Nitrogen in fluids and melts

Nitrogen forms a number of oxidation states from +5 (NO_3^-) to −3 (NH_4^+) (Sharp, 2007), however, the speciation of nitrogen in mantle fluids is not well constrained (Mikhail and Sverjensky, 2014, and references therein). Recently, however, it has been shown that in the aqueous fluids of the oxidised upper mantle and mantle wedge, nitrogen is present mostly as N_2 (Li and Keppler, 2014; Mikhail and Sverjensky, 2014), but NH_3 is also a stable species (Li and Keppler, 2014). However in the rest of the Earth's upper mantle, the dominance of N_2 or NH_4^+ in the fluids is dependent upon the nitrogen concentration and the pH of the fluids (Mikhail and Sverjensky, 2014), and in the deep reduced upper mantle, NH_3 is the dominant nitrogen species (Li and Keppler, 2014). Recently, melt and fluid inclusions in octahedral diamonds from several locations have been found to have high nitrogen contents, indicating that nitrogen can constitute a major mantle volatile, in the context of diamond-related fluids/melts (Smith et al., 2014).

Generally, nitrogen solubility in basaltic melts is low (Busigny and Bebout, 2013) and is thought to be similar to that of argon, based on the measurement of near constant $N_2/^{40}Ar$ ratios in MORB vesicles (Marty, 1995). However, as with aqueous fluids, this varies with oxidation state. Nitrogen physically dissolves in basaltic melt under highly oxidising conditions, whereas it chemically dissolves in silicate melts as nitrides (Si–N) or cyanides (C–N) under highly reducing conditions (Miyazaki et al., 2004). The nitrogen content of silicate melts strongly depends on oxygen fugacity (Figure 1.11; Libourel et al., 2003). For fO_2 from air to IW, the nitrogen content is very low and near-constant at ca. 10^{-9} mol g^{-1}, but below the iron wüstite (IW) buffer (IW to IW−7) the nitrogen content increases drastically by four to five orders of magnitude with decreasing fO_2 (Libourel et al., 2003). Further decreasing oxygen fugacity below IW−7 does not affect the nitrogen solubility which reaches a plateau at ca. 5×10^{-5} mol g^{-1} (Libourel et al.,

2003). Additionally, the solubility of nitrogen in silicate melt also increases with pressure up to 3–4 GPa (Roskosz et al., 2012). Roskosz et al. (2006) showed that in the case of depolymerized melts (eg. basalt) at pressures in the range 1–3 GPa, the nitrogen solubility does not show Henry's Law behaviour, in contrast to the behaviour of noble gases. This was thought to be due to a fraction of nitrogen (up to 60%) interacting strongly with the silicate melt to form nitrosyl groups (an NO group directly bound to a metal via the N atom). They found that the nitrogen content of the silicate melt was 0.3–0.7 wt.% (Roskosz et al., 2006).

1.2.1.3 Nitrogen in mantle minerals

Nitrogen in peridotite xenoliths has been shown to be bound in crystal structures with minerals such as phlogopite and amphibole particularly rich in nitrogen, with olivine containing approximately 0.1 ppm of nitrogen (Yokochi et al., 2009). Additionally, a significant amount of nitrogen in the deep mantle could be stored as NH_4^+ in clinopyroxene (Watenphul et al., 2010). The lower pressure and more oxidised conditions in the shallower mantle would lead to the oxidation and volatilisation of nitrogen to N_2 and subsequent loss by degassing (Busigny and Bebout, 2013).

Possibly the most important nitrogen-bearing mineral in the mantle, in terms of relevance, is diamond (see Section 1.2.2), which could yield information regarding global nitrogen concentrations, the isotopic composition of nitrogen and the generation of nitrogen-bearing melt/fluid in the mantle (Busigny and Bebout, 2013). Lithospheric diamonds typically contain measureable quantities of nitrogen, whereas super-deep diamonds generally have very low nitrogen contents (Cartigny et al., 2014). This is most likely due to a lack of available nitrogen in the deep mantle, where other phases may preferentially partition nitrogen. One possibilty is carbides and nitrides. Iron carbide inclusions in super-deep diamonds have been reported to contain up to 9 at.% nitrogen (Kaminsky and Wirth, 2011), and nitrides such as osbornite (TiN) and iron nitrides are thought to be stable un-

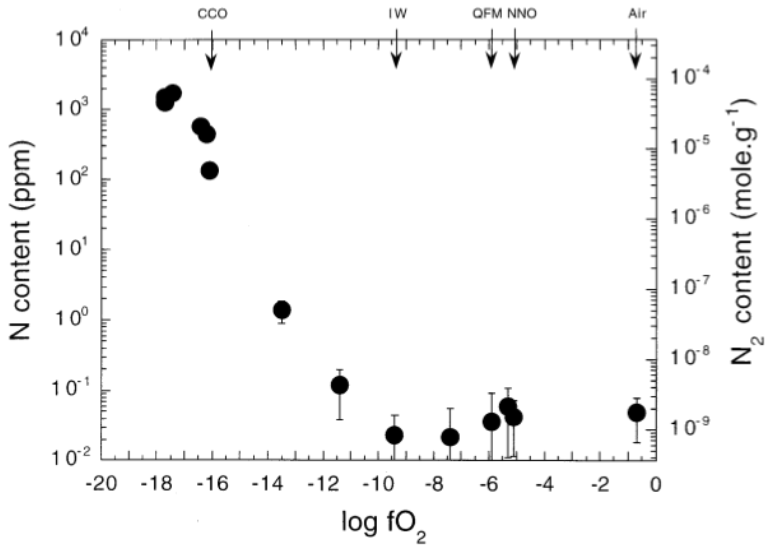

Figure 1.11: Nitrogen contents (in ppm or mol g^{-1} units) in CM-1 MORB-like melt as function of oxygen fugacity at 1425℃. Redox conditions are indicated in the upper part of the graph. From Libourel et al. (2003).

der reducing conditions at very high pressures in the mantle, and could also be significant nitrogen hosts within the Earth's core (Adler and Williams, 2005; Busigny and Bebout, 2013; Kaminsky and Wirth, 2011). Although common in meteorites, natural osbornite (TiN) is very rare on Earth but has been reported alongside cubic boron nitride as inclusions within coesite estimated to have formed at depths below 300 km (Dobrzhinetskaya et al., 2009). Experiments have shown that at any P, T, fO_2 conditions, osbornite is the most easily formed nitride, suggesting that nitrogen may be preferentially associated with Ti-bearing phases in the upper mantle, e.g. clinopyroxenes (Martinez and Javoy, 1998).

1.2.2 Nitrogen compatibility in diamond

The presence of nitrogen as a lattice-bound impurity within diamond was introduced in Section 1.1.2. Nitrogen concentrations in diamonds range from 0 to 3830 ppm (Stachel and Harris, 2009), and in general nitrogen is strongly enriched in diamonds relative to primitive mantle concentrations . The actual K value (partition coefficient) for nitrogen in diamond and silicates is inferred and not quantified (Mikhail, 2011). In a study on

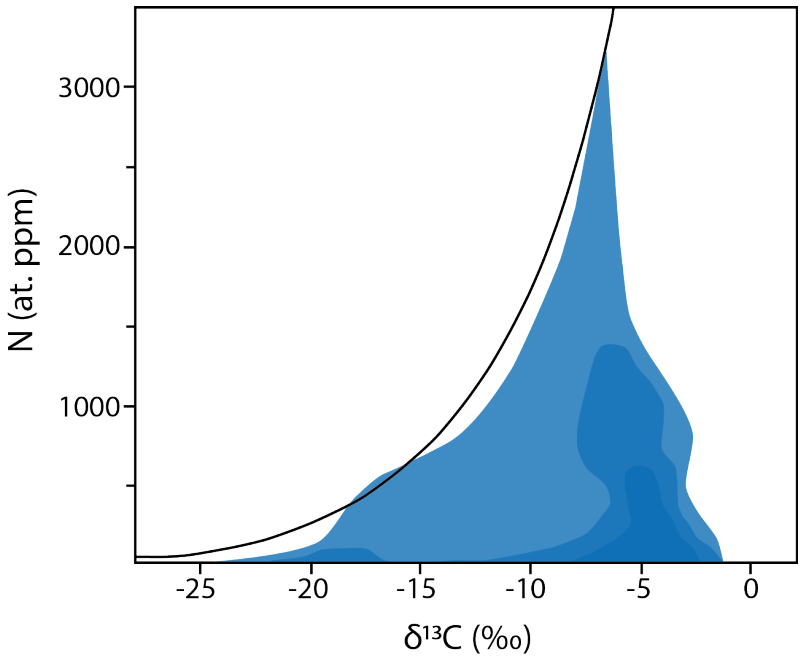

Figure 1.12: δ^{13}C–N diagram of known paragenesis diamonds. Modified from Cartigny et al. (2001).

octahedral diamonds from worldwide locations, Cartigny et al. (2001) found that diamonds with low δ^{13}C values are clearly characterised by low nitrogen contents, whereas diamonds with high δ^{13}C have more variable nitrogen contents and a high upper limit. A limit sector curve can be drawn defining the upper extent of nitrogen concentration for a given δ^{13}C value (Figure 1.12). This was interpreted to be the result of slow growth fractionation from various stages in mantle melt evolution (Cartigny et al., 2001). The authors suggested that the nitrogen content of diamond is primarily a function of its rate of growth, and that the Type IIa low nitrogen diamonds represent the equilibrium growth state - nitrogen being incompatible in the diamond structure. Fibrous diamonds result from rapid growth evidenced by the trapping of many impurities, and they also contain high levels of nitrogen (Figure 1.13), whereas well-crystallised octahedral diamonds have slower growth rates (Cartigny et al., 2001; Sunagawa, 2005). However, given that ∼90 % of lithospheric diamonds are Type I (D. Fisher, pers. comm. 2015), and the majority of these are octahedral (Boyd et al., 1987; Sunagawa, 2005), is it plausible that these are all incorporating nitrogen at disequilibrium? Support for this theory can be found in fluid

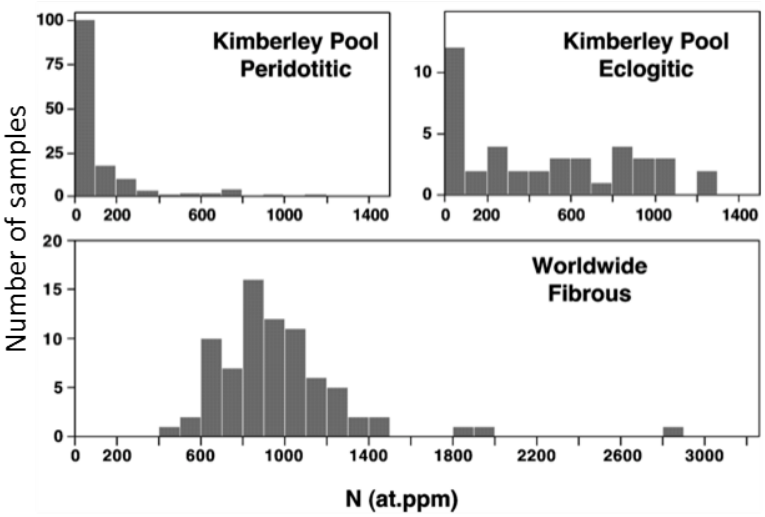

Figure 1.13: Histograms comparing the nitrogen concentrations of peridotitic, eclogitic and fibrous diamonds. From Cartigny et al. (2001).

inclusions containing high nitrogen contents and low C/N ratios. For these to be achieved, no more than 5% of the available nitrogen can be sequestered into the diamond, therefore, the majority of nitrogen remains in the growth medium, therefore nitrogen incorporation into diamond is a function of growth kinetics (Smith et al., 2014).

Alternatively, there are some indications that nitrogen is a compatible element within the diamond structure. The decrease of nitrogen content and the systematic increase of δ^{13}C and δ^{15}N (Equation (1.1)) towards the rim are suggestive of compatible behaviour of nitrogen during continuous growth by fractional crystallisation from an oxidised fluid/melt from which nitrogen was progressively depleted during growth (Bulanova et al., 2002; Smart et al., 2011). Model calculations of δ^{13}C–N covariations have yielded partition coefficients from $K_N = 2$ for diamond precipitating from reduced fluids (Thomassot et al., 2007) to $K_N = 4 - 5$ for diamond precipitating from oxidised fluids, indicating that nitrogen is strongly compatible in diamond relative to the growth medium (Smart et al., 2011; Stachel et al., 2009). High nitrogen diamonds have been grown experimentally using both metal catalysts and in the presence of silicates from de-carbonation reactions (Stachel and Harris, 2009). Experiments by Pal'yanov et al. (2002) showed high nitrogen

concentrations of up to 800 ppm in diamonds grown by carbonate–silicate interactions. Experimental growth of diamond occurs at significantly higher temperatures than the conditions of natural diamond formation, therefore speeding up diffusion and permitting better equilibration between the diamond and its growth medium (Stachel and Harris, 2009). It seemed implausible to Stachel and Harris (2009) that synthetic diamonds incorporate nitrogen under disequilibrium conditions whereas octahedral natural diamonds form much closer to equilibrium conditions, leading them to conclude that the strong enrichment of nitrogen in diamond relative to the mantle reflects the compatibility of nitrogen in the diamond lattice. However, modelling of the diffusive relaxation of isotopic zoning in diamonds has shown that nitrogen isotope zoning relaxes incredibly slowly, with 1 μm zoning preserved after a million years at temperatures of 2000 K (comparable to HPHT experimental temperatures) (Koga et al., 2003). This indicates that diffusion of nitrogen through diamond is too slow to equilibrate the nitrogen composition of the diamond with the growth medium during the short durations of laboratory experiments. It is possible that the high nitrogen concentrations seen in synthetically grown diamonds are a function of the high growth rate. Therefore, it is difficult to say whether nitrogen is compatible or incompatible in the diamond lattice.

1.3 Nitrogen isotopes in diamond

Nitrogen has two stable isotopes – ^{14}N and ^{15}N (Sharp, 2007). The isotope ratios are expressed using the 'delta' notation (Equation (1.1)) which is defined as a part per thousand (‰) deviation from the internationally recognised 'Air' standard (Boyd, 1988; Cartigny et al., 1998a; Fischer et al., 2002, 2005; Gautheron et al., 2005; Javoy and Pineau, 1991; Javoy et al., 1984; Marty and Humbert, 1997; Mohapatra et al., 2009; Palot et al., 2009; Thomassot et al., 2009).

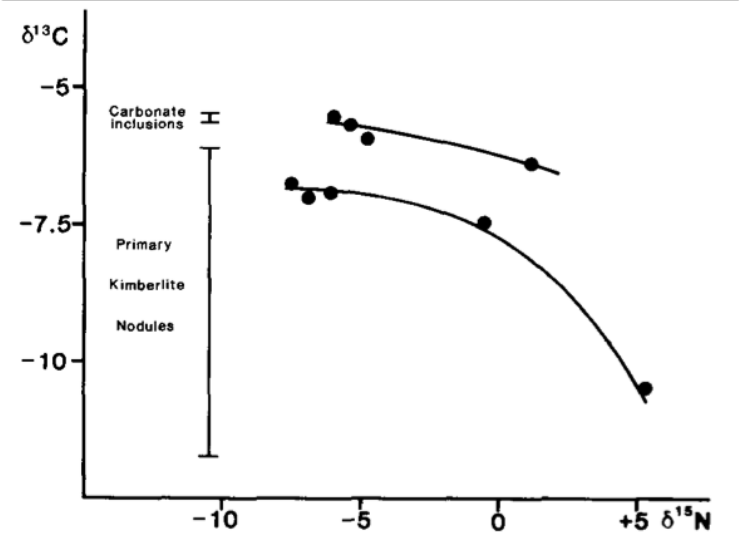

Figure 1.14: δ^{15}N – δ^{13}C relationship in large diamonds. From Javoy et al. (1984).

$$\delta^{15}\mathrm{N} = \left(\frac{^{15}\mathrm{N}/^{14}\mathrm{N}_{\mathrm{sample}}}{^{15}\mathrm{N}/^{14}\mathrm{N}_{\mathrm{standard}}} - 1 \right) \times 1000 \tag{1.1}$$

The isotopic compositions of carbon and nitrogen for crustal and mantle derived samples are, on average, distinct (Hoefs, 2009), making the carbon and nitrogen isotopic systems potentially useful indicators of interactions between crustal and mantle volatiles. Over the last ∼60 years the stable isotopes of carbon have been used to trace the origin of diamond-forming carbon. These studies have shown that monocrystalline diamonds from both the upper and lower mantle, and containing peridotitic, eclogitic and sulphide inclusions, show a strong mean δ^{13}C of -5 ± 3 ‰ (Cartigny, 2005; Craig, 1953; Deines, 1980; Deines et al., 1984, 1989). Nitrogen isotopes have the potential to complement carbon isotope data from mantle-derived diamonds with the aims of providing a more accurate insight into the origins of diamond-forming carbon and tracing the deep carbon cycle through geological time (Boyd and Pillinger, 1994; Cartigny et al., 1998b; Javoy et al., 1984; Klein-BenDavid et al., 2010; Palot et al., 2014; Thomassot et al., 2009) which is still poorly understood (Hazen and Schiffries, 2013).

An early study of diamonds of known origin by Javoy et al. (1984) analysed a number of

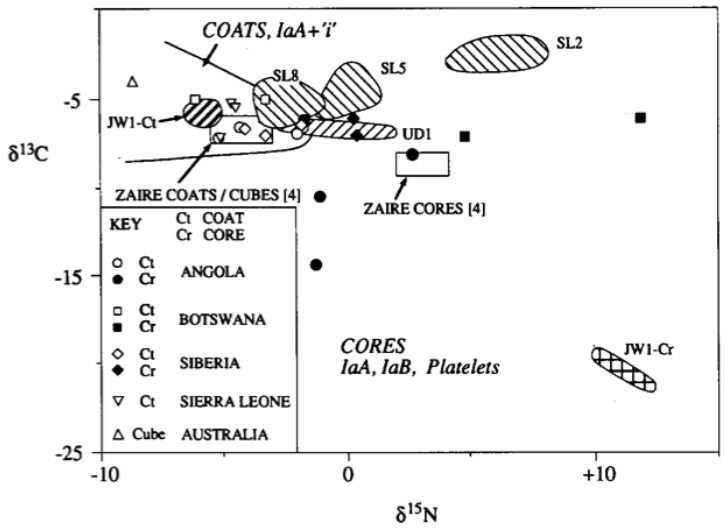

Figure 1.15: Summary plot of isotope data from Boyd et al. (1992). Also included are the regions occupied by the samples from Zaire (Javoy et al., 1984). The shaded areas indicate the range in isotope composition displayed by the sectioned diamonds. Apart from the field labelled 'JW1 Ct' (the coat of sample JW1) the fields shown are for the cores of the sectioned diamonds.

crystal aggregates from Mbuji-Mayi, Zaire for nitrogen isotopes. They found that the δ^{15}N values varied from -11.2 to $+6.0$ ‰ and that all the average concentrations of nitrogen for each diamond were greater than 750 ppm, with only one exception. Javoy et al. (1984) also found that the relationship between δ^{15}N and δ^{13}C defines two groups and an inverse correlation (Figure 1.14). They suggested that this may represent two stages of distillation effects corresponding to the two episodes of kimberlitic activity suggested by a geologic study. However, numerous later studies show that there is no evidence of a correlation between carbon and nitrogen isotope ratios.

Coated diamonds analysed by Boyd et al. (1992) showed marked differences in δ^{15}N and δ^{13}C values between the fibrous coats and the cores, which were free from micro-inclusions. Fig. 1.15 shows that the cores are extremely variable (Boyd et al., 1992). These results compared favourably with those of Boyd et al. (1987) which also showed considerable differences between the N isotope compositions of the coats and cores, with the cores generally being more enriched in ^{15}N with respect to the coats (Figure 1.16). Their results

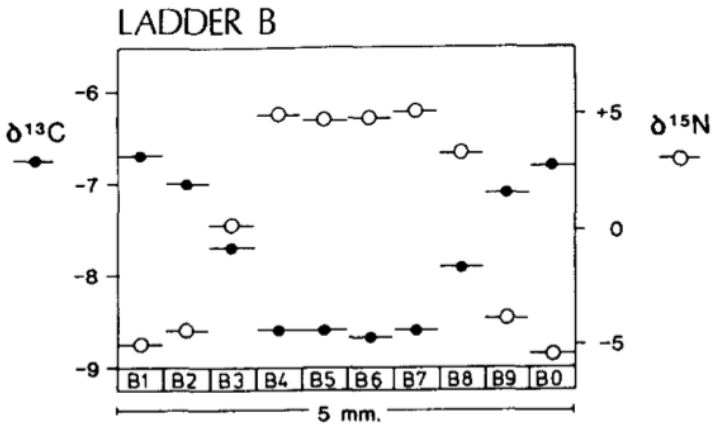

Figure 1.16: Profile showing the covariation of carbon and nitrogen isotope composition within a laser sectioned coated diamond. From Boyd et al. (1987).

also showed an apparent anti-correlation between the δ^{15}N and δ^{13}C values.

A preliminary study of octahedral diamonds of unknown paragenesis by Boyd and Pillinger (1994) found that the diamonds could be separated into two groups defined by their δ^{13}C values: 'high-δ^{13}C' (δ^{13}C = -6.4 to -2.9 ‰) and 'low-δ^{13}C' (δ^{13}C = -19.4 to -9.5 ‰). They found that the high-δ^{13}C diamonds were generally characterised by nitrogen that is depleted in ^{15}N relative to atmospheric nitrogen, whereas the low-δ^{13}C diamonds contained nitrogen generally enriched in ^{15}N relative to the atmosphere (Figure 1.17). Further data from Cartigny et al. (1998b) overlaps both the low and high δ^{13}C groups, calling into question the significance of the distinction (Figure 1.18).

A study of 55 diamonds of peridotitic paragenesis from Fuxian, China were analysed by Cartigny et al. (1997). They found that the δ^{15}N values ranged from -24.2 to $+7.5$ ‰, with a mean of δ^{15}N = -8.0 ± 5.2 ‰, and with all but one sample having negative δ^{15}N values. About 25% of the samples were characterised by δ^{15}N lower than -12 ‰ and down to -25 ‰, while the δ^{13}C values showed much less variation ranging from -6.22 to $+0.81$ ‰ (Cartigny et al., 1997). Peridotitic diamonds from a number of locations including Africa and Siberia, largely support the observations from Fuxian. While only the diamonds from China showed extreme δ^{15}N variations, a major part of the sample was within a -12

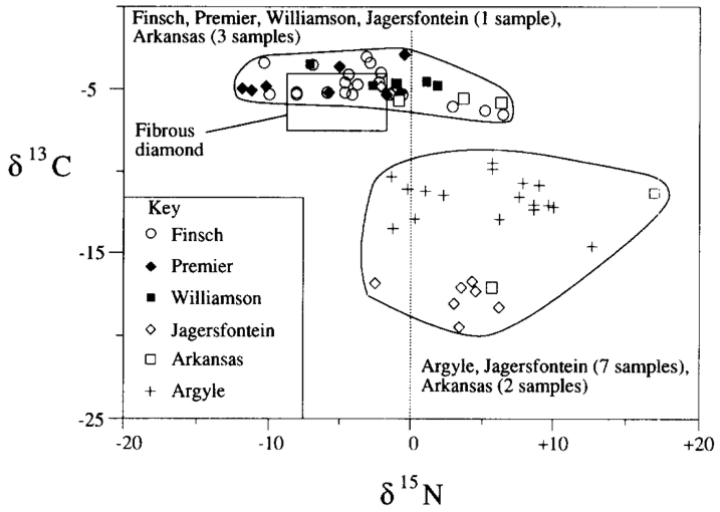

Figure 1.17: Summary plot of the isotope data from Boyd and Pillinger (1994). Included is the region defined by fibrous diamonds. The dotted line is the N isotopic composition of the atmosphere (0 ‰). The high-δ^{13}C samples are generally depleted in ^{15}N relative to air and are quite similar to fibrous diamonds, whereas the low-δ^{13}C samples are generally enriched in ^{15}N relative to air.

to +6 ‰ interval, with most δ^{15}N values being around −5 ‰ (Cartigny et al., 1998b). The lowest recorded terrestrial δ^{15}N values were found recently in diamonds from Kankan, Guinea. Two peridotitic diamonds had δ^{15}N values of −30.4 and −39.4 ‰, with 'normal mantle' δ^{13}C values, and a lower mantle diamond had a δ^{15}N of −24.9 ‰ (Palot et al., 2012). The other lower mantle diamonds analysed by Palot et al. (2012) fell within the region defined by lithospheric peridotitic diamonds (Figure 1.19).

The summary chart (Figure 1.19) shows the δ^{15}N vs. δ^{13}C for diamonds from published literature. It clearly shows that for peridotitic diamonds in particular there is a very large range in δ^{15}N (−40 to +15 ‰) with only a small range in δ^{13}C (−5 ± 3 ‰ with a few outliers). Coated diamonds show a very narrow range for both carbon and nitrogen, suggesting that the mean mantle composition has a δ^{15}N of −5 ± 3 ‰. The overall range for eclogitic diamonds is narrower for nitrogen, but larger for carbon. A very large majority of samples plot in the negative region for both δ^{15}N and δ^{13}C, suggesting limited, if any, recycling of crustal material into the diamond source region during diamond formation.

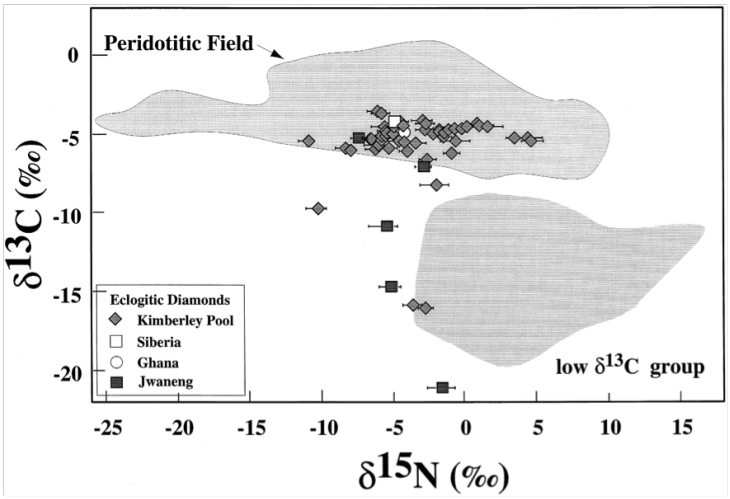

Figure 1.18: δ^{15}N – δ^{13}C diagram of diamonds belonging to the eclogitic paragenesis from the Kimberley Pool, a single eclogitic diamond from Ghana, one from Siberia and five from Jwaneng. From Cartigny et al. (1998b).

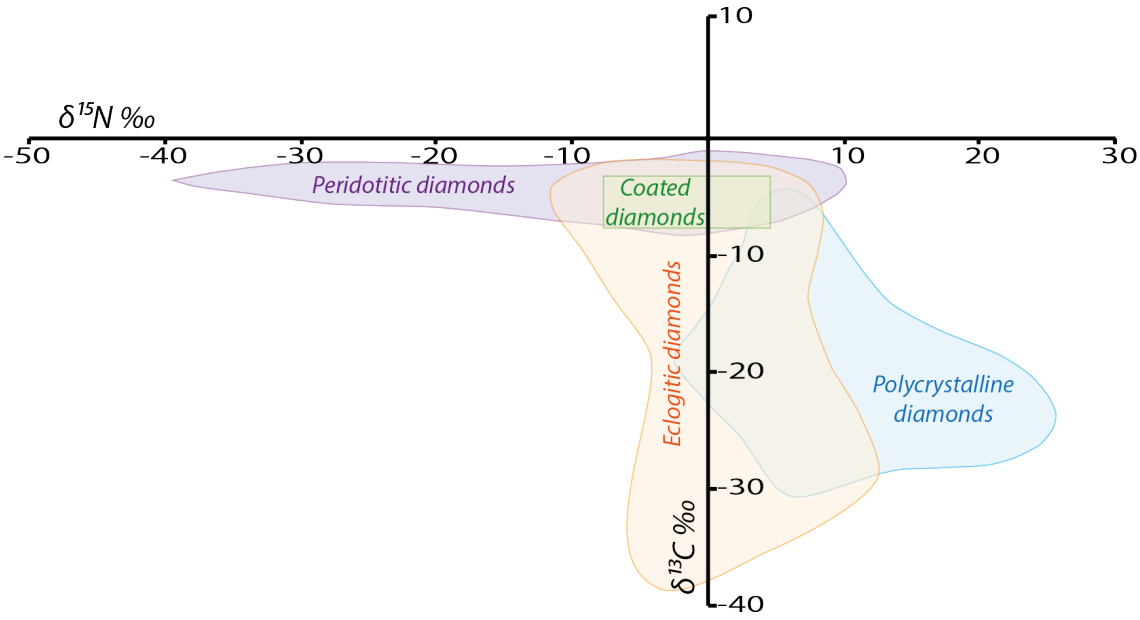

Figure 1.19: A summary of the δ^{15}N vs. δ^{13}C data from the literature for diamonds of known paragenesis (with the exception of the polycrystalline diamonds). All δ^{15}N and δ^{13}C values are relative to the AIR and V-PDB standards respectively.

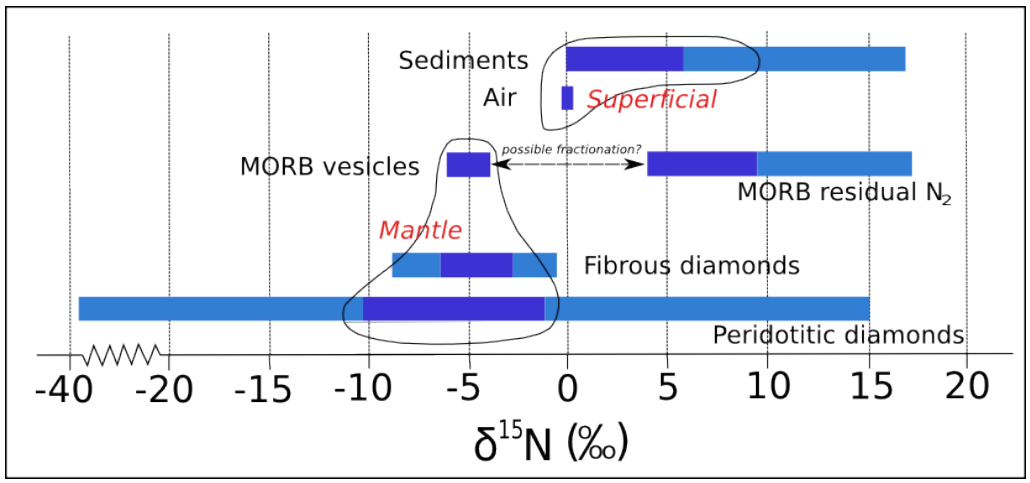

Figure 1.20: Illustration of the isotopic imbalance between mantle and superficial nitrogen. With mantle nitrogen of negative δ^{15}N it is impossible to make outgassed products (superficial nitrogen) and their complement, outgassing residue, both with positive δ^{15}N. Modified from Javoy (1997).

1.4 Variation of nitrogen isotopes

Peridotitic diamonds, in particular, show a large range of δ^{15}N values but only a small range of δ^{13}C values. Additionally, individual diamonds can be zoned with respect to their carbon and nitrogen isotope composition, nitrogen abundance and nitrogen aggregation state (Boyd et al., 1987), and some individual samples can show a very large range of δ^{15}N values with a comparably small range of δ^{13}C values (Mikhail et al., 2014b). These variations in diamonds can be attributed to multistage growth from isotopically distinct reservoirs or to fractionation processes operating during single growth steps (Boyd et al., 1987), or perhaps both.

1.4.1 Mantle heterogeneity

Positive δ^{15}N values can be explained by the contribution of a recycled N component, whereas negative δ^{15}N values suggest the occurrence of pristine N in the mantle region where diamonds were formed, presumably the sub-continental mantle which may have been isolated from the convective mantle for a long time (Marty and Humbert, 1997).

Most evidence indicates that there is an isotopic disequilibrium with respect to nitrogen between external (atmosphere and crust) and internal (mantle) reservoirs of the Earth (Cartigny et al., 1998b). An important question is how did the positive and negative δ^{15}N reservoirs originate? According to Javoy (1997), both the superficial nitrogen reservoir and the outgassing residue have positive δ^{15}N signatures, which couldn't have been generated from a negative δ^{15}N mantle (Figure 1.20). A model was proposed where the Earth was initially of enstatite (EH) chondrite composition with a δ^{15}N of -20 to -40 ‰, with a late veneer of CI chondrite with a δ^{15}N of $+43$ ‰, which later mixed in the upper mantle to produce an upper mantle with δ^{15}N of ca. -6 ‰, with the more negative δ^{15}N seen in diamonds representing preserved very negative δ^{15}N which can be found in the lower mantle, or in the cold lithospheric domains, where no convection occurs (Javoy, 1997). The model implies through mass-balance calculations that the upper and lower mantle are mostly decoupled with respect to volatiles.

Dauphas and Marty (1999) found heavy nitrogen (δ^{15}N of -0.2 to $+6.5$ ‰) in carbonatites from the Kola Peninsula. They suggested nitrogen fractionation during core formation as a method of enriching the lower mantle in ^{15}N relative to the shallow mantle. Nitrogen is a siderophile element so uptake of N by the core would lower the $N_2/^{36}$Ar ratio of the mantle. The ^{14}N–^{14}N bond is weaker than the ^{15}N–^{14}N bond and the ^{15}N–^{15}N bond, so the residual N in the mantle would be enriched in ^{15}N. They also considered recycling and suggested that if heavy nitrogen was recycled into the Earth it should, over time increase the δ^{15}N and $N_2/^{36}$Ar ratio of the deep mantle relative to the shallow mantle, which is apparently not the case. A way around this difficulty is to consider that the nitrogen isotopic composition of the mantle is not primordial. There is evidence that a considerable amount of nitrogen could be recycled into the mantle. During subduction, devolatilisation would preferentially release ^{14}N as N_2, leaving the slab enriched in ^{15}N, meaning that subducted nitrogen will have a positive δ^{15}N signature (Figure 1.21) (Bebout and Fogel, 1992; Busigny et al., 2003; Haendel et al., 1986). This could provide a mechanism for adding ^{15}N-enriched nitrogen into the deep mantle. Existing observations have shown that

a significant fraction of the initially subducted nitrogen could be retained to great depths in the subducting sections to either return to the surface in arcs or enter the deeper mantle beyond the sub-arc regions (Busigny et al., 2003; Halama et al., 2010, 2012; Sadofsky and Bebout, 2004). The total flux of subducted nitrogen has been estimated as 13.2×10^{11} g yr^{-1}, which is almost five times higher than the flux of N output from arc volcanism (2.8×10^{11} g yr^{-1}), suggesting that ca. 80% of N input is transferred to the mantle, and not recycled to the surface (Busigny et al., 2011; Cartigny and Marty, 2013). Other estimates have suggested that the recycling is much more efficient with the N output from arcs estimated at 2.0×10^{10} mol yr^{-1} and N-input from subducted sediments estimated at 1.37×10^{10} mol yr^{-1} (Fischer et al., 2002). Data from the Central American Volcanic Arc estimate a sedimentary input N flux of 2.3 to 9.3×10^{8} mol yr^{-1}, which is at the low end of the calculated output flux of 7.4 to 46×10^{8} mol yr^{-1} (Elkins et al., 2006). However, evidence suggests that altered oceanic crust (AOC) is a significant reservoir for subducting nitrogen, for example, the basement section of the Mariana margin is annually subducting 5.1×10^{6} g km^{-1} N into the trench at a rate twice as large as that of sedimentary input at the same margin (Li et al., 2007). If N input from AOC is added to the inventory of N in subducting sediments, the return of N to the surface through arc volcanism appears to be far less efficient, ca. 15–40% (Elkins et al., 2006; Halama et al., 2010).

The low $\delta^{13}C$ values seen in some eclogitic diamonds have been suggested as evidence of diamonds growing from recycled organic matter which had been subducted in the mantle. However, organic matter should also have a strong positive $\delta^{15}N$ signature, but an analysis of a suite of eclogitic diamonds from Jwaneng showed the $\delta^{15}N$ values were also negative and therefore could not represent the presence of recycled organic matter during diamond growth (Cartigny et al., 1998a). These results were further corroborated by coupled $\delta^{13}C$ and $\delta^{15}N$-values in octahedral peridotitic and eclogitic diamonds (Cartigny et al., 1998b). The presence of very high Fe and chrome contents in inclusions of some highly ^{13}C-depleted diamonds from Orapa also make it highly unlikely that the low $\delta^{13}C$ carbon can be attributed to recycled organic material (Deines et al., 1993). However,

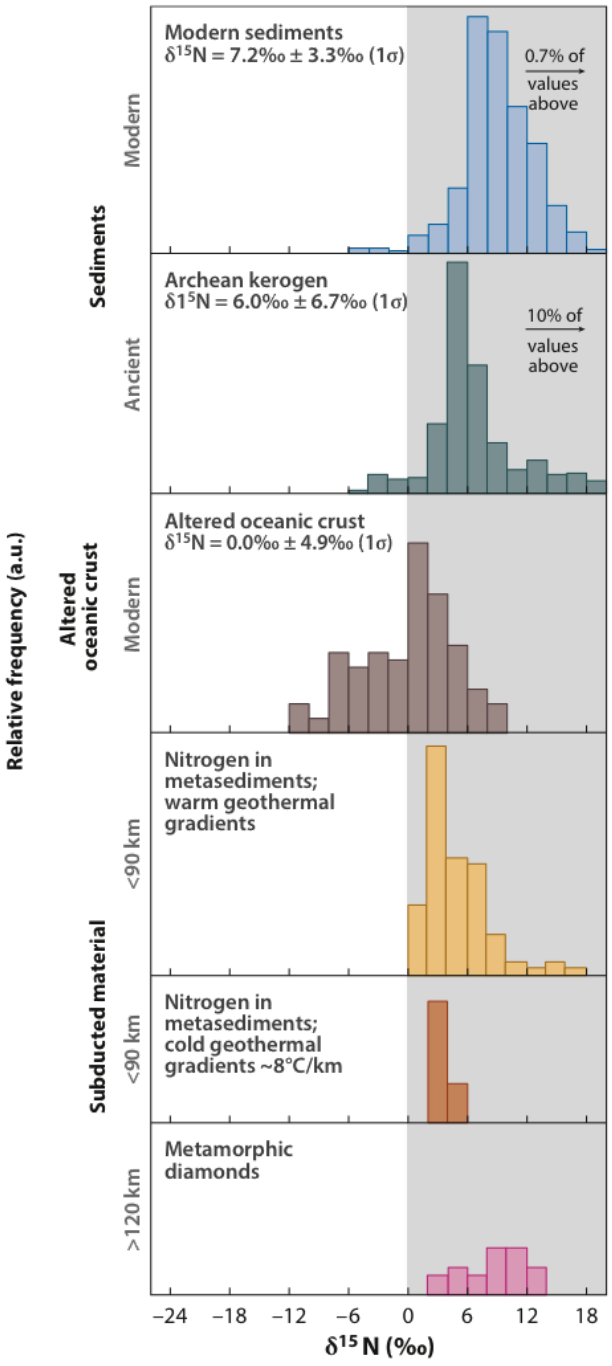

Figure 1.21: Comparative histograms of the δ^{15}N values of modern and ancient sediments, and subducted nitrogen from both warm and cold slab environments. Modified from Cartigny et al. (2014).

evidence for subduction is clear from many studies, including sulphur isotopes of sulphide inclusions, and oxygen isotopes of eclogitic inclusions and nodules, meaning that subduction may require some decoupling of carbon from other elements (Shirey et al., 2013). Therefore, further investigation is required before a recycled source of diamond-forming carbon can be ruled out.

1.4.2 Isotopic fractionation

1.4.2.1 Mass dependent stable isotope fractionation

Mass dependent isotope exchange reactions can be classified as either kinetic or equilibrium reactions. Kinetic mass dependent fractionation of isotopes describes numerous one-directional processes occurring under conditions of incomplete isotope exchange (Schauble, 2004). It occurs because it requires more energy to transport a heavy mass than a light mass, therefore, for a given amount of energy, heavy isotopes will travel slower than the light isotopes resulting in a residue which is enriched in the heavier isotope, if the transfer process is interrupted prior to completion (Hin, 2012). Equilibrium fractionation occurs when heavy isotopes prefer to reside in one phase rather than a second phase, relative to the light isotopes (Hin, 2012). Natural variations in stable isotopes can be expressed in terms of a mass fractionation factor, α, from a standard isotope composition, n:

$$\left(\frac{^{h}X}{^{l}X}\right) = \left(\frac{^{h}X}{^{l}X}\right)_{n} \left(\frac{^{h}m}{^{l}m}\right)^{-\alpha} \tag{1.2}$$

where ^{h}X and ^{l}X are the heavy and light isotopes, respectively, of the element investigated, and ^{h}m and ^{l}m are the atomic weights of the two isotopes (Rudge et al., 2009). The isotope fractionation factor can be further expressed in terms of 'α':

$$\alpha_{A-B} = \frac{\left(^{h}X/^{l}X\right)_{A}}{\left(^{h}X/^{l}X\right)_{B}} \tag{1.3}$$

where α_{A-B} is the fractionation factor between two phases, A and B (Schauble, 2004). In geochemistry, the symbol Δ is more commonly used to describe the fractionation factor, which can be defined as the difference between the measured compositions of the two phases, A and B (Hin, 2012). For geological purposes, α generally does not deviate from 1.00 by more than 0.01, therefore α and Δ can be related simply as:

$$1000 \ln(\alpha_{A-B}) = \Delta^{h/l} X_{A-B} = \delta^{h/l} X_A - \delta^{h/l} X_B \tag{1.4}$$

where $\delta^{h/l} X$ is the measured isotopic composition given as a ratio of isotopes h and l of element X (Hin, 2012).

The equilibrium fractionation between two phases is based on the differences in bond strength of the different isotopes of an element (Sharp, 2007). The heavy isotopes will tend to be concentrated in the phase where that element forms the stiffest bonds, except where the element of interest is bonded directly to hydrogen (Schauble, 2004). Equilibrium fractionation generally decreases with increasing temperature, roughly proportional to $1/T^2$ (Schauble, 2004), without a first order pressure dependence (Hin, 2012). This relationship can be summarised as:

$$\ln(\alpha_{A-B}) \propto \frac{\Delta m}{m_a^2} \frac{\Delta F_{A-B}}{T^2} \tag{1.5}$$

where Δm is the difference in the mass of the two isotopes, m_a is the average atomic mass, ΔF_{A-B} is the different in the sum of force constants acting on the atom in phase A vs. B, and T is the absolute temperature (Schauble, 2007). It follows from Equation (1.5) that stable isotope fractionation can always occur as long as there is a mass difference between isotopes and a difference in bond stiffness between the phases. In a general classification of bond types, covalent bonds are stronger than ionic bonds while metallic bonds are weakest (Hin, 2012). Fractionations are largest in low temperature environments, and

for light elements (eg. H, C, O, N) which have relatively large differences between their isotopic masses (Hin, 2012).

1.4.2.2 Evidence for nitrogen isotopic fractionation in natural samples

The tendency for nitrogen to exsolve (aggregate) implies that it is not readily incorporated into the diamond structure and therefore, fractionation of nitrogen isotopes during diamond growth might be expected (Boyd et al., 1987). However, equilibrium fractionations at temperatures in excess of 1000°C should be small, as in the case of simple molecules of nitrogen compounds, e.g. $\Delta(N_2\text{–}NH_3) = \delta_{N_2} - \delta_{NH_3}$ becomes negative for T < 675°C but never exceeds −1.5 ‰ (Javoy et al., 1984). The diamond-reservoir fractionation factor for nitrogen may be larger than those for simple molecules, but if diamond were controlling nitrogen, the latter is more likely to become enriched in the residual volatiles as the tendency of nitrogen to exsolve suggests that it will preferentially partition into the volatile phase (Boyd et al., 1987).

On the basis of co-variations with N-content, positive $\delta^{15}N$ values, which occur most frequently among monocrystalline diamonds of peridotitic and eclogitic paragenesis, were thought by (Cartigny et al., 2009) to reflect high-temperature fractionations rather than source effects, although little is known about the N-bearing phases involved and about nitrogen fractionation factors at mantle temperatures.

It is probable that, relative to fibrous diamonds, octahedral diamonds grow in stages most likely from a limited supply of volatiles linked to percolating melts or fluids (Boyd and Pillinger, 1994; Cartigny et al., 1997). These melts or fluids could be isotopically differentiated during percolation through the continental lithosphere (the less abundant nitrogen would be more sensitive to this effect than carbon), which could produce the general range of $\delta^{15}N$ of −12 to +5 ‰, but perhaps not the stronger depletion (−25 ‰) seen in diamonds from China (Cartigny et al., 1998b). The trends observed in a Yakutian diamond, decreasing N content and increasing $\delta^{13}C$ and $\delta^{15}N$ during diamond formation

are suggestive of isotopic fractionation occurring during crystallisation in a closed system (Bulanova et al., 2002), however, this is unlikely to apply to the majority of diamonds.

Yokochi et al. (2009) suggested that while equilibrium isotope fractionation at high temperatures cannot produce δ^{15}N variations of several per mil, diffusive fractionation could produce a significant isotope effect. They used a diffusive mixing model, where the nitrogen from a host magma diffuses in or out of a mineral phase with the lighter isotope ^{14}N diffusing faster than ^{15}N, to calculate that N uptake from the host magma can bring the δ^{15}N value of the mineral up to 12 ‰ below that of the host magma.

1.5 Aims of this thesis

There are several questions which can be raised based on a review of the literature.

- Why is the range of δ^{15}N in peridotitic diamonds so large when the range in δ^{13}C is so narrow?
- What is the main control on the variation in δ^{15}N in diamonds - source variations (mixing between reservoirs), or isotope fractionation (between phases)?
- Does equilibrium or kinetic nitrogen isotope fractionation occur in diamond in nature?
- What is the equilibrium fractionation factor for nitrogen during diamond formation?

In order to answer the questions set out above, I have used both natural samples and experiments. I have used natural samples to investigate kinetic isotope fractionation between growth sectors, co-variation of C and N isotope systems and internal variability within individual stones. I have used experiments to determine the possibility of isotope fractionation occurring during diamond growth. Multi-anvil experiments have been used to examine diamond growth itself, and piston-cylinder experiments have been used

to investigate isotopic equilibrium using graphite at lower pressure and a much-shorter timescale.

Chapter 2

Methodology

2.1 Determination of carbon and nitrogen isotope ratios

The C and N isotope analyses in this thesis were carried out at the Open University using the FINESSE machine. The FINESSE apparatus is a custom-built, computer operated facility which utilises three static-mode mass spectrometers fed from a common extraction system under high vacuum (Verchovsky et al., 1998). It uses stepwise oxidation/pyrolysis (heating under vacuum) to measure carbon and nitrogen isotopes from very small aliquots of gas (<10 ng for carbon, and <5 ng for nitrogen). Operating in static mode enables the analysis of smaller aliquots of sample gas, relative to continuous flow facilities, however it does compromise the precision with typical errors of ± 0.5 ‰ for carbon and nitrogen. This is still good enough to study mantle geochemical systems as the terrestrial range for mantle samples is > 40 ‰ for both systems (Cartigny, 2005), and the ability to use much smaller samples is a great advantage when studying precious and rare samples such as diamond. A second key advantage of the Finesse is the ability to operate with extremely low nitrogen blanks. This is achieved by operating under high vacuum, with stainless steel pipework and by using copper valve tips for the nitrogen section of the facility.

2.1.1 Introduction to FINESSE

The mechanical components that make up the FINESSE machine were previously described in detail by Shelkov (1997). A later update to the automated procedure to allow simultaneous determinations of $^{15}N/^{14}N$ and $^{13}C/^{12}C$ ratios and the carbon and nitrogen abundances from a single sample was described by Mikhail (2011). Therefore, I will provide a brief introduction to the key components of the FINESSE machine and their role in the analytical procedure.

The FINESSE apparatus has a number of components which are connected by steel piping (Figure 2.1).

- Vacuum pumps (five ion pumps and one turbo pump)
- Combustion furnace
- CuO (O_2 supply) and CuOcl (O_2 clean-up)
- Molecular sieve
- Three cold fingers
- Baratron® capacitance manometer
- Quadrupole mass spectrometer
- Two static-mode multi-collector mass spectrometers
- Reference gas sources (Air, CO_2, N_2)

The components are separated using several manual and computer controlled valves. The manual valves are not used during the sample analysis procedure, and along with the liquid nitrogen supply, are the only components which are not fully automated. The liquid nitrogen supply must be topped up manually, but the administration of the liquid nitrogen to the cooling devices is automated. Once the sample has been loaded, the entire

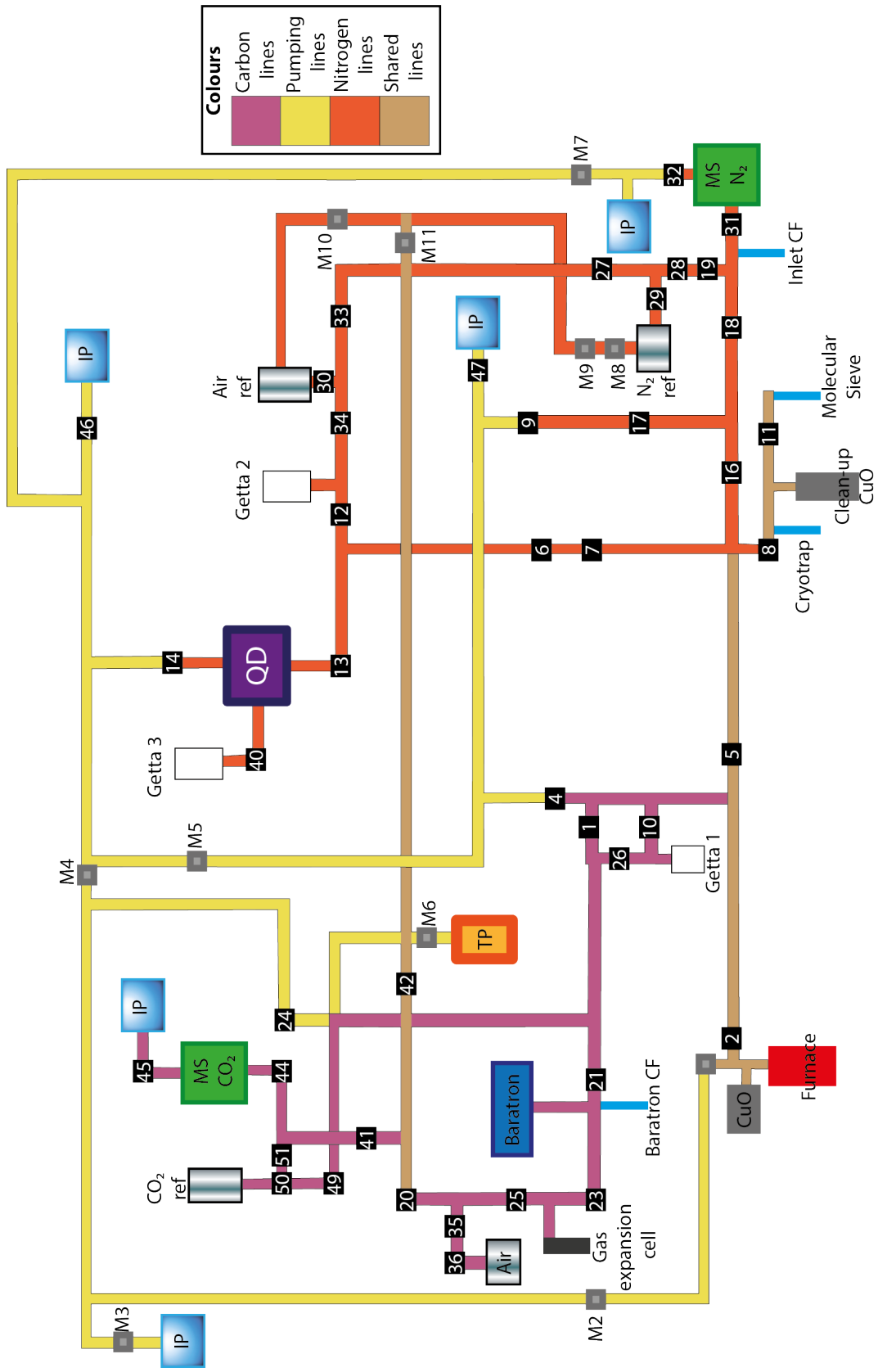

Figure 2.1: Schematic layout of the FINESSE machine. The black squares with white numbers are automated (pneumatic) valves. M1-11 indicates manual valves. IP is an ion pump and TP is the turbo pump. Air and Air ref refer to air standards. CO_2 ref is the CO_2 reference gas and N_2 ref is the N_2 reference gas. CF stands for cold finger, QD for quadrupole, and MS for mass spectrometer.

analytical procedure is fully automated and controlled using LabVIEW™ software. The following parameters can be controlled by the operator prior to the experiment: number of analyses (temperature steps), combustion or pyrolysis (for each step), step duration, and the temperature ranges of the CuO, CuOcl, cryotrap, molecular sieve, baratron cold finger and the inlet cold finger. If at any point the liquid nitrogen source is exhausted, the system produces an error message and pauses indefinitely until it is restarted by the operator. There is an inbuilt failsafe to stop any analyses without liquid nitrogen, as these would result in a complete failure.

2.1.1.1 Overview of components

Combustion furnace The combustion furnace consists of a doubly insulated quartz tube. The double insulation is achieved by situating the quartz tube within a second tube which is pumped to vacuum (Figure 2.2). This reduces the external confining pressure on the furnace enabling higher temperatures to be reached. At high temperatures (>1100℃) the quartz is mechanically weakened and atmospheric pressure would cause it to collapse. The vacuum insulation has the secondary benefit of reducing the diffusion of atmospheric gases into the furnace. The heater is made of SiC and the temperature within the furnace is measured using a thermocouple. The thermocouple and heating system can achieve temperature increments of ∼25℃ in the range 200–1400℃ (Shelkov, 1997).

CuO (O_2 supply) and CuOcl (O_2 clean-up) The furnaces used to heat the CuO and CuOcl are of a similiar design to the combustion furnace. The main difference is the lack of vacuum tube insulation, and a gap in the existing insulation to allow rapid cooling (Figure 2.3). The temperature gradient for cooling is >500℃ in 20 minutes. The CuO and CuOcl furnace use a high-resistance alloy wire as the heater, and the CuOcl is a single-wall furnace.

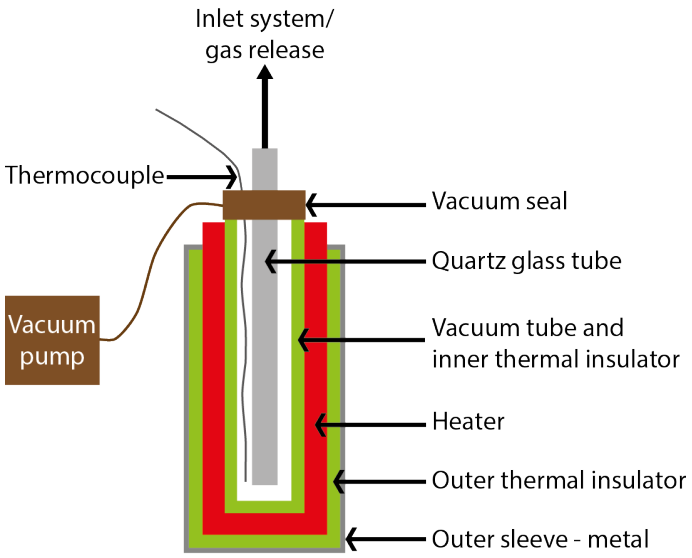

Figure 2.2: Design of the combustion furnace (not to scale).

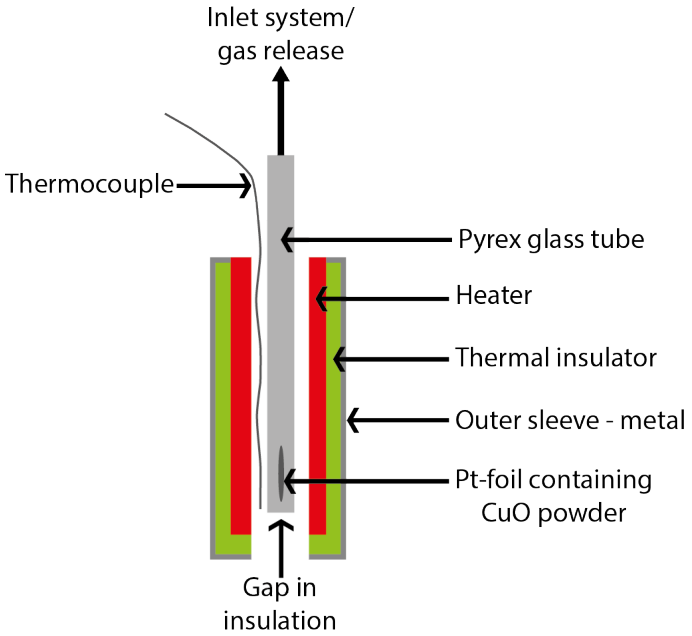

Figure 2.3: Design of the furnaces used to heat the CuO and CuOcl (not to scale).

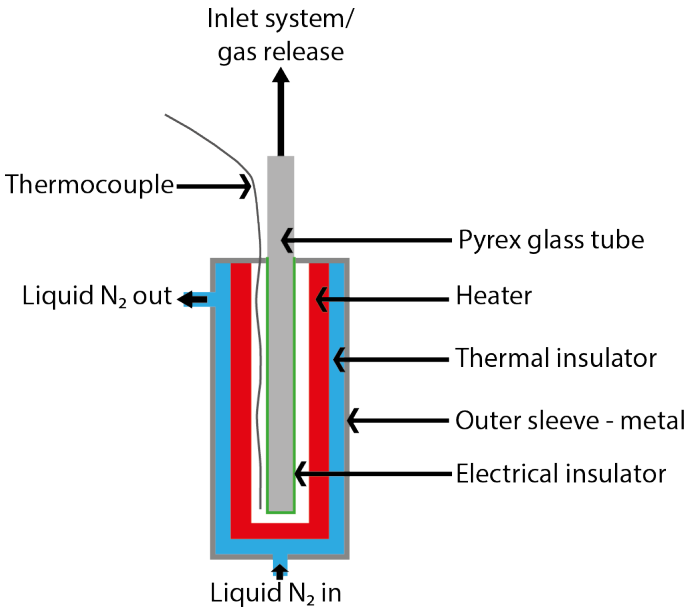

Figure 2.4: Design of a variable temperature trap, e.g. the cryotrap. The molecular sieve is placed within the pyrex tube in the design of the molecular sieve trap. The heater is never in physical contact with liquid nitrogen. The inlet cold finger design does not require the heater (not to scale).

Cryotrap and molecular sieve These components consist of a Pyrex® tube doubly encased in metallic sleeves (Figure 2.4). Using rotary pumps, liquid nitrogen can be pumped around the inner sleeve to cool the Pyrex® tube to low temperatures. This allows for cooling below the condensation temperature of CO_2 (<-160℃) in the cryotrap, and N_2 (<-190℃) in the molecular sieve. In addition, the cryotrap and molecular sieve have an inner heater as part of the assembly which allows them to be heated. The cryotrap can be heated above the evaporation temperature of H_2O ($\sim$60 ℃) and the molecular sieve can be heated to 250 ℃ in order to purify it and maintain a low nitrogen blank.

Baratron cold finger and inlet cold finger Like the cryotrap and molecular sieve, the cold fingers consist of Pyrex® tubes doubly encased in metallic sleeves to allow cooling by liquid N_2 (Figure 2.4). The baratron cold finger can be cooled below the condensation point of CO_2 and the inlet cold finger is cooled to below the condensation point of N_2. The outer sleeve of the baratron cold finger is wrapped with an electrically insulating thermal

wire to allow for rapid heating once pumping of liquid N_2 has ceased. The inlet cold finger does not need to be heated rapidly during the analytical procedure, therefore it does not have a heating system.

Temperature controls Eurotherm® microprocessors control the temperatures in all the heating/cooling components. These automatically adjust the power input where necessary to maintain the temperature required at each stage of analysis.

Baratron® and mass spectrometers The functions of the Baratron®, quadrupole and the two static-mode mass spectrometers will be described in section 2.1.4.

2.1.1.2 Reference gases and calibration

For static mode measurements, the sample and reference gases are analysed in sequence. It is therefore required that there are equal amounts of sample and reference gases used in the mass spectrometer during analysis. In order to automate the amount of reference gas that is used during calibrations and for analysis of carbon and nitrogen isotopes and concentration analysis (Baratron® and quadrupole mass spectrometer), the bleed time technique is implemented (Shelkov et al., 1997). This involves the bleeding of the reference gas through a capillary gas pipette (located between the reference gas cylinders and valves 50 or 28 (Figure 2.1) for carbon or nitrogen respectively).

2.1.2 Sample preparation

Sample preparation takes place in a clean room. For analysis, the diamond samples are wrapped in Pt foil which is twice cleaned before use. Firstly, its is placed in a quartz tube with CuO powder and attached to a vacuum line. The tube is then sealed and heated in a furnace to ∼900℃ for 24 hours to oxidise contaminants. Next, it is placed in a pure O_3

environment and treated with UV light for a further 24 hours. Platinum is used because it facilitates the combustion of CH_4 and CO to CO_2, and it also catalyses the decomposition of nitrous oxides to N_2. This is important as there could otherwise be low temperature mass dependent isotopic fractionation between nitrous oxides and N_2. It also reduces the occurrence of isotopologues that could interfere with analyses, such as CO and $^{14}N_2$ which both have a mass of 28 (Mikhail, 2011).

The diamonds are crushed into small pieces (0.04–0.3 mg) and cleaned using propanol . The equipment is cleaned thoroughly between each use to prevent cross contamination of the samples. Prior to wrapping the sample in Pt foil, the foil is weighed and the balance set to zero. The sample is removed from the propanol and dried, before being wrapped in the foil and returned to the balance. The weight is measured and recorded three times, then an average is taken. This is the most reliable way to obtain an accurate weight for the sample. Recording the starting weight is important to ensure a 100% yield during combustion. The Pt foil containing the sample is then wrapped in Al foil for transport from the clean room to the Isotope Lab.

2.1.3 Sample loading

The sample loading procedure takes approximately one hour in total. The sample loading assembly is shown in Figure 2.5. Firstly, the sample loading system is closed off from the furnace and main vacuum lines using a manual valve – glass valve 1. A second valve, glass valve 2, can then be removed to allow the samples to be loaded into the tube. Up to three samples can be loaded at any one time, but it is safer to only load two as there is no way of labelling them inside the tube, so it is important to keep them separated. A metal 'slug', which is manipulated from the outside by a magnet, is used to move the samples once they have been loaded. Once the samples are loaded, glass valve 2 can be replaced, but it must be left open. Using the 'Global Control' interface, valves 20, 22, 27, 33, 49, are closed and the TP valve and valve M3 are closed manually, then valve 42 can be opened.

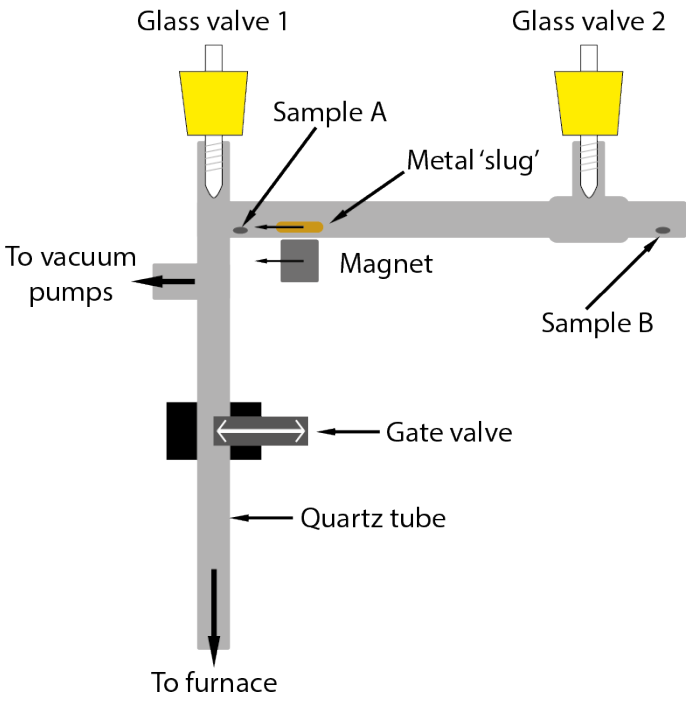

Figure 2.5: Design of the sample loading assembly. Samples are loaded by removing glass valve 2. An additional sample can be stored in the assembly as indicated by 'Sample B' (not to scale).

Next, glass valve 1 can be re-opened. The sample-loading assembly then pumps to the turbo pump and should be left for 15 minutes. Once the 15 minutes are complete, glass valve 2 may now be closed and valve M3 opened. The system will then pump to the ion and turbo pumps. Again, it should be left for 15 minutes. After 15 minutes, valve 22 can be opened. The baratron pressure should now be within normal limits. If it is, the sample can be dropped into the furnace. To do this, the gate valve must be opened. It is important to check the pressure on the main-line gauge prior to dropping the sample. Using the metal 'slug' and a magnet, the sample is gently moved along the tube until it drops. The pressure on the main-line gauge should rise if the sample has dropped into the furnace. Once it is certain that the sample has dropped into the furnace, the gate valve should be closed. Finally, valve 42 can be closed and valves 20, 27, 33 and 49 opened. The 'Experimental Control' interface is used to set the temperature steps for the experiment. For each sample, a series of temperature steps is used to make sure all of the carbon and

nitrogen is oxidised. These steps can vary from 200 to 1400 ℃. Next, 'Experiment setup' is used to select the analyses to run – for the purposes of this thesis they are CO_2 – N_2 – QF. To return to the main interface the 'Go' icon should be selected. Finally, to start the experiment, the 'Run' icon must be selected. The computer will then issue several prompts. It is very important not to append the data to the previous file, unless you are continuing a paused experiment. 'No' must be selected when asked if the step is ready, unless it is the continuation of a paused experiment which has already completed the current combustion phase. The experiment will now begin.

2.1.4 Experimental procedure

The experimental procedure is described in detail in Shelkov (1997) and Mikhail (2011) and summarised here.

2.1.4.1 Combustion

The sample is heated in the quartz furnace either under vacuum (pyrolysis) or oxygen (combustion), which releases the sample gas. For combustion, the oxygen source is pure CuO powder which is heated to 850℃. The pyrolysis/combustion stage lasts for 30 minutes. When oxygen has been used, the CuO is subsequently cooled to 600℃, then 350℃ to withdraw the excess oxygen from the furnace.

2.1.4.2 Gas separation and purification

Once combustion is complete and the CuO has cooled to blow 500℃, the cryotrap begins cooling to −172℃. When this temperature is reached, the sample gas is released from the furnace. The CO_2 gas is condensed onto the cryotrap, but the N_2 is not. Once the CO_2 is completely transferred to the cryotrap, valve 11 (Figure 2.1) is opened and the N_2 is then condensed using a molecular sieve cooled to −250℃ (liquid nitrogen temperature).

All non-condensible gases are pumped away from the clean-up section . The furnace is closed off so combustion can begin on the next step.

2.1.4.3 Carbon measurements

Abundance Once separated, the condensates are returned to the gas phase, and remain separated by valve 11 isolating the N_2 on the molecular sieve (Figure 2.1). The CO_2 is transferred into the Baratron® capacitance manometer, which determines the abundance with an accuracy of ± 1 %. This equipment measures true pressure (force/unit area) which means it is not gas-type sensitive. To avoid saturation of the mass spectrometer, the CO_2 gas is split into smaller aliquots.

Carbon isotopic ratio determination The $^{13}C/^{12}C$ ratio is determined by measuring the mass of the CO_2 gas (Craig, 1953). The important isotopologues of CO_2 are $^{12}C^{16}O_2$, $^{13}C^{16}O_2$, $^{12}C^{16}O^{17}O$ and $^{12}C^{18}O^{17}O$ that correspond to masses 44, 45 and 46. The ratio of masses 45/44 and 46/44 are measured using a triple collector mass spectrometer.

The mass spectrometer first performs a 'zero' measurement to enable the background to be subtracted from the sample and reference gas measurements. Once this is complete, the sample CO_2 gas is expanded into the mass spectrometer and the measurements are taken. Next, the sample gas is pumped away from the mass spectrometer, and then an aliquot (of a similar size to the sample) of reference gas is fed in. If the size of the reference gas is not within 5% of the sample gas, the measurement is repeated with a new aliquot of the correct size. The ratio of $^{13}C/^{12}C$ of the sample is determined relative to the reference gas, then normalised to $\delta^{13}C$ relative to the Pee Dee Belemnite standard. The precision of the measured $\delta^{13}C$ value is determined using the reference gas.

2.1.4.4 Nitrogen measurements

Abundance Once the CO_2 and H_2O have been removed from the cryotrap, the molecular sieve is heated to 250℃ to release the N_2 (including small amounts of noble gases and CO). The CuOcl is heated to 800℃ in order to oxidise any CO to CO_2 and remove any remaining O_2. The CuOcl is then cooled to 450℃ to withdraw the oxygen, and the cryotrap is cooled to −140℃ to trap any residual CO_2. The initial N abundance measurement is taken using the quadrupole mass spectrometer by measuring the intensity of mass 14 of an aliquot of gas of known volume because the background for this mass is very low. This gives an estimate of the amount of gas present, and is used to enable the correct amount of splitting to be performed.

The gas to be analysed is stored between valves 18, 19 and 31 (Figure 2.1) where the inlet cold finger is cooled to condense any remaining condensible gases. The nitrogen mass spectrometer first performs a 'zero' measurement to subratct the background from the sample and reference gas measurements, and then the mass of the nitrogen in the sample is determined in the mass spectrometer and calibrated against the reference gas.

Nitrogen isotopic ratio determination The nitrogen isotopic ratio ($^{15}N/^{14}N$) is determined using the same principles as the carbon isotopic ratio, but using a different mass ratio (29/28 corresponding to the two potential masses of N_2). The intensities of mass 29 and 28 are calibrated against the reference gas and corrected using the air reference gas as a standard, then expressed as $\delta^{15}N$ relative to air. The $^{15}N/^{14}N$ in the reference gas gradually becomes fractionated over time, which can be corrected for by regular calibrations with the air reference gas. The precision of the measured $\delta^{15}N$ value is determined using the reference gas.

2.1.5 Blank levels

The blank levels are quantified using the same procedure detailed above but using an empty Pt-foil as the sample. The fully automated system with metal piping in the nitrogen section enables the blank levels to be kept extremely low. Carbon blank levels are maintained at <30 ng, which is negligible for the scope of this thesis where all samples contain considerably more carbon. Nitrogen blank levels are maintained at <1 ng, but are often below 0.5 ng. For diamonds containing >500 ppm of nitrogen, the blank contribution is negligible and does not need to be considered. For diamonds containing <500 ppm, the blank contribution is subtracted from the nitrogen mass and isotopic measurements. In this thesis, where the blank contribution is >50% the data have been discarded.

2.1.5.1 Nitrogen blank stability versus time

Blanks were analysed during each of my four visits to the Open University. The results are presented below (Figure 2.6). Throughout the experiments, the nitrogen blank was maintained below 0.5 ng, and with a δ^{15}N within normal terrestrial values (>−50 ‰ and <50 ‰).

2.2 High-pressure experiments

2.2.1 Multi-anvil press

The multi-anvil press experiments have been performed at the Bayerisches Geoinstitüt, Bayreuth, Germany, using a 1000 ton Kawai-type split-cylinder press (Kawai et al., 1970). The multi-anvil press is capable of reaching pressures up to 25 GPa and temperatures of 2200°C. This apparatus consists of an octahedron-within-cubes geometry (Walker et al., 1990, and references therein), where the sample is contained within an octahedral void held between eight tungsten carbide cubes. The octahedral void is created by the truncation of

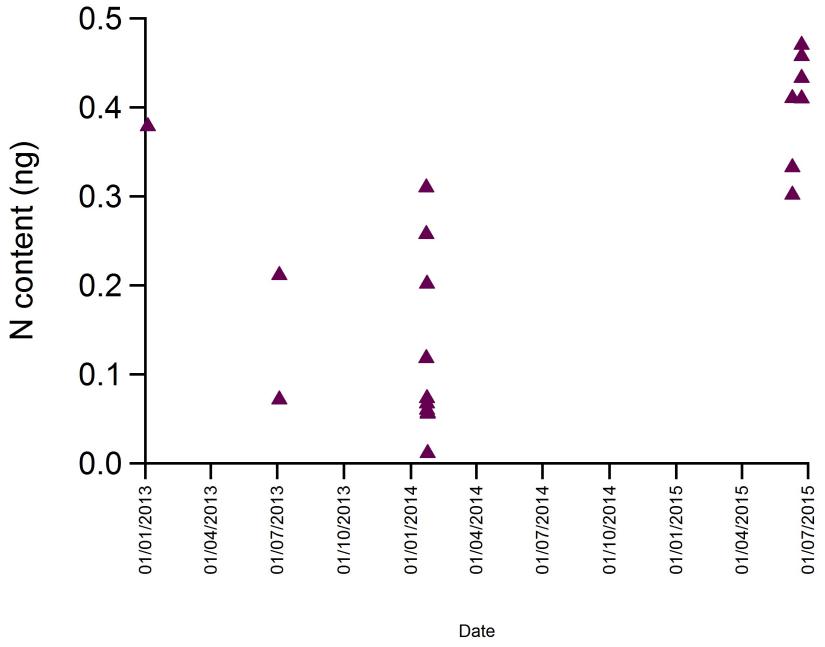

(a)

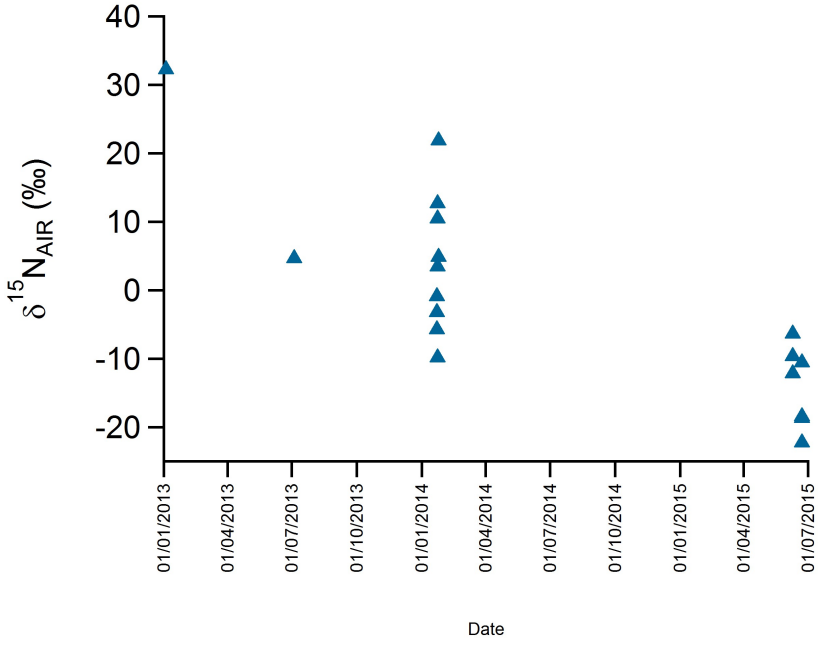

(b)

Figure 2.6: Graphs showing the stability of the N blank through time. (a) N content and (b) δ^{15}N.

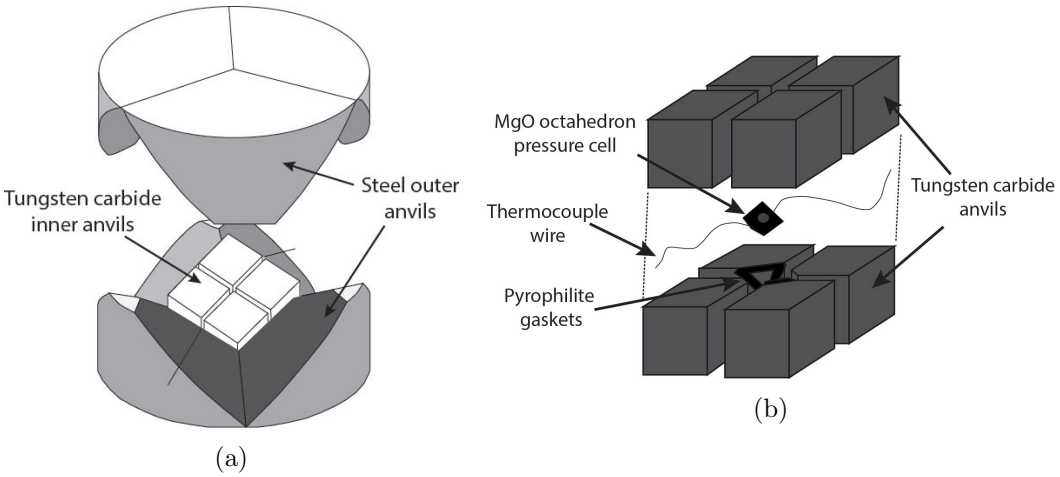

Figure 2.7: Schematic of the Kawai-type anvil sets and assembly. (a) The arrangement of the split-cylinder outer anvils of a Walker cell after Dobson et al. (2004) and (b) the eight inner anvils with the pressure cell and gaskets after Rubie (2006).

the cubes on the three-fold axis. These cubes are compressed from the outside by a cylindrical cluster of six wedges contained within a ring, creating the confining pressure. The octahedral pressure medium is made from MgO and pyrophillite gaskets are used between the carbide anvils to transfer pressure to the sample. The sample assembly consists of several parts: an MgO octahedron (size depends on the size of the anvil truncations), a ZrO_2 sleeve, a thermocouple, a furnace (eg. graphite, $LaCrO_3$), and a capsule (eg. boron nitride, rhenium foil) in which the sample powder is placed. The sample is heated by passing an electric current across the resistance furnace within the octahedron, which is controlled using a Eurotherm®. The temperature is measured using a thermocouple placed within the sample assembly adjacent to the capsule.

2.2.2 Piston-cylinder press

The piston-cylinder experiments have been performed at UCL using a typical $^1/_2$ inch Boyd–England type press (Boyd and England, 1960). The piston-cylinder press can perform high pressure and high temperature experiments over relatively long periods of time (weeks to months), and can reach pressures of up to 5 GPa and temperatures of up to

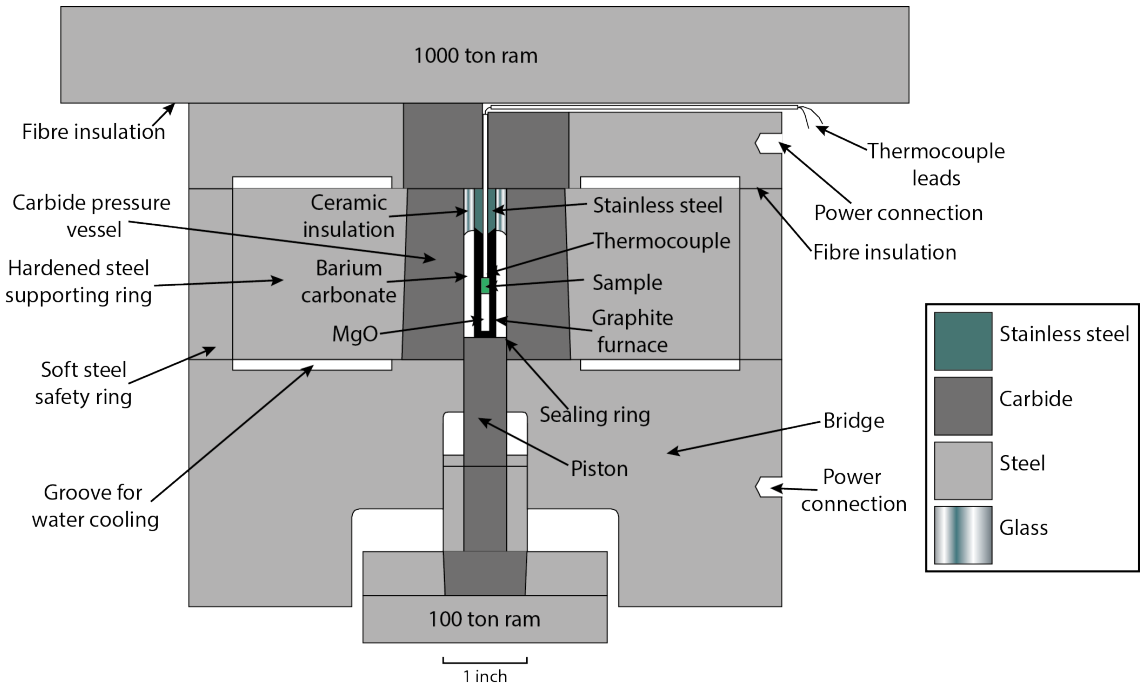

Figure 2.8: Schematic diagram of the piston cylinder press. Modified from Boyd and England (1960).

2200 ℃. Sample volumes are typically 200 mm^3. The piston-cylinder apparatus achieves high pressures by using the principle of pressure amplification: converting a small load on a large piston to a large load on a small piston (Figure 2.8). The pressure vessel is end-loaded during a run with a thrust of 150–250 tons delivered by a hydraulic press. Pressure is applied to the sample and furnace assembly with a $^1/_2$ inch diameter carbide piston driven by a second hydraulic press. Copper piping around the edge of the pressure vessel allows for water cooling. The sample assembly consists of a solid pressure medium (e.g. barium carbonate), a resistance heater (e.g. graphite), and a small central volume for the sample. The sample is heated by applying a large voltage to steel plates above and below the pressure vessel, which is then passed across the resistance furnace. This is controlled by a Eurotherm®. The temperature is monitored with a thermocouple placed close to the sample.

Chapter 3

Carbon and nitrogen isotope systematics of mixed-habit diamonds

3.1 Introduction

Mixed habit diamonds (Figure 3.1) are examples of crystals that form by two growth mechanisms occurring at the same time (Frank, 1967; Howell et al., 2015) – octahedral and cuboid growth (Lang, 1974; Moore and Lang, 1972; Suzuki and Lang, 1976). Octahedral growth produces flat {111} facets, whereas cuboid growth produces characteristic hummocky non-faceted surfaces which can be inclined by up to 30° from {100} (Howell et al., 2015; Sunagawa, 2005). The growth mechanisms for these two types of growth are explained in Section 1.1.1.1. Two different growth mechanisms occurring at the same time within a single crystal produces different impurity characteristics between the growth sectors (Howell et al., 2015). Nitrogen concentrations in mixed-habit diamonds are typically high (900–>2000 ppm) with N preferentially partitioned into the octahedral sectors,

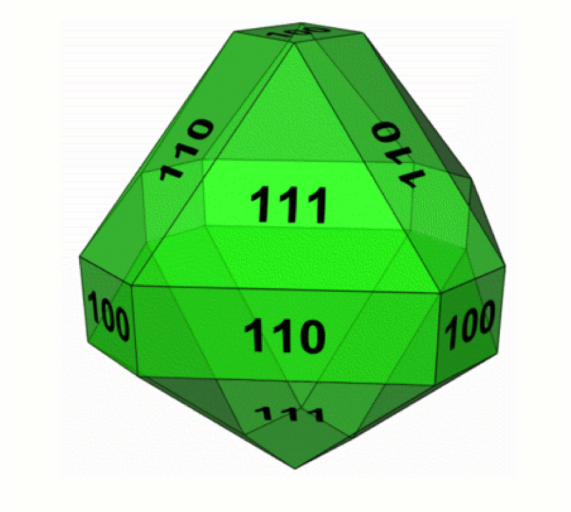

Figure 3.1: A three-dimensional cubic crystal with {100}, {110} and {111} faces. In this study, diamonds with only {100} and {111} faces were analysed. From ElementSix (2015).

with enrichment of 107–157% relative to the cuboid sectors (Howell et al., 2013b, 2015; Lang et al., 2004; Welbourn et al., 1989; Zedgenizov and Harte, 2004). No study has ever observed fractionation of carbon isotopes in mixed-habit diamond; therefore, herein the focus is nitrogen as fractionation of nitrogen isotopes has been observed in synthetic diamonds.

An analysis of a large, laser-sectioned synthetic cubo-octahedral diamond by Boyd et al. (1988) showed a large kinetic fractionation of nitrogen isotopes of ∼40 ‰ between cubic and octahedral growth sectors. The cubic [100] sector of the stone contained about half the concentration of nitrogen and was enriched by ca. 4.5 % in ^{15}N relative to the octahedral [111] growth region (Boyd et al., 1988). The nitrogen-rich octahedral part of the stone had δ^{15}N values close to atmospheric (−0.4 to −2.4 ‰) whereas the nitrogen poor cubic regions had δ^{15}N values of +30.7 to 42.1 ‰, but the δ^{15}N of the initial nitrogen is unknown (Boyd et al., 1988). A more recent study performed in situ analysis (SIMS) of a further two synthetic stones and found that the nitrogen abundance in cubic sectors is reduced relative to octahedral sectors by a factor of two to four, with some cubic zones containing only 20% of the nitrogen content of octahedral zones growing at the same time (Reutsky et al., 2008b). This marked difference in nitrogen concentration was accompanied by a

large variation in δ^{15}N of 27–33 ‰ (Reutsky et al., 2008b), which clearly corresponds with the earlier investigation by Boyd et al. (1988).

Table 3.1: Summary of the existing data on mixed-habit diamonds from Boyd et al. (1988); Cartigny et al. (2003); Howell et al. (2013b); Reutsky et al. (2008b).

	Sample	**Sector**	**N ppm**	**N content ratio (c/o)**	**$\Delta(\delta^{15}$N) (‰)**
Natural	MC01	cuboid	1565	0.8	
		octahedral	1995		
	MC07	cuboid	1558	0.9	
		octahedral	1681		
	MC08	cuboid	1802	0.8	
		octahedral	2335		
	MC10	cuboid	1192	0.6	
		octahedral	1851		
	MC13	cuboid	1675	0.7	
		octahedral	2250		
	Cartigny	cuboid	29	0.7	−0.1
		octahedral	42		
Synthetic	Boyd	cubic	40	0.3	40
		octahedral	115		
	Reutsky 150	cubic	75	0.3	27
		octahedral	257		
	Reutsky 140	cubic	136	0.3	33
		octahedral	475		

Kinetic isotope fractionation of this magnitude could explain the large range of δ^{15}N seen in mantle-derived diamonds, however, there has so far been limited work on whether a similar effect occurs in natural diamonds. A systematic FTIR and SIMS analysis of a

single mixed-habit diamond from Yakutia showed that there is no significant or consistent fractionation of carbon or nitrogen isotopes between cuboid and octahedral growth sectors (Bulanova et al., 2002), however the nitrogen isotope data was associated with a large error of ca. ±6 ‰. Cartigny et al. (2003) considered the possibility of a similar fractionation occurring in natural diamond but also found that the δ^{15}N values of octahedral and cuboid growth sectors in a single macro-diamond were the same (within error), but the octahedral sectors contained more nitrogen than the cuboid sectors. They concluded that kinetic fractionation does not occur in natural diamonds. Howell et al. (2013b) used FTIR to analyse 13 mixed crystal habit diamonds and found large differences in nitrogen content between growth sectors of up to 700 ppm. Like the synthetic diamond analysed by Boyd et al. (1988), the octahedral sectors contained considerably more nitrogen than cuboid sectors(Table 3.1).

3.2 Samples and methodology

The samples which were analysed were the subject of the initial investigation by Howell et al. (2013b). They were obtained through the gem industry (provided by Prof. W. Griffin), therefore their geographical source is unknown. They were initially in the form of doubly polished {100} plates less than 1 mm thick. The spectroscopic data showed that all the samples had high nitrogen concentrations with N preferentially partitioned into the octahedral sectors (2100–2650 ppm) compared to the cuboid sectors (1450–1870 ppm) (Table C.1) (Howell et al., 2013b). Additionally, trace element measurements showed that nickel and cobalt preferentially partitioned into the cuboid growth sectors (Figure C.1), which contained up to two orders of magnitude more Ni and Co than the octahedral sectors (Howell et al., 2013a). However, there was no evidence of carbon isotope fractionation between growth sectors.

The original diamond plates were laser cut by Dr. D. Howell to isolate the octahedral and cuboid sectors of the following diamonds: MC01, MC07, MC08, MC10, and MC13

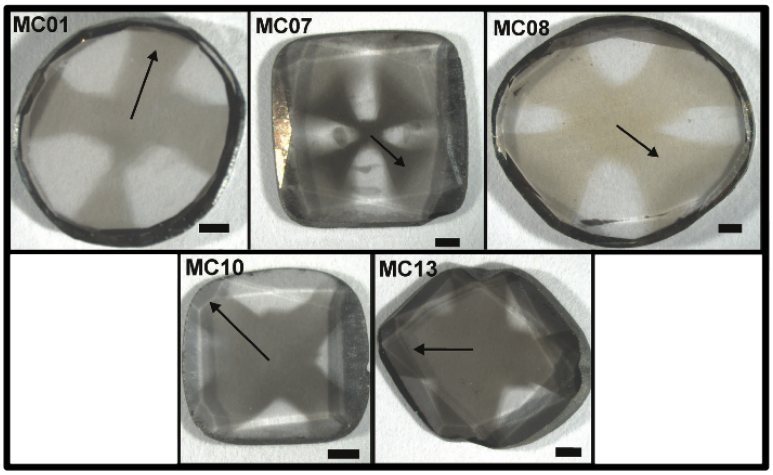

Figure 3.2: Images of the five mixed-habit diamonds analysed in this study. All are doubly polished plates. All are cut within 10° of a {100} face. The black arrows point in a <100> direction. The black bars represent 1 mm scales. From Howell et al. (2013b).

(Figure 3.2). The samples were analysed using the FINESSE by the procedures described in Section 2.1. Cuboid sectors from four additional diamonds (MC02, MC03, MC04, MC09) were also analysed, but the octahedral sectors were not available for comparison. Each analysis used the following temperature steps:

1. 1100 ℃ pyrolysis
2. 500 ℃ combustion
3. 1100 ℃ combustion
4. repeat stage 3 until the sample has fully combusted.

The pyrolysis/combustion of each step is performed for 30 minutes. Steps 1 and 2 are used as cleaning steps to remove any surficial contaminants from the sample. In many of the experiments, only two main combustion steps were required as the sample had fully combusted after one step.

3.3 Results

The summarised results are shown below in Table 3.2. These data presented are weighted mean values for each sector analysed (stepped data can be found in Table B.1). Due to the high nitrogen contents of these diamonds, the blank contribution was negligible, therefore blank corrections were not necessary.

3.3.1 Nitrogen concentration

The similarity between in situ (FTIR) and combustion datasets demonstrate that the C and O sectors were adequately separated prior to analysis (Figure 3.3). The results compare favourably with the initial N-concentration data obtained by Howell et al. (2013b), which showed that octahedral growth sectors contain considerably more nitrogen than cuboid growth sectors (Figure 3.3). The cuboid sectors contain 1190–1800 ppm of nitrogen, compared with 1680–2350 ppm in the octahedral sectors, meaning an enrichment of nitrogen in the octahedral sector of 10–155% relative to the cuboid sector. The discrepancies between the mass spectrometry data and the FTIR data can be explained by the fact that the FTIR takes a mean measurement from multiple analyses each of a very small volume of sample, whereas the mass spectrometry remeasures a larger volume of sample, so there may be small variations within each sector, accounting for the differences in concentration measurements.

3.3.2 Carbon isotopic values

The δ^{13}C values range from -5 to -10 ‰. For Δ^{13}C ($\delta^{13}C_{\text{cuboid}} - \delta^{13}C_{\text{octahedral}}$), the values range from -1.5 to 1.5 ‰. With an associated error of ca.$\pm$1 ‰, these values show that there is no resolvable variation in δ^{13}C between cuboid and octahedral growth sectors. The carbon isotope ratios for MC07 and MC08 were previously measured using SIMS (Howell et al., 2013b). For MC07, the octahedral sectors have a mean δ^{13}C of -8.79

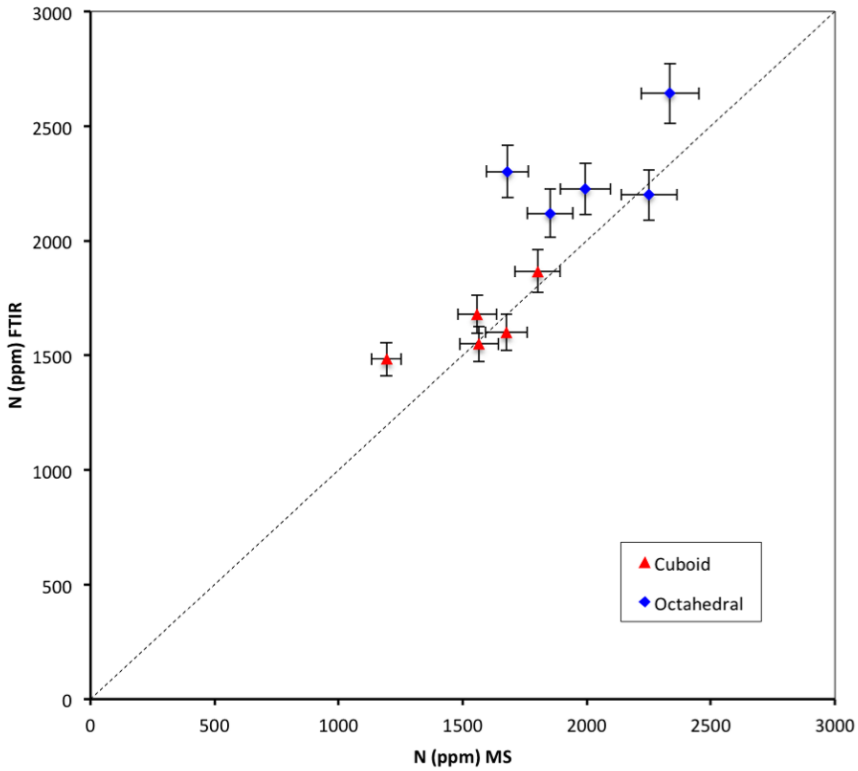

Figure 3.3: A comparison between the nitrogen concentration measured using FTIR and stepwise combustion mass spectrometry.

‰, and the cuboid sectors have a mean δ^{13}C of −8.83 ‰. For MC08, the octahedral sectors have a mean δ^{13}C of −8.98 ‰, and the cuboid sectors have a mean δ^{13}C of −8.90 ‰. The carbon isotope ratios of MC10 and MC13 were also measured using SIMS (Howell et al., 2015), with mean δ^{13}C values of the cuboid sectors measured as −8.7 and −8.5 ‰, respectively, and −8.5 and −8.3 ‰, respectively, in the octahedral sectors. There are small differences between the δ^{13}C values for MC08 (-10.5 ± 1.1 ‰ cuboid, and -10.2 ± 1.0 ‰ octahedral) and MC10 (-5.6 ± 0.4 ‰ cuboid, and -7.1 ± 3.8 ‰ octahedral) in this study and the δ^{13}C values measured using SIMS, however, this can be explained by small differences within each diamond, as SIMS uses surface measurements, whereas the mass spectrometer measures a larger volume of sample.

3.3.3 Nitrogen isotopic values

The δ^{15}N values range from 1.5 to −2.5 ‰. For Δ^{15}N ($\delta^{15}N_{cuboid} - \delta^{15}N_{octahedral}$), the values range from −3.9 to 1.2 ‰ (as with carbon, the associated error is ±1 ‰). Due to the high nitrogen contents of these diamonds, the blank contribution was negligible and therefore blank corrections did not need to be applied. In this case, only MC10 (Δ^{15}N of −3.9 ‰) shows a possibly significant fractionation between cuboid and octahedral growth sectors, with the octahedral sector enriched in ^{15}N relative to the cuboid sector (Figure 3.4). Concurrent to this study, the δ^{15}N values for three of these samples (MC08, MC10 and MC13) were determined by SIMS (Howell et al., 2015). The SIMS analyses also found the octahedral sector of MC10 to be enriched in ^{15}N relative to the cuboid sector but the fractionation was not as large ($\sim 0.5 \pm 0.4$ ‰). Both MC08 and MC13 also showed very small differences in δ^{15}N values of ∼1 ‰, which are within the error of the method applied here. The SIMS-obtained δ^{15}N values for the cuboid and octahedral growth sectors of MC08, MC10 and MC13 (Table C.2) are within 1.5 ‰ of the values measured by combustion, with the exception of the cuboid sector of MC10 which differs by ∼2.5 ‰. As with carbon, these small differences can be explained by small heterogeneities within the diamonds which may or may not be seen by the differing measurement techniques. As

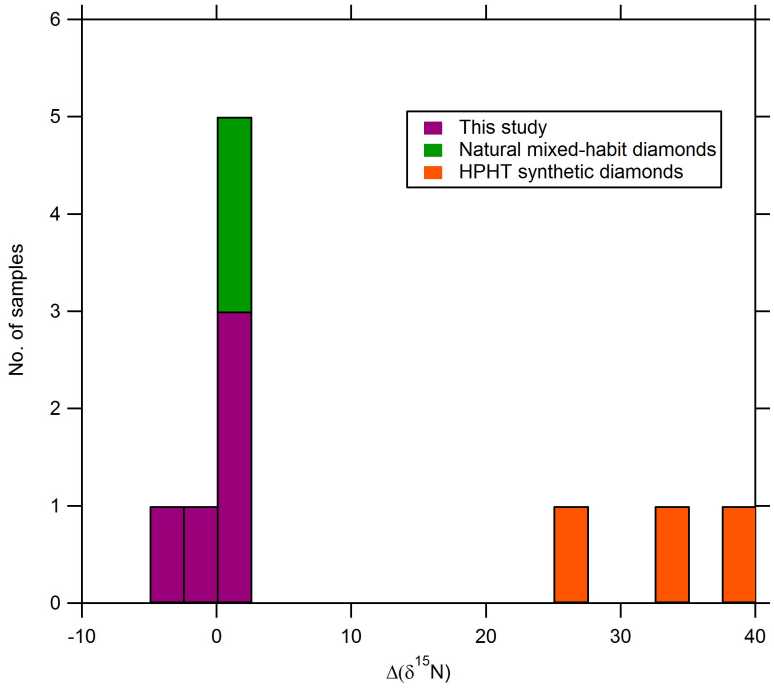

Figure 3.4: Histogram showing the fractionation of nitrogen isotopes ($\Delta(\delta^{15}N)$) in this study compared with other studies on natural diamonds (Bulanova et al., 2002; Cartigny et al., 2003), and synthetic diamonds (Boyd et al., 1988; Reutsky et al., 2008b). The fractionation is calculated from the cubic or cuboid sector to the octahedral sector.

these differences are small, they do not affect the conclusions of this study.

3.4 Discussion

3.4.1 Nitrogen isotope fractionation between growth sectors

These data have shown that while synthetic mixed habit diamonds exhibit a large (∼40 ‰) fractionation of nitrogen isotopes, there is no resolvable difference between the $\delta^{15}N$ values of the cuboid and octahedral sectors in natural mixed-habit diamonds, in all but one sample (Figure 3.4). The largest fractionation in the natural samples is in MC10, with a fractionation of ∼4 ‰. However, in this case it is the octahedral sector that is enriched in ^{15}N, whereas in the synthetic diamonds, it is the cubic sector that is enriched in ^{15}N.

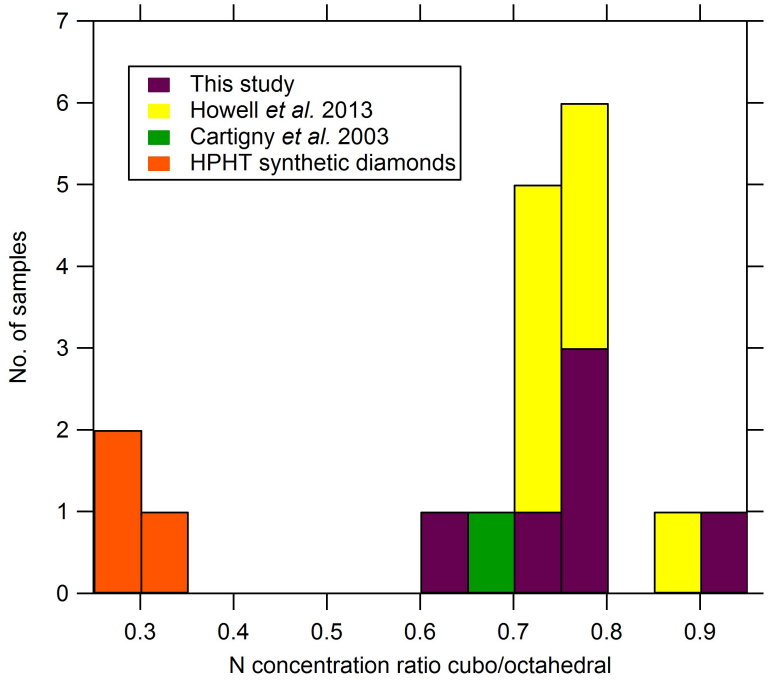

Figure 3.5: Histogram showing the ratio of nitrogen concentration between cubic or cuboid and octahedral growth sectors in this study compared with other studies on natural diamonds (Cartigny et al., 2003), synthetic diamonds (Boyd et al., 1988; Reutsky et al., 2008b) and FTIR data from (Howell et al., 2013b).

The main reason for this differing behaviour between natural and synthetic samples is the difference in growth mechanisms involved. Octahedral growth in both natural and synthetic diamonds occurs via the spiral growth mechanism (Sunagawa, 2005). The cube faces of a diamond grown from a metal solvent also form via the spiral growth mechanism. However, cuboid growth for natural diamonds in a C-O-H fluid occurs via an adhesive growth mechanism (Sunagawa, 2005). Therefore, natural mixed habit diamonds grow by two different growth mechanisms, while HPHT synthetic diamonds grow by just one mechanism on two crystallographically different surfaces.

In both natural and synthetic mixed habit diamonds, the cuboid/cubic sector is depleted in nitrogen relative to the octahedral sector, although the difference is more pronounced in the synthetic diamonds with an N_{cub}/N_{oct} ratio of ~0.3 vs. an N_{cub}/N_{oct} ratio of ~0.6–0.9 in natural diamonds (Figure 3.5). This preferential nitrogen uptake in the octahedral sectors is possibly the result of more bonding opportunities on the {111} face compared

to the {100} face (Howell et al., 2013b; Sunagawa, 2005). However, it has been shown that the nitrogen concentration in synthetic diamonds depends on the growth rate of each sector (Satoh et al., 1990). At higher temperatures, the nitrogen uptake is greater in the (111) sector (octahedral) than the (100) sector (cubic) (Burns et al., 1990; Satoh et al., 1990), whereas at lower temperatures the nitrogen concentration is greater in the (100) sector than the (111) sector (Satoh et al., 1990). This is likely due to the fact that at lower temperatures (1350℃) the growth rate of (111) sectors exceeds that of the (100) meaning that nitrogen would be more easily contained in the (100) growth sector, and vice versa at higher temperatures (1400℃) (Satoh et al., 1990). This could explain why the octahedral sectors of HPHT synthetic diamonds are enriched in ^{14}N relative to the cubic sectors, as bonding with lighter isotopes requires less energy (Schauble, 2004). It it is possible that the adhesive growth mechanism occurring in cuboid sectors of natural mixed-habit diamonds minimises this effect, due to a faster uptake of nitrogen onto the rough crystal surface which counteracts the greater bonding opportunities/slower growth rate on the octahedral face, therefore evening out the differences. However, there is still a preferential uptake of nitrogen in the octahedral sectors of natural diamonds indicating that the greater bonding opportunities or effects of the slower growth rate are not fully nullified by the increased uptake speed. Therefore, one might expect to still see an enrichment of ^{14}N in the octahedral sector. However, these data show this is not the case, so a different explanation is required.

Boyd et al. (1988) speculated that if the initial nitrogen δ^{15}N in HPHT synthetic diamonds was assumed to be close to atmospheric ($\sim$0 ‰), only the cubic sectors showed any fractionation. The data from Reutsky et al. (2008b) also show a similar relationship, with the octahedral sector close to 0 ‰ and the cuboid sector enriched in ^{15}N. If this is the case, it would indicate that the fractionation process is related to the growth on the cubic sector alone, assuming that the initial δ^{15}N value of the diamond-forming medium was 0 ‰. Further evidence can be found in the analysis of a HPHT synthetic cube-form diamond described in Stern et al. (2014). The bulk δ^{15}N value was found by combustion

to be +9.5 ‰, which again indicates that cubic growth preferentially incorporates ^{15}N relative to the growth medium, if the $\delta^{15}N$ of the growth medium is assumed to be ∼0 ‰. A synthetic cubic face should be rough, and as such should grow by the same adhesive growth mechanism as natural cuboid faces. However, synthetic {100} faces show evidence of spiral growth, indicating that a {100} face transforms from a rough face to a smooth face in the presence of a metallic solvent (Sunagawa, 2005). This process is called surface reconstruction. It is probable that this reconstructive process is responsible for the enrichment of ^{15}N in cubic sectors of synthetic diamonds. Surface reconstruction does not occur in natural diamond growth when silicate is acting as a solvent as it only takes place in a solution in which the metallic element has a small ionic radius as the solvent (Sunagawa, 2005). As surface reconstruction does not occur in nature, it is unlikely that the subsequent isotope fractionation could occur in nature, which is consistent with the data presented here.

3.4.2 Compatibility of nitrogen in diamond

Whether nitrogen is compatible or incompatible in the diamond lattice is still unclear and has been interpreted to be both by different authors (see Section 1.2.2). The data presented here provide some evidence for a decoupling of nitrogen concentration and nitrogen isotope composition during diamond growth. Octahedral and cuboid growth sectors contain differing concentrations of nitrogen despite having been precipitated under the same P–T–X conditions. The differences between nitrogen concentrations of octahedral and cubic sectors in synthetic diamonds can be even larger than those in natural diamonds. This indicates that even at higher temperatures, diamond is not in equilibrium with the growth medium i.e. diffusion is not occurring fast enough to equilibrate the diamond and the growth medium as was suggested by Stachel and Harris (2009). This suggests that the nitrogen concentration of a diamond is unrelated to the nitrogen concentration of the growth medium. The nitrogen concentration of a diamond may be controlled kinetically, and therefore the nitrogen content of diamond is primarily a function of its growth rate,

as suggested by Cartigny et al. (2001). However, investigations of synthetic mixed habit diamonds showed that the higher nitrogen concentration was found in the slower growing sector (Burns et al., 1990; Satoh et al., 1990). Indeed, crystal growth theory also indicates that the octahedral sectors should grow more slowly than cuboid faces in natural diamonds (Sunagawa, 2005).

3.4.3 Implications for diamond formation

Both the C and N isotope ratios of these mixed habit diamonds fall well within the mean range for mantle-derived diamonds. The δ^{13}C values are at the low end of the peridotitic range (-5 ± 3 ‰; Cartigny (2005)), but are within the normal range for eclogitic diamonds. Therefore, they can be considered representative of global diamond populations, in terms of their isotopic composition.

The analysis of these natural mixed-habit diamonds has shown no evidence of large (>10 ‰) kinetic fractionations between growth sectors, unlike that which has been shown in HPHT synthetic diamonds. The difference between natural and synthetic diamonds is most likely due to differences in growth mechanism as explained above, and the fractionation is caused by processes which are unique to HPHT synthetic diamond growth. This implies it is unlikely that kinetic isotope fractionation could be responsible for the large range of δ^{15}N seen in mantle-derived diamonds. If two different growth mechanisms operating contemporaneously do not fractionate the nitrogen isotopes, it seems implausible that such fractionation could occur during the growth of diamond in more 'normal' circumstances. There is a possibility that both cuboid and octahedral sectors are affected equally by an equilibrium fractionation between diamond and the growth fluid. However, given that the octahedral growth sectors preferentially partition nitrogen, and cuboid sectors preferentially partition nickel and cobalt (Howell et al., 2013a), it is unlikley that if an isotopic fractionation were occurring, it would be completely equal between the two growth mechanisms, although it could potentially be very small (<1 ‰) and therefore

undetectable by combustion methods. Such a small equilibrium fractionation would be unable to produce large variations in δ^{15}N such as those seen in global diamond populations. This combination of evidence indicates that the δ^{15}N values measured in diamonds are dependent on the δ^{15}N composition of the source-fluid. The large range of δ^{15}N in mantle-derived diamonds can therefore be explained by isotopic heterogeneities within the source-mantle regions and/or diamond-forming fluids, which is consistent with the conclusions of Mikhail et al. (2014b).

Table 3.2: Summary of the carbon and nitogen isotope data for the five mixed-habit diamonds. The parameters $\Delta(\delta^{13}C)$, $\Delta(\delta^{15}N)$ and ΔN represent the difference in carbon isotope value, nitrogen isotope value and nitrogen content respectively, between the cuboid and octahedral growth sectors.

Sample	**Sector**	**C (mg)**	δ^{13}**C (‰)**	±	$\Delta(\delta^{13}$**C)** **(‰)**	δ^{15}**N (‰)**	±	$\Delta(\delta^{15}$**N)** **(‰)**	**N (ppm) MS**	**ΔN (ppm) MS**	**N (ppm) FTIR**	**ΔN (ppm) FTIR**
MC01	cuboid	0.08	−7.0	0.6	1.2	−0.1	0.2	1.16	1565	−430	1549	−677
	octahedral	0.04	−8.2	0.4		−1.2	0.1		1995		2226	
MC07	cuboid	0.07	−9.5	9.7	−1.4	0.4	2.9	1.14	1558	−123	1679	−623
	octahedral	0.05	−8.2	0.3		−0.8	0.1		1681		2302	
MC08	cuboid	0.21	−10.5	1.1	−0.3	0.0	1.0	0.3	1802	−533	1866	−776
	octahedral	0.24	−10.2	1.0		−0.3	0.7		2335		2642	
MC10	cuboid	0.04	−5.6	0.4	1.5	−2.4	0.2	−3.9	1192	−659	1483	−637
	octahedral	0.05	−7.1	3.8		1.5	0.1		1851		2120	
MC13	cuboid	0.19	−9.3	1.7	−1.5	−1.1	0.3	−0.1	1675	−575	1600	−600
	octahedral	0.08	−7.8	1.1		−1.0	0.3		2250		2200	

Chapter 4

Co-variation of carbon and nitrogen isotopes in diamondites

4.1 Introduction

For monocrystalline diamonds, the general relationship of large δ^{15}N variations compared with much smaller δ^{13}C variations has been well established. However, polycrystalline diamonds (e.g. diamondites) have been studied much less, and their origins are much less well-constrained (Heaney et al., 2005). The aim of this study was to analyse a suite of diamondites for their carbon and nitrogen isotopes to look at the relationships between the two, and to determine whether their origins are the same as for monocrystalline diamonds, or whether their history is entirely different.

4.2 Samples

The 15 samples analysed in this study originate from the main Orapa kimberlite in Botswana. This is the largest of 23 pipes in the Orapa cluster in northeastern Botswana

and was emplaced 93.1 Ma ago (Mikhail et al., in review). The samples were previously studied by Mikhail et al. (in review) whose data is summarised in Table C.3. All of the samples in this study contained intergrowths of silicates, with all the samples containing garnet and one with additional clinopyroxene (ORF7). The mutual intergrowth of the diamond and garnets suggest that they are syngenetic. Twelve of the samples have been determined to be of websteritic paragenesis, two are of eclogitic paragenesis (ORF7, ORF61) and one shows a mixed paragenesis (ORF53) where one garnet is lherzolitic and another is websteritic. The parageneses were determined based on the garnet discrimination diagram of Aulbach et al. (2002). The carbon isotope composition has been previously determined for all the samples with δ^{13}C values ranging from -5.3 to -22.5 ‰. Additionally, the oxygen isotopes of the garnets have been determined for seven samples, with δ^{18}O (V-SMOW) values ranging from 6.0 to 8.0 ‰ (Mikhail et al., in review). All the samples with oxygen isotope data are of websteritic paragenesis. The nitrogen composition of three samples was determined using FTIR with values ranging from 260 to 900 ppm, with relatively low nitrogen aggregation states of 14 to 36 %B (Mikhail et al., in review).

4.3 Methodology

The large diamondite crystal aggregates were broken up into individual grains. Inclusion free fragments were selected for analysis, with each fragment weighing between 0.050 mg and 0.350 mg. The samples were analysed using the FINESSE by the procedures described in Section 2.1. Each analysis used the following temperature steps:

1. 1100 ℃ pyrolysis
2. 500 ℃ combustion
3. 1100 ℃ combustion
4. repeat stage 3 until the sample has fully combusted.

The pyrolysis/combustion of each step is performed for 30 minutes. Steps 1 and 2 are used as cleaning steps to remove any surficial contaminants from the sample. In many of the experiments, only two main combustion steps were required as the sample had fully combusted after one step.

4.4 Results

The results of the carbon and isotope analyses are shown in Table C.3. Two samples, ORF897 and ORF145, are not included as they did not drop into the furnace and were lost. For discussion, the samples used in this study have been divided into two groups: those with oxygen isotope data, and those without. The δ^{15}N values have been corrected for the blank contribution, and the errors propagated accordingly. The effects of the blank correction increase with decreasing nitrogen abundance. The blank corrected values and the associated uncertainty are calculated using the following equations.

$$Mass\ of\ nitrogen\ in\ sample = \mathrm{N}_m - \mathrm{N}_b \tag{4.1}$$

where N_m is the measured nitrogen mass of the sample, and N_b is the nitrogen mass of the blank. The corrected nitrogen isotope values ($\delta^{15}\mathrm{N}_c$) are calculated using the following equation:

$$\delta^{15}\mathrm{N}_c = \frac{(\delta^{15}\mathrm{N}_m \cdot \mathrm{N}_m) - (\delta^{15}\mathrm{N}_b \cdot \mathrm{N}_b)}{\mathrm{N}_m - N_b} \tag{4.2}$$

where $\delta^{15}\mathrm{N}_m$ is the measured δ^{15}N of the sample, is the corrected δ^{15}N and $\delta^{15}\mathrm{N}_b$ is the δ^{15}N of the blank. The errors on each corrected value are calculated as follows:

$$\Delta\delta^{15}\mathrm{N}_c = \frac{1}{(\mathrm{N}_m - \mathrm{N}_b)^2} \cdot \sqrt{\Big[(1-\delta^{15}\mathrm{N}_m)^2(\Delta\mathrm{N}_m)^2 + (1-\delta^{15}\mathrm{N}_b)^2(\Delta\mathrm{N}_b)^2 + (\mathrm{N}_m - \mathrm{N}_b)^2 \cdot \Big((\Delta\mathrm{N}_m)^2(\Delta\delta^{15}\mathrm{N}_m)^2 + (\Delta\mathrm{N}_b)^2(\Delta\delta^{15}\mathrm{N}_b)^2\Big)\Big]} \tag{4.3}$$

where $\Delta\delta^{15}\mathrm{N}_m$ is the measured error in per mil, $\Delta\delta^{15}\mathrm{N}_b$ and $\Delta\mathrm{N}_b$ are the standard deviation of multiple blank analyses, and $\Delta\delta^{15}\mathrm{N}_c$ is the blank corrected precision on the δ^{15}N value.

Table 4.1: Carbon and nitrogen isotope and nitrogen concentration data for Orapa diamondites. All data are weighted mean values, and blank-corrected values where applicable. [a]Data from Mikhail et al. (in review) – N concentration measured by FTIR and $\delta^{18}\mathrm{O}_{\mathrm{garnet}}$ measured by mass spectrometry.

	δ^{13}**C**	±	δ^{15}**N**	±	**N (ppm)**	δ^{13}**C**[a]	**N (ppm)**[a]	$\delta^{18}\mathbf{O}^{a}_{\mathrm{garnet}}$
ORF9	−21.2	0.7	1.6	2.7	20	−5.3		8
ORF13	−3.5	0.2	0.6	1.4	27	−9.4	261	6
ORF20	−6.8	0.7	3.8	0.3	31	−10.7		6.7
ORF78	−11.9	0.7	1.0	0.2	550	−14.4	408	6.9
ORF114	−7.4	0.3	12.0	0.8	13	−15.7		7.6
ORF119	−21.5	0.3	3.2	0.4	24	−22.5		7.3
ORF144	−18.6	0.7	1.0	3.8	20	−19.8		7.2
ORF7	−1.7	0.7	0.9	0.1	506	−8.2	900	
ORF32	−18.5	0.7	−0.4	0.6	31	−17.9		
ORF49	−13.0	0.5	2.1	0.1	43	−16.5		
ORF53	−20.7	1.2	41.2	2.3	28	−21.9		
ORF61	−2.8	0.4	23.7	0.3	64	−5.6		
ORF?	−17.7	0.7	11.7	6.7	10	−15.6		

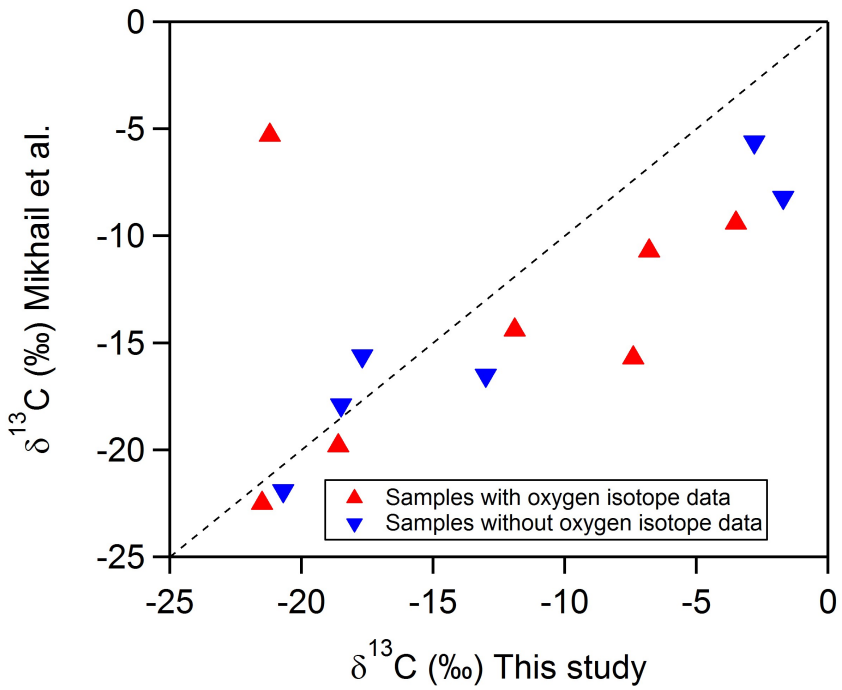

Figure 4.1: A comparison of the δ^{13}C values obtained by this study and Mikhail et al. (in review). The dashed line represents 1:1.

4.4.1 Samples with oxygen isotope data

The δ^{13}C values range from -3.5 to -21.5 ‰, which is similar to the range determined by Mikhail et al. (in review). However, two of the samples show large differences in the δ^{13}C measured by the two studies (Figure 4.1). ORF9 has a difference of 15.9 ‰ and ORF114 has a difference of 8.3 ‰. The nitrogen abundances range from 13 ppm to 550 ppm, however all but one sample (ORF78 – 550 ppm) have nitrogen abundances below 35 ppm. This is in contrast to the data from Mikhail et al. (in review) which indicated that ORF13 contained 261 ppm of nitrogen, whereas only 27 ppm was measured in this study. The data for ORF78 are similar, however, across the two studies with 408 ppm measured by Mikhail et al. (in review). The largest blank contribution in a single combustion step was 38.9 %. The blank-corrected δ^{15}N values range from 0.6 to 12.0 ‰.

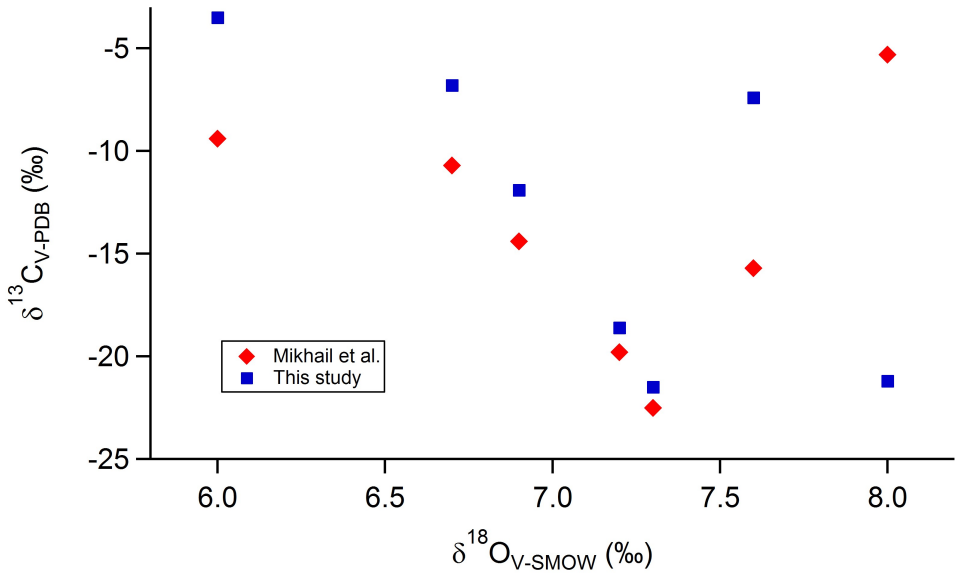

Figure 4.2: δ^{13}C vs. δ^{18}O from this study and Mikhail et al. (in review).

4.4.2 Samples without oxygen isotope data

The δ^{13}C values range from -1.7 to -20.7 ‰(Figure 4.1), which is again similar to the range determined by Mikhail et al. (in review). In this case, only one sample shows a large difference (>5 ‰) in the δ^{13}C measured by the two studies. ORF7 has a difference of 6.5 ‰. The nitrogen abundances range from 10 ppm to 506 ppm, but all but one sample (ORF7) have nitrogen abundances below 65 ppm. There is a large difference in the nitrogen abundance of ORF7 measured in this study and by Mikhail et al. (in review), who determined the nitrogen abundance to be 900 ppm. In these samples the largest blank contribution in a single step was 81.7 %. This step was therefore not included. The largest blank contribution to be included in the study was 44.5 %. The blank corrected δ^{15}N values range from -0.4 to 41.2 ‰.

4.5 Discussion

4.5.1 Relationship between δ^{13}C and δ^{18}O

These data show a clear inverse relationship (with three exceptions) for $\delta^{18}O_{garnet}$ vs. $\delta^{13}C_{diamond}$ (Figure 4.2) where progressive ^{13}C-depletion of the diamond is coupled by ^{18}O-enrichment of the syngenetic garnets. Although there are some small differences in the δ^{13}C values between the data from this study and the data from Mikhail et al. (in review), this relationship is clear in both data sets. In both cases, there are three samples which do not fit on the curve. These are also the three samples which show the largest difference between δ^{13}C values – ORF13, ORF9 and ORF114. This suggests that these two diamondites have experienced a different formation history to that of the other samples in the suite.

The large range of δ^{13}C values, particularly those which show a large ^{13}C-depletion could be explained by either high-temperature fractionation of carbon isotopes (Mikhail et al., 2014a), although this could only account for $\sim$7 ‰ variation, or by growth from fluid sourced from crustal organic carbon (Mikhail et al., in review). However, the range of δ^{18}O values cannot by explained by fractionation as stable oxygen isotope fractionation factors for mantle conditions are incredibly small (Chacko et al., 2001). Therefore, the occurrence of δ^{18}O values away from the mean mantle value for garnet ($+5.5 \pm 0.5$ ‰; Mattey et al., 1994) are best explained by subducted lithosphere which has been altered previously in a low-temperature environment (Mikhail et al., in review). The most likely source of a websteritic component with ^{13}C-depletion and ^{18}O-enrichment would be hydrothermally altered oceanic lithosphere with ^{13}C-depleted organic carbon (Mikhail et al., in review). Mixing of such a component with pristine mantle could produce the relationship shown in Figure 4.2.

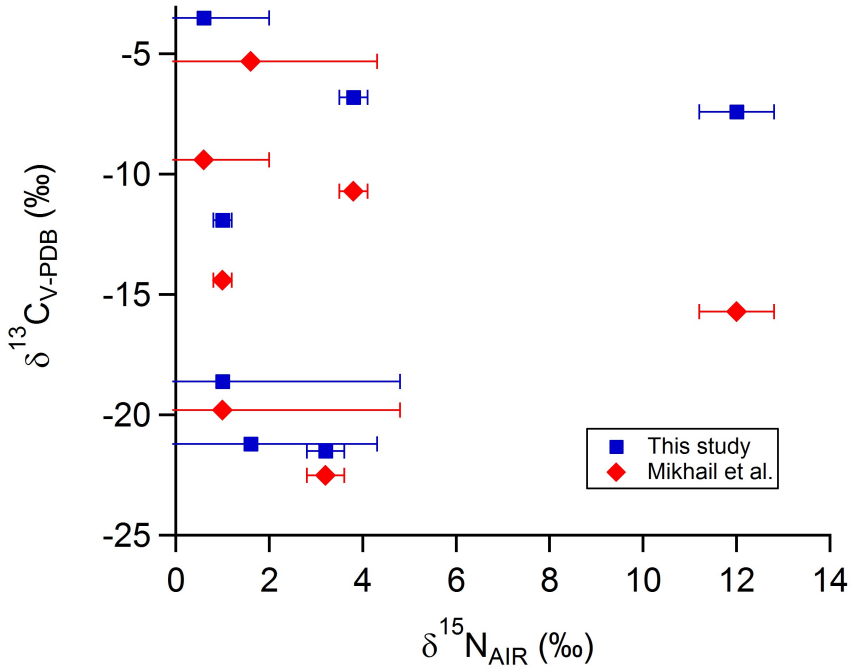

Figure 4.3: δ^{15}N vs. δ^{13}C data for samples with oxygen isotope data from this study and Mikhail et al. (in review).

4.5.2 Relationship between δ^{13}C and δ^{15}N

The δ^{15}N values for all the diamondites in this study show an enrichment in ^{15}N relative to the mean mantle (-5 ± 3 ‰). Previously studied polycrystalline diamonds from Orapa have also shown this enrichment, with δ^{15}N values between +4.5 ‰ and +15.5 ‰ (Gautheron et al., 2005). Evidence from MORB and coated diamonds indicates that the convecting mantle has a consistent δ^{15}N value of around -5 ± 3 ‰. Additionally, monocrystalline diamonds, whilst variable, have a mean value of, again, -5 ± 3 ‰ (Cartigny, 2005), suggesting that there is a relationship between these diamonds and the convecting mantle. The diamondites in this study, and those in previous studies (Gautheron et al., 2005), have almost entirely positive δ^{15}N values – a relationship which is not seen in monocrystalline diamonds from Orapa (Figure 4.4). With the absence of age data, it is impossible to say when each population formed, but it is likely that their formation occurred at different times from a different source fluid. There is only one main source of

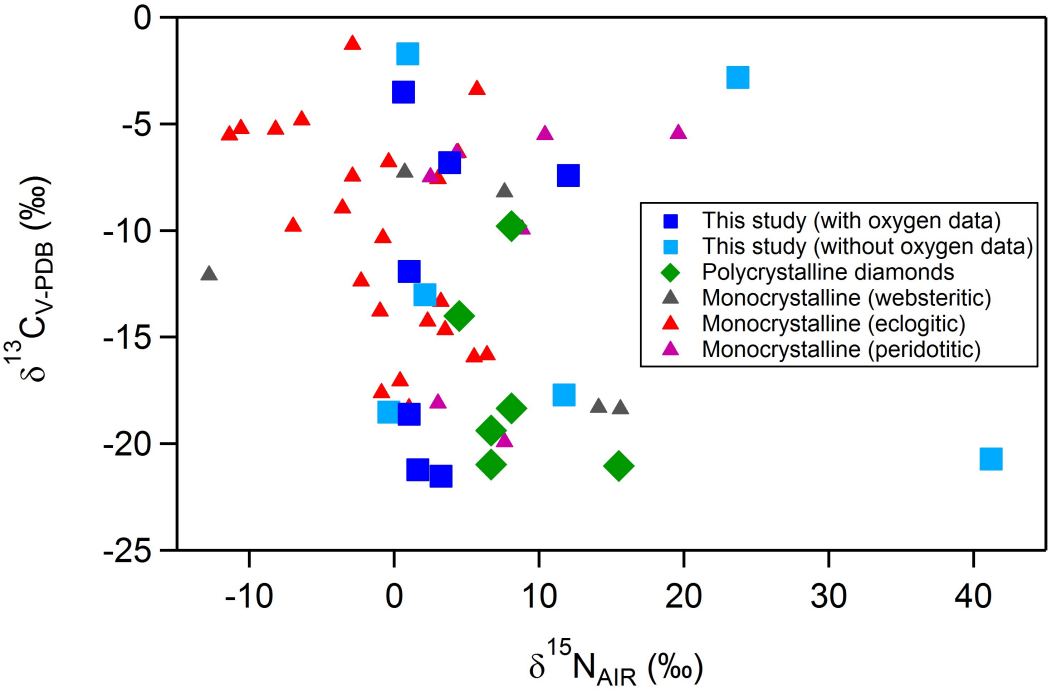

Figure 4.4: δ^{15}N vs. δ^{13}C in Orapa diamonds from this study, polycrystalline diamonds from Orapa from the literature (Gautheron et al., 2005), and monocrystalline diamonds from Orapa (Cartigny et al., 1999).

'heavy' nitrogen in the Earth system and that is surficial – i.e. sedimentary or organic. There is a well-established inbalance between 'light' nitrogen in the mantle and 'heavy' nitrogen at the surface (Javoy, 1995, 1997). Heavy nitrogen, with δ^{15}N values of up to 12 ‰, has been shown to be subducted into the mantle within sediments (Bebout and Fogel, 1992; Busigny et al., 2003) and within altered oceanic crust (Halama et al., 2010, 2012). This nitrogen is further enriched in ^{15}N by devolatilisation during metamorphism (Bebout and Fogel, 1992), however, it has been shown that significant amounts of nitrogen can be retained within the slab to depths below 100 km (Halama et al., 2012). This subducted nitrogen is believed to be the source of 'heavy' nitrogen in carbonatites sourced from the deep mantle (Dauphas and Marty, 1999).

The evidence from the δ^{18}O values of syngenetic garnets from some of the diamondites in this study, and the occurrence of ^{13}C-depletion also indicate a subduction origin. The positive correlation between δ^{18}O and δ^{15}N (Figure 4.5) also indicates that the ^{15}N-enrichment and ^{18}O-enrichment are linked to the same source. It is therefore likely that the source-fluid of the diamondites originated from subducted hydrothermally altered oceanic lithosphere with an organic carbon component. The large range of δ^{13}C values indicates a large amount of ^{13}C-depletion relative to a limited range of ^{15}N-enrichment. This could be explained by subduction in a cold slab environment (Busigny and Bebout, 2013), where organic carbon is responsible for the ^{13}C-depletion but the cold temperatures would limit the amount of devolatilisation and subsequent ^{15}N-enrichment in the downgoing slab.

4.5.3 Differences in carbon isotope values

Three of the samples in this study ORF7, ORF9 and ORF114 show large differences in δ^{13}C values (>5 ‰) between this study and the measurements by Mikhail et al. (in review). These large variations could be explained by fractionation, but it has been shown previously (see Chapter 3) that large fractionations are unlikely to occur in nature. A more likely explanation would be variations in the isotopic composition of the source fluid. To

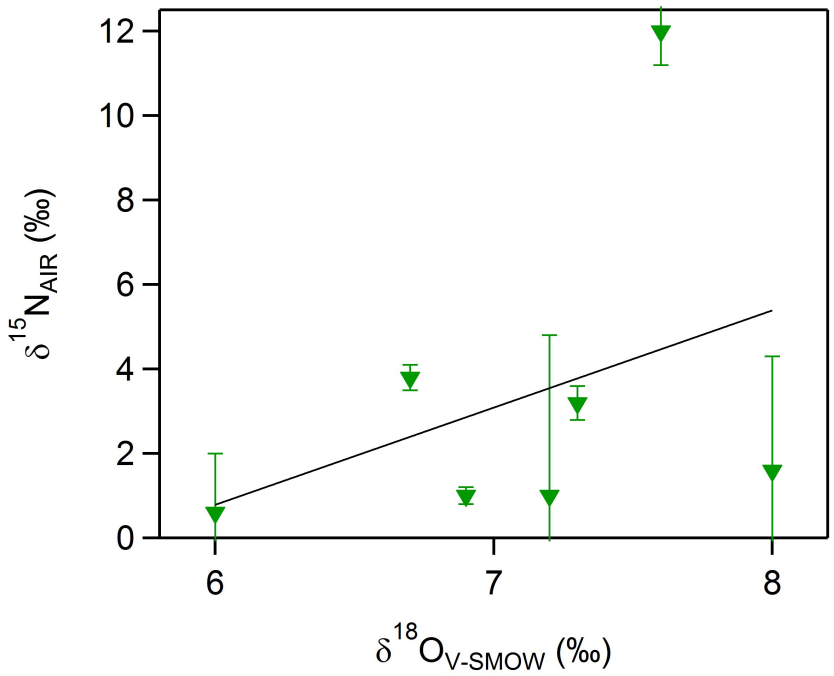

Figure 4.5: δ^{15}N vs. δ^{18}O in Orapa diamonds from this study (δ^{18}O data from Mikhail et al. (in review)).

explain variations of this scale, it is likely that these samples experienced multi-stage growth from multiple distinct fluids.

4.5.4 Origin of 'heavy' nitrogen

Three of the diamondites in this study produce δ^{15}N values significantly higher than typical values for sedimentary nitrogen (∼8 ‰), including two of the most positive δ^{15}N values recorded in terrestrial diamonds: ORF61 (23.7 ‰) and ORF53 (41.2 ‰). This large enrichment in ^{15}N could have been produced by fractionation, however, other studies have shown that this is unlikely (Chapter 3; Howell et al., 2015). It is possible that these diamondites are recording a primordial nitrogen source. Javoy (1997) proposed a model for the accretion of the Earth where the composition was predominantly enstatite chondrite, with a late veneer of carbonaceous chondrite. The nitrogen isotopic composition of carbonaceous chondrites could account for the 'heavy' nitrogen seen in these diamondites

(Kung and Clayton, 1978; Sephton et al., 2003), but this is not supported by the carbon isotope ratios. This could, however, be evidence of decoupling of the carbon and nitrogen isotope systems. Another possible source of this highly ^{15}N-enriched fluid would be high amounts of devolatilisation during subduction. However, only values of up to 12 ‰ have been recorded in metamorphic rocks (Bebout and Fogel, 1992; Busigny et al., 2003), and the nitrogen isotope data for the remaining Orapa diamondites can be best explained by only a limited amount of devolatilisation. A further explanation could be fractionation of nitrogen during core formation, where nitrogen would act as a siderophile element, so uptake of nitrogen by the core would preferentially incorporate ^{14}N and also reduce the $N_2/^{36}$Ar ratio of the mantle (Dauphas and Marty, 1999). A possible test for these theories would be to measure the noble gas isotopes of the Orapa diamondites to see if they exhibit a primordial signature.

4.6 Conclusions

The evidence from carbon, oxygen and nitrogen isotope systems indicates that diamondites from Orapa form from a fluid which is a mixture of a 'mantle-like' source with a ^{13}C-depleted, ^{15}N-and-^{18}O-enriched source. The most likely origin of this fluid is subducted oceanic lithosphere. It is also possible that there is a component of very ^{15}N-enriched primordial mantle present.

Chapter 5

Internal variations in mantle-derived diamonds

5.1 Introduction

The mean nitrogen isotope value for peridotitic diamonds is -5 ± 4 ‰ (Cartigny, 2005). However, these data are derived from bulk stable isotope determinations, which does not provide information for the internal variability of a sample. Some individual samples can show a very large range of δ^{15}N values with a comparably small range of δ^{13}C values (Figure 5.1b; Mikhail et al., 2014b), meaning that the bulk nitrogen isotope value of a given sample may not reflect all of the components that contributed to the formation of the sample. The aim of this study is to further investigate the possibility of mantle nitrogen isotope heterogeneity, using diamonds from Juina, Brazil.

Bulk stable isotope data show that diamonds from Juina have a narrow range of bulk δ^{13}C values for upper and lower mantle-derived diamonds (∼4 ‰), with a corresponding range of ∼10 ‰ for their bulk δ^{15}N values (Figure 5.1a; Kaminsky et al., 2001; Palot et al., 2012). The narrow range for both upper and lower mantle peridotitic diamonds were used

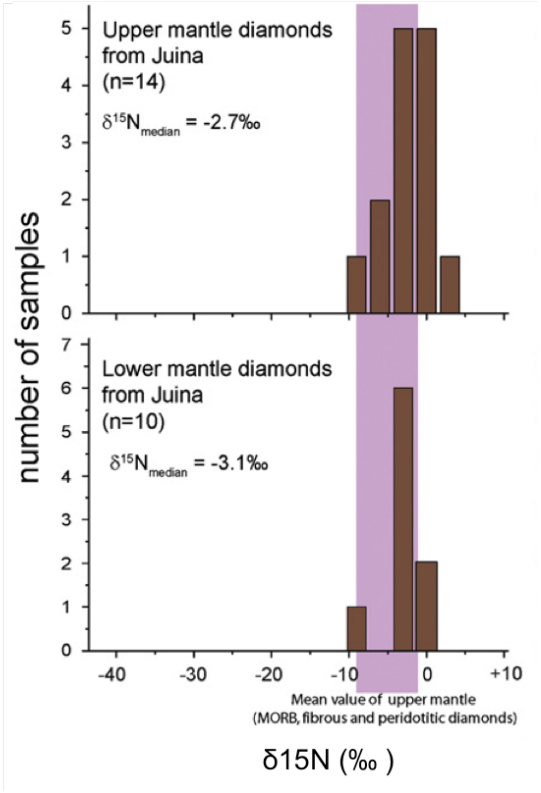

(a)

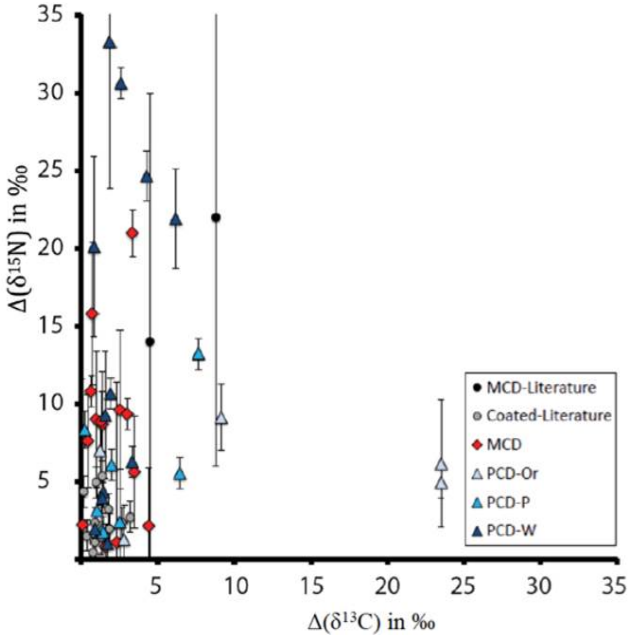

(b)

Figure 5.1: (a) bulk data for diamonds from Juina (Palot et al., 2012) show little variation in δ^{15}N for both upper and lower mantle diamonds, however, (b) shows that there can be large variations in δ^{15}N within a single sample (Mikhail et al., 2014b), which is not shown in simple bulk data.

to propose a homogeneous mantle source beneath the Amazonian craton (Brazil) produced through mixing linked to whole mantle convection (Palot et al., 2012). However, it was shown in Mikhail et al. (2014b) that δ^{15}N within an individual monocrystalline diamond from Juina can vary by up to ∼20 ‰ with a corresponding range of δ^{13}C values of <3.0 ‰. There is also evidence for large variations in δ^{13}C in diamonds from the Juina area. Zedgenizov et al. (2014) found variations in δ^{13}C of up to 15 ‰ in sublithospheric diamonds from São Luiz, corroborating the findings of previous studies of sublithospheric diamonds from the Juina area (Bulanova et al., 2010). These data cast doubts on whether or not the mantle is well-mixed with respect to nitrogen and carbon isotopes, and suggests single diamonds can be formed from multiple isotopically distinct fluid sources.

5.2 Samples and methodology

The samples used in this study are ten monocrystalline diamonds from Juina in Brazil. The pieces analysed were transparent sections laser-cut from the original samples by Dr. Dan Howell. FTIR data were obtained by Dr. Frank Brenker for five of the samples: RS01, RS14, RS51, RS55 and RS68. Of these, all are type IaB, with the exception of RS14, which is type II. Two of the diamonds, RS30 and RS68, are suggested to be of lower mantle origin. RS30 contains inclusions of ferropericlase, and RS68 contains inclusions of $CaSiO_3$, $CaTiO_3$, carbonates and olivine (see Brenker et al., 2007, for a detailed description). The remaining eight samples are of unknown paragenesis.

The δ^{13}C, δ^{15}N and N-concentrations were obtained simultaneously using the Finesse machine at the Open University (see Section 2.1). Each analysis used the following temperature steps:

1. 1100 ℃ pyrolysis
2. 500 ℃ combustion

3. 1100 ℃ combustion

4. repeat stage 3 until the sample has fully combusted.

Steps 1 and 2 are used as cleaning steps to remove any surficial contaminants from the sample. Each sample required at least two steps to fully oxidise.

5.3 Results

The data presented are both 'bulk' and 'stepped' data. Bulk data are derived from weighted mean δ^{13}C–δ^{15}N values and nitrogen concentrations for a given sample. Stepped data are individual δ^{13}C-δ^{15}N values and nitrogen concentrations released during each stage of oxidation. Bulk data reflect the average composition of the whole sample, whereas the stepped data reveal variations within the sample. The δ^{15}N values have been corrected for the blank contribution (see Chapter 4), and the errors propagated accordingly.

A summary of the data can be seen in Table 5.1 and the full dataset can be found in Table B.3. The blank corrected data show a range of δ^{15}N values from -16.4 to $+26.1$ ‰ (Figure 5.2) and there is no relationship between nitrogen concentration and δ^{15}N or δ^{13}C values, other than a grouping around the mean mantle values (Figure 5.2). Samples with > 50 % blank contributions were omitted from this study. The average blank percentage is 5.8 %, and the largest blank contribution is 23.4 %.

5.3.1 Bulk combustion data

The bulk data for the lower mantle diamonds show a range in N-concentration of 21–249 ppm (Figure 5.3). RS68 has a δ^{13}C value within normal mantle range (-5 ± 3 ‰), whereas RS30 shows a ^{13}C-enrichment of ≥ 2 ‰ relative to the mean mantle value (Figure 5.3). For both samples the bulk δ^{15}N values are within the normal mantle range

Table 5.1: Summary of the bulk data for the diamonds from Juina. $\Delta(\delta^{13}C)$ and $\Delta(\delta^{15}N)$ refer to the difference between the maximum and minimum carbon and nitrogen isotope values respectively. The stepped data can be found in Table B.3.

	Bulk δ^{13}C	±	**$\Delta(\delta^{13}C)$**	**Bulk δ^{15}N**	±	**$\Delta(\delta^{15}N)$**	±	**Bulk N ppm**	**ΔN ppm**	**ΔN ppm % of bulk**
RS01	−3.9	0.4	1.3	−5.1	0.1	1.3	0.1	545	154	28
RS14	−8.6	0.7	0.6							
RS30	−0.9	5.6	1.6	−3.5	0.4	0.3	0.4	248	176	71
RS51	−3.5	0.6	0.7	−4.9	0.5	1.4	0.4	133	80	60
RS55	−1.6	0.8	4.2	−4.4	2.9	4.6	2.8	182	69	38
RS60	−4.3	0.6	0.8	0.4	2.0	9.3	2.0	43	27	64
RS68	−3.9	0.7	2.3	−2.1	10.0	21.1	5.6	10	14	140
RS101	−3.3	3.8	0.8	−14.8	4.9			2		
RS104	−3.8	0.6	2.1	−1.6	0.9	30.5	0.8	462	674	146
RS108	−4.8	0.4	1.4	−6.1	0.1	1.3	0.1	912	213	23

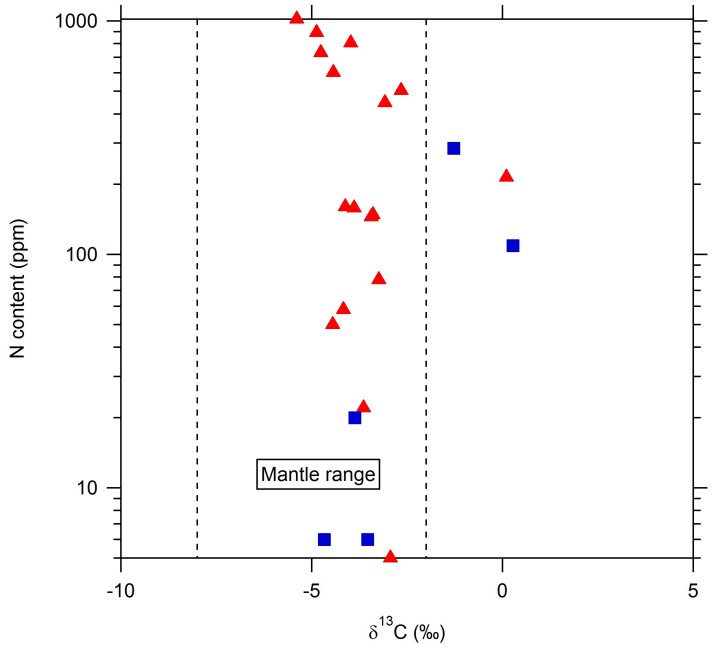

(a)

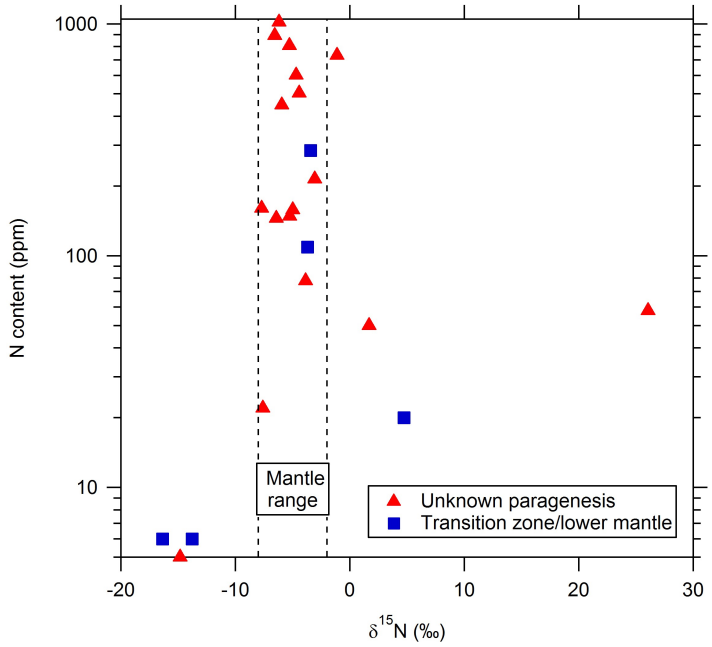

(b)

Figure 5.2: Graphs showing (a) the δ^{13}C vs. nitrogen content and (b) the δ^{15}N vs. nitrogen content for each combustion step. The regions defined by the dashed lines indicate the average mantle range.

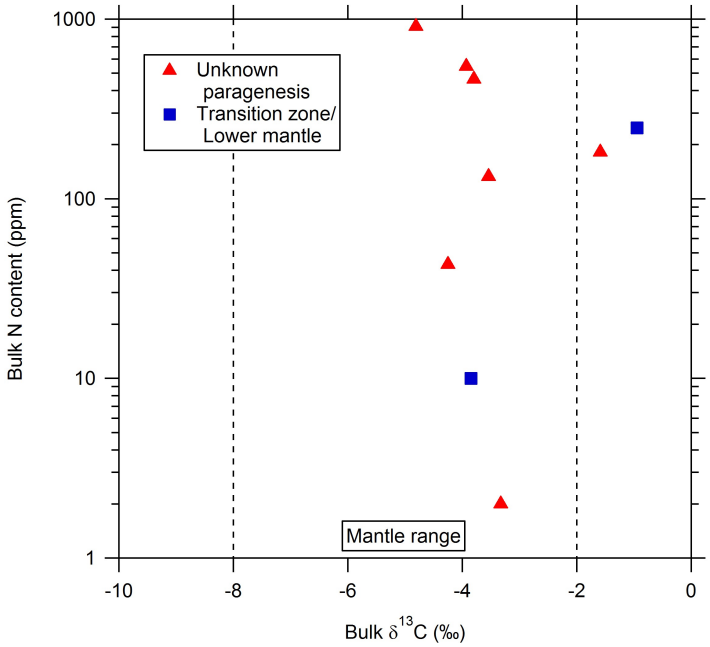

(a)

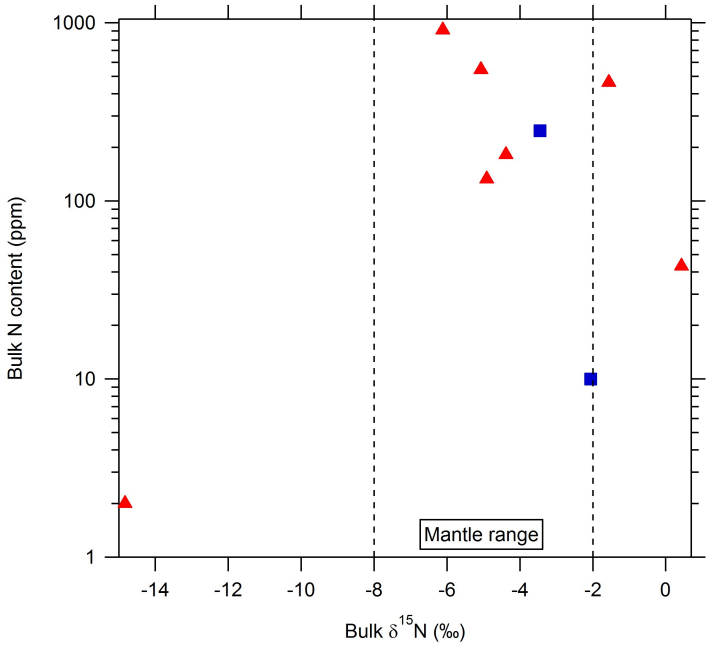

(b)

Figure 5.3: Graphs showing (a) the bulk δ^{13}C vs. bulk nitrogen content and (b) the bulk δ^{15}N vs. bulk nitrogen content for each sample. The regions defined by the dashed lines indicate the average mantle range.

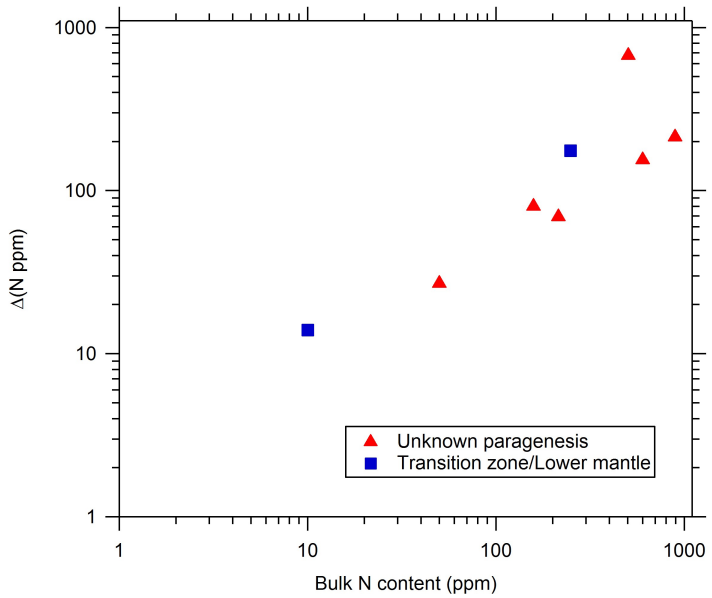

Figure 5.4: The bulk nitrogen content of each sample vs. the variation in nitrogen content within each sample.

(-5 ± 3 ‰). The bulk data for the remaining 8 samples show N-concentrations ranging from <2–914 ppm (Figure 5.3). Of these eight, all have δ^{13}C values within the normal mantle range, with the exception of RS14 that shows a ^{13}C-depletion of ≥ 1 ‰ relative to the mean mantle value (Figure 5.3). RS60 shows a ^{15}N-enrichment of ≥ 2 ‰ relative to the mean mantle value, whereas RS101 shows a ^{15}N-depletion of ≥ 12 ‰ (Figure 5.3). The remaining samples have δ^{15}N values within the normal mantle range.

5.3.2 Stepped combustion data

To express the stepwise oxidation, the parameters $\Delta(\delta^{13}\text{C})$, $\Delta(\delta^{15}\text{N})$ and Δ(N ppm) are used. These are defined as the maximum – minimum carbon and nitrogen isotope value and nitrogen concentration for an individual diamond produced by stepwise oxidation respectively. All the samples show heterogeneous nitrogen abundances. Generally, the stepped data for stable isotope values show a relationship where $\Delta(\delta^{15}\text{N}) > \Delta(\delta^{13}\text{C})$ (Figure 5.5). There are three samples that do not show this relationship, however, in all 3 cases both $\Delta(\delta^{15}\text{N})$ and $\Delta(\delta^{13}\text{C})$ are less than 2 ‰ (with minimum total uncertainties

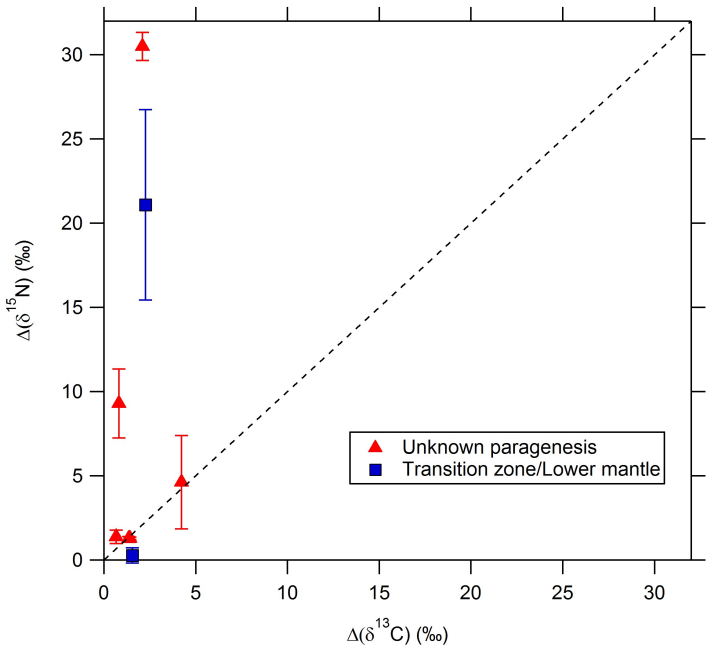

Figure 5.5: The $\Delta(\delta^{13}C)$ vs. $\Delta(\delta^{15}N)$ for each sample. The dashed line represents a 1:1 ratio. The error bars represent the blank-corrected uncertainty.

of ca. ± 1 ‰). With the exception of RS104, $\Delta(\delta^{15}N)$ shows a decrease with increasing bulk N-concentration and Δ(N ppm) (Figure 5.6). There appears to be no relationship between $\Delta(\delta^{13}C)$ and bulk N-concentration or Δ(N ppm) (Figure 5.6). There is a possible relationship between $\Delta(\delta^{15}N)$ and $\delta^{15}N$ where the samples with bulk values close to the 'mean' mantle value show the largest $\Delta(\delta^{15}N)$ (Figure 5.7). There is no correlation between $\Delta(\delta^{15}N)$ and $\delta^{13}C$, or between $\Delta(\delta^{13}C)$ and $\delta^{13}C$ or $\delta^{15}N$ (Figure 5.7).

5.4 Discussion

5.4.1 Nitrogen concentration variability

All the nitrogen-bearing samples in this study show heterogeneous nitrogen concentrations (Figure 5.4). This observation concurs with that of Mikhail et al. (2014b), however, it is not possible to identify the cause of the N/C heterogeneity from these data. Nitrogen abundance in diamonds has previously been shown to be heterogeneous (Fitzsimons

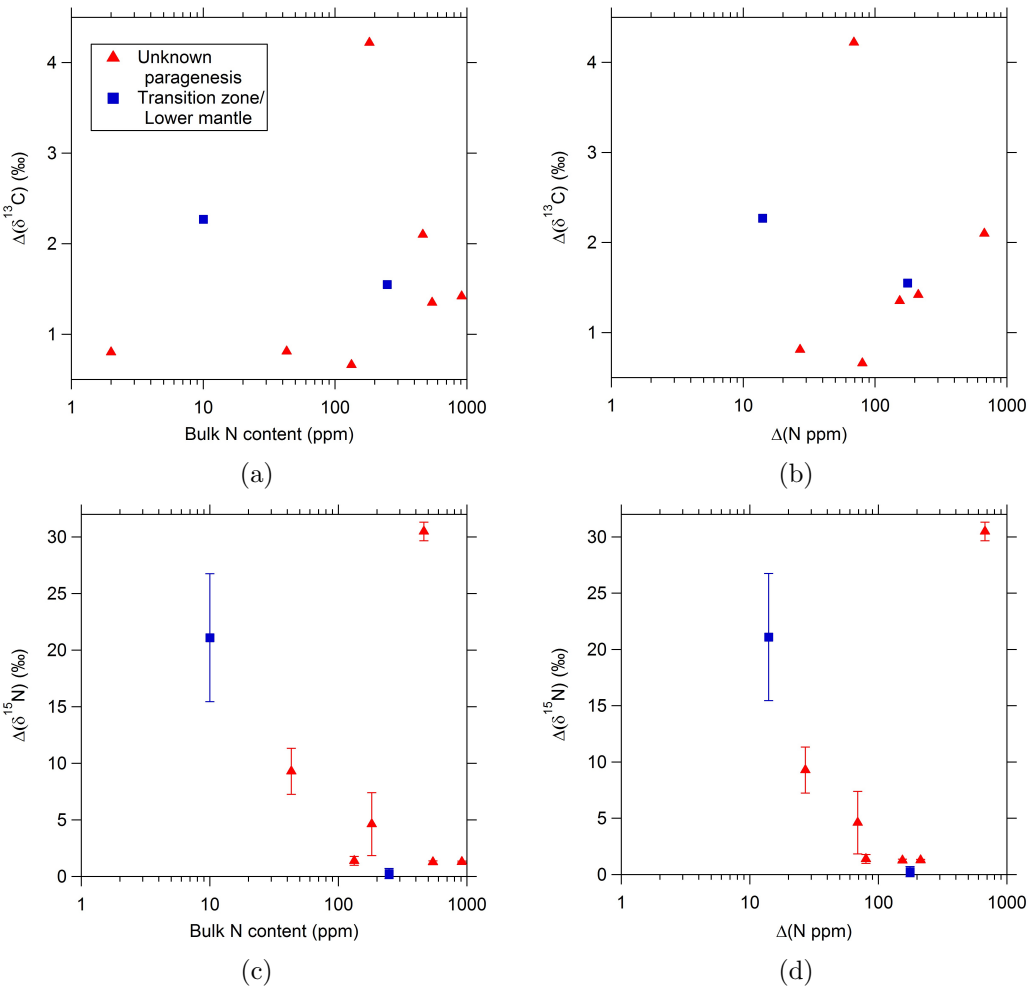

Figure 5.6: Graphs showing (a) the bulk nitrogen content vs. $\Delta(\delta^{13}\mathrm{C})$, (b) Δ(N ppm) vs. $\Delta(\delta^{13}\mathrm{C})$, (c) bulk nitrogen content vs. $\Delta(\delta^{15}\mathrm{N})$ and (d) the Δ(N ppm) vs. $\Delta(\delta^{15}\mathrm{N})$ for each sample. The error bars indicate the blank-corrected uncertainty.

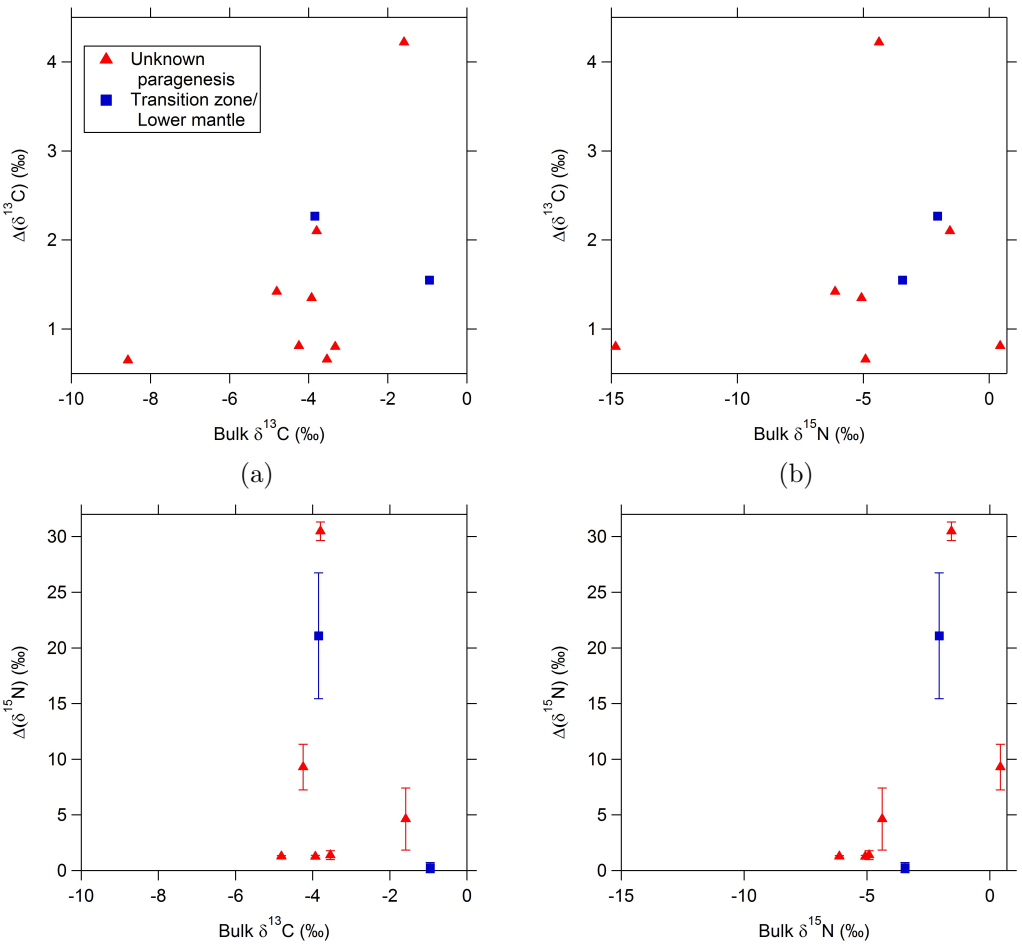

Figure 5.7: Graphs showing (a) the bulk δ^{13}C vs. $\Delta(\delta^{13}$C), (b) bulk δ^{13}C vs. $\Delta(\delta^{15}$N), (c) bulk δ^{13}C vs. $\Delta(\delta^{15}$N) and (d) the bulk δ^{15}N vs. $\Delta(\delta^{15}$N) for each sample. The error bars indicate the blank-corrected uncertainty.

et al., 1999; Harte et al., 1999; Westerlund and Gurney, 2004; Zedgenizov and Harte, 2004). In some cases, there is an observed decrease in nitrogen concentration from core to rim (Bulanova et al., 2002; Hayman et al., 2005). Other studies have shown that nitrogen abundances can vary by several hundred ppm across individual growth layers on the micron-scale, with no systematic increase or decrease from core to rim (Chen et al., 2012; Harte et al., 1999; Palot et al., 2013; Wiggers de Vries et al., 2013; Zedgenizov et al., 2014). One possible explanation is a changing nitrogen concentration in the source fluid. Alternatively, it could be due to variations in the compatibility of nitrogen due to changes in the oxygen fugacity or pH of the source fluid (Mikhail and Sverjensky, 2014).

5.4.2 Carbon and nitrogen isotope variability

The variability for nitrogen isotope values is typically larger than the variability for carbon isotope values (Figure 5.5). The majority of the samples show variations that are comparable to the standard deviation of the mean mantle δ^{13}C and δ^{15}N values ($\pm$ 3 and $\pm$ 4 ‰; Cartigny, 2005). Small variations like these can be explained by stable isotope fractionation during diamond formation in an open system (Cartigny et al., 2001; Mikhail et al., 2014b; Petts et al., in press; Thomassot et al., 2007).

Three samples show $\Delta(\delta^{15}\text{N})$ values of > 5 ‰ that cannot be explained by equilibrium stable isotope fractionation under mantle temperatures, based on the available stable isotope fractionation factors (Richet et al., 1977). These large $\Delta(\delta^{15}\text{N})$ values (up to ca. 30 ‰) could be explained by an incomplete mixing of crustal and mantle end-member components (Mikhail et al., 2014b). Another possible explanation for the large variations is kinetic isotope fractionation during diamond formation. Boyd et al. (1988) and Reutsky et al. (2008b) both found a large kinetic fractionation of nitrogen isotopes of up to 40 ‰ between cubic and octahedral growth sectors in synthetic diamonds. They also show a large difference in N-concentration between the growth sectors. Unlike in Mikhail et al. (2014b), some of the data presented in this thesis show a relationship between Δ(N

ppm) and $\Delta(\delta^{15}N)$ which could indicate the occurrence of kinetic isotope fractionation (Figure 5.6d). Studies on natural mixed-habit diamonds have shown that this effect is unlikely to occur in natural diamonds (Chapter 3), but based on these data alone, kinetic nitrogen isotope fractionation cannot be ruled out.

The possible relationship between $\Delta(\delta^{15}N)$ and $\delta^{15}N$, where the samples with 'average' bulk values show the largest $\Delta(\delta^{15}N)$ (Figure 5.7d), could be due to a homogenisation of more extreme values from multiple fluid sources. The extreme values recorded by stepwise oxidation are mixed to produce a 'mean mantle' signature. This could mean that the 'mean mantle' value simply represents a mixing of a number of different components.

5.4.3 Comparison between upper and lower mantle diamonds

The bulk $\delta^{15}N$ values for both lower mantle diamonds in this study are within the normal mantle range. However, RS68 (LM) shows the second largest $\Delta(\delta^{15}N)$ of all the samples in this study (21.1 ‰; Figure 5.8). Although none of the samples from this study have been determined to be of upper mantle origin, examples from Mikhail et al. (2014b) (Figure 5.8) show that upper mantle diamonds from Juina can have $\Delta(\delta^{15}N)$ values in the region of 15–20 ‰ (Table C.4). The occurrence of such large variations in both upper and lower mantle diamonds suggests that the mantle is not well-mixed with respect to nitrogen isotopes, but more work is required to affirm how consistent this observation is. Interestingly, the negative $\delta^{15}N$ components in RS68 (LM) are significantly more negative than the negative $\delta^{15}N$ components of BZ270 (P-type), J-17 (E-type) and J-19 (E-type) from Mikhail et al. (2014b) (Figure 5.8). The upper mantle diamonds contain negative $\delta^{15}N$ similar to that of the mean mantle from -4.9 to -2.5 ‰, whereas the lower mantle diamond contains $\delta^{15}N$ of -16.4 to -13.8 ‰. This could indicate the existence of a primordial heterogeneity between the upper and lower mantle (Cartigny et al., 1997; Palot et al., 2012).

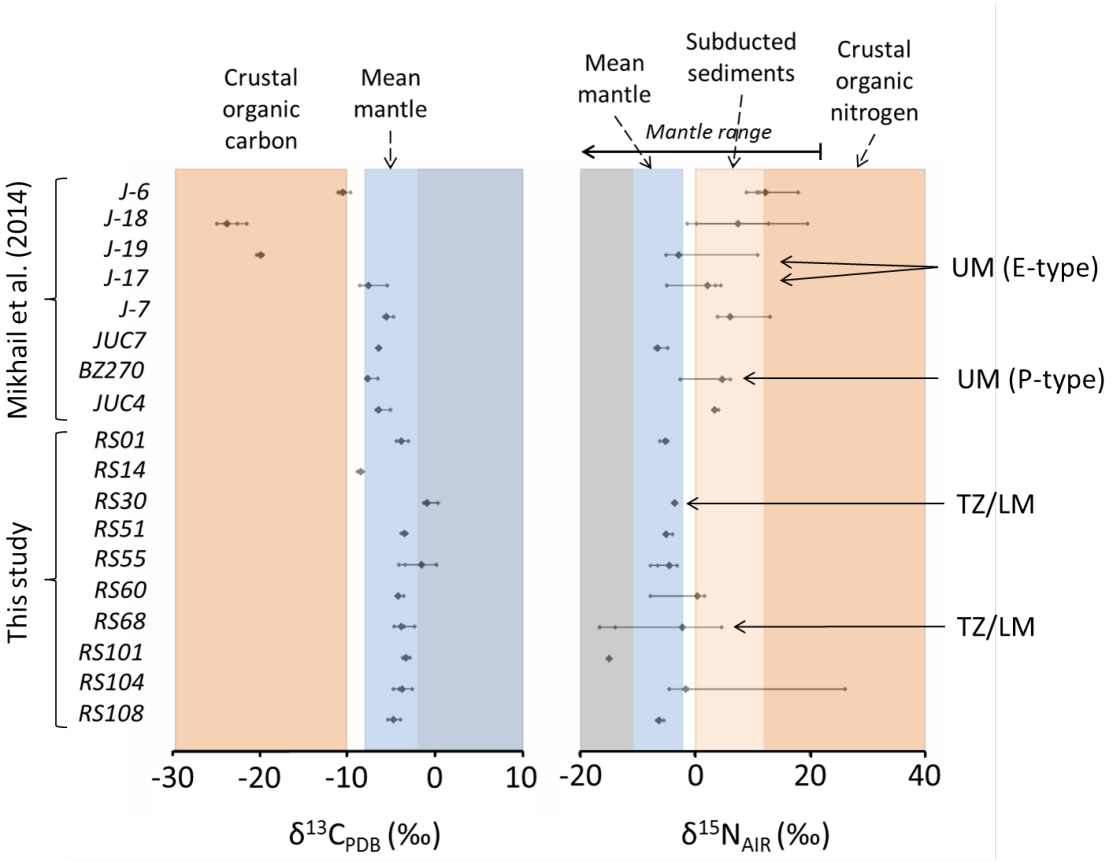

Figure 5.8: The range of carbon (left) and nitrogen (right) isotopes for the diamonds in this study, compared with diamonds from Juina analysed previously (Mikhail et al., 2014b). The orange areas represent the region occupied by crustal materials (Thomazo et al., 2009), and the blue areas represent the region occupied by mantle values (Cartigny, 2005). The large symbols represent the bulk figure for each sample, whereas the small symbols represent the values recorded at each stage of combustion.

5.4.4 Implications for the origin of diamond-forming volatiles beneath the Amazonian craton

Of the three samples with $\Delta(\delta^{15}N)$ values of > 5 ‰, all contain both positive and negative $\delta^{15}N$ components. This suggests that there is both a mantle and crustal influence in diamond-forming fluids beneath the Amazonian craton. In particular, RS104 was found to contain a $\delta^{15}N$ component of +26.06 ‰ (Figure 5.8), strongly indicating the presence of subducted metasedimentary nitrogen (Thomazo et al., 2009). Although this value is higher than what might be expected for subducted sediments (ca. 6 ‰), devolatilisation during subduction would enrich the remaining nitrogen in ^{15}N and decrease the abundance, resulting in the values seen in RS104 (Haendel et al., 1986; Palot et al., 2014). However, the bulk $\delta^{13}C$ and $\delta^{15}N$ values of −3.80 ‰ and −1.56 ‰ respectively, could easily be misinterpreted as being of mantle origin alone. In addition to the isotopically light nitrogen discussed in Section 5.4.3, RS68 also contains a significant proportion of heavy nitrogen – $\delta^{15}N$ of +4.7 ‰. This suggests there was a crustal component in the diamond-forming fluid. The $\delta^{13}C$ value of this component, −3.9 ‰, suggests the most likely source would be subducted carbonate. This supports the conclusions of Brenker et al. (2007) who suggested the coexistence of $CaSiO_3$-walstromite and olivine with syngenetic calcite inclusions in RS68 meant that the carbonate was incorporated into the diamond in the lowermost part of the transition zone (> 580 km depth), or even the lower mantle. Further evidence of a crustal origin for diamond-forming carbon has been shown in diamonds from Juina (Bulanova et al., 2010; Mikhail et al., 2014b; Zedgenizov et al., 2014). These studies presented diamonds with low $\delta^{13}C$ values typical of biogenic carbon, ca. −25 ‰. Bulanova et al. (2010) found that the low $\delta^{13}C$ values were associated with diamonds containing inclusions of a subducted oceanic sediment origin, and Mikhail et al. (2014b) showed that the low $\delta^{13}C$ values were accompanied by significant positive $\delta^{15}N$ components. Additionally, the trace element signature of a number of type II ultra-deep diamonds from Juina indicate that the fluid-source is a low-degree partial melt of subducted, carbonated oceanic crust, which produces trace element rich carbonatitic melts

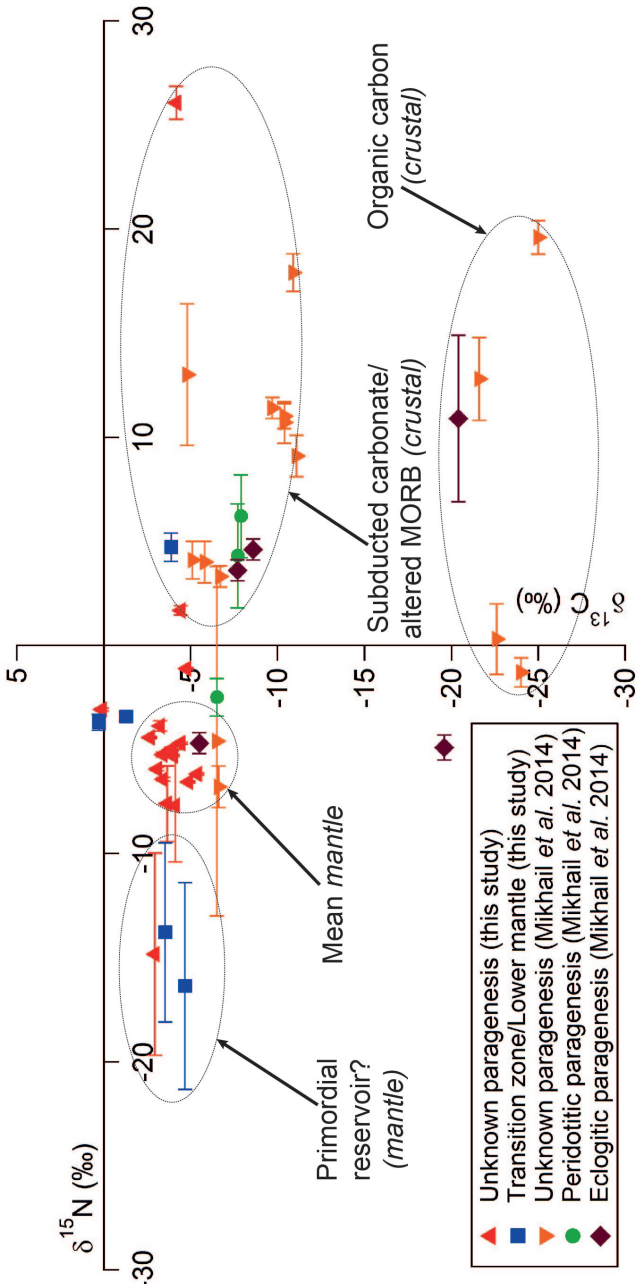

Figure 5.9: The stepped $\delta^{13}C$ vs. $\delta^{15}N$ for analyses from this study in addition to data from Juina published by Mikhail et al. (2014b). The error bars represent the blank-corrected uncertainty.

(Walter et al., 2008). All this evidence strongly suggests there is a significant contribution from subducted carbon involved in diamond-formation beneath the Amazonian craton.

The data from the 10 samples in this study, together with the 8 samples from Juina studied by Mikhail et al. (2014b), suggest that there may at least four isotopically distinct sources of diamond-forming fluid (Figure 5.9) recorded by diamonds from beneath the Amazonian craton. These are:

1. an average mantle carbon (ca. -5 ‰) and isotopically light nitrogen (ca. -15 ‰) mantle source (eg. RS68) which could represent a primordial reservoir;
2. an average mantle carbon and average mantle nitrogen (ca. -5 ‰) mantle source (eg. RS01, RS51, RS104);
3. a subducted oceanic crust source containing carbonate and/or altered MORB (δ^{13}C > -10 ‰, δ^{15}N > 0 ‰; eg. RS68, RS104, and JUC4, J-7 (Mikhail et al., 2014b));
4. and an organic carbon source (δ^{13}C < -10 ‰, δ^{15}N > 0 ‰; eg. J-19, J-18, J-6 (Mikhail et al., 2014b)).

The evidence of multiple fluids within single diamonds suggests a multistage growth history for this diamond population.

5.5 Conclusions

The δ^{13}C, δ^{15}N and nitrogen contents from 10 monocrystalline Juina diamonds have been determined using stepwise oxidation. The variation of δ^{15}N is typically larger than the variation of δ^{13}C within a single diamond, and some individual samples show a large range of nitrogen isotope values that cannot be explained by equilibrium fractionation. Both kinetic isotope fraction, and mantle heterogeneity can be invoked to explain the data shown here. The large variations for δ^{15}N within single diamonds have now been shown to

occur in both upper and lower mantle diamonds, suggesting that mantle heterogeneities exist throughout the sampled mantle.

Chapter 6

Experimental determination of equilibrium nitrogen isotope fractionation

6.1 Nitrogen isotope fractionation between diamond and carbonate

Carbon isotope fractionation has been shown to occur in diamond synthesis experiments using a metal solvent (Mikhail et al., 2014a; Reutsky et al., 2008a). However, there has been little work on carbon isotopes using a carbonate catalyst and the behaviour of nitrogen isotopes during diamond synthesis. Magnesite ($MgCO_3$) was chosen as the catalyst for my experiments due to its carbon release peak of 500–600°C which is sufficiently different to that of diamond (Figure 6.1). However, magnesite does not behave as a typical solvent catalyst (Sato et al., 1999; Taniguchi et al., 1996; Utsumi et al., 2004). At 7.7 GPa spontaneous nucleation of diamond was achieved when the magnesite was in the molten state (above 2100°C) (Akaishi et al., 1990; Sato et al., 1999), however, at 9.5 GPa, diamond

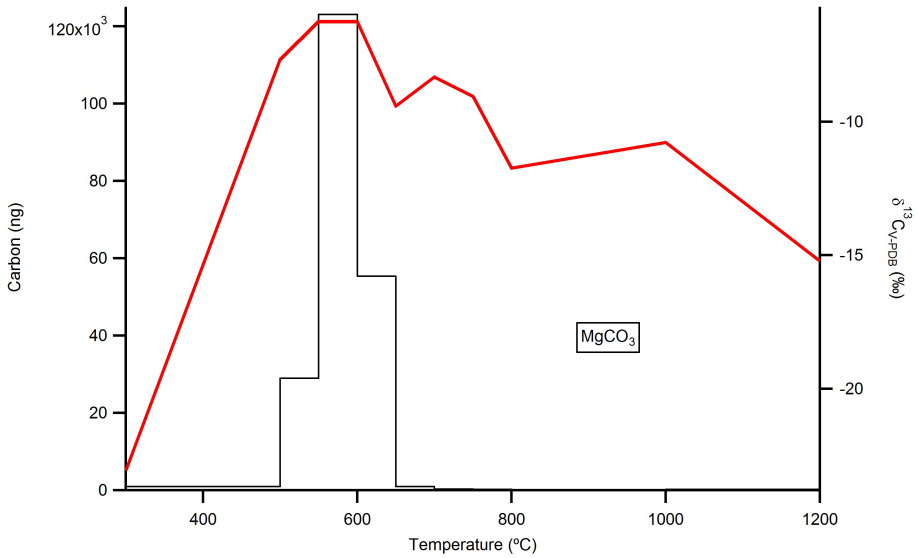

Figure 6.1: Step plot showing the carbon release (the histogram shows carbon abundance corresponding to the left-hand y-axis) during combustion of $MgCO_3$ and the $\delta^{13}C$ of each step (red line corresponding to the right-hand y-axis).

can be formed at 1600–1800℃, considerably below the melting temperature of magnesite at this pressure (Taniguchi et al., 1996; Utsumi et al., 2004). It was suggested in Utsumi et al. (2004) that a partial decomposition of $MgCO_3$ releasing CO_2 could catalyse the graphite–diamond transition. Potentially, this could be tested by determining the isotopic composition of the carbonate and graphite/diamond. It was concluded in Taniguchi et al. (1996) that there was no isotopic exchange of carbon between the carbonate catalyst and the carbon-source; however, only the final diamond compositions were analysed in this case. The aim of my experiments is to synthesise diamond from graphite using magnesite as a catalyst to investigate whether there is carbon isotope exchange and nitrogen isotope fractionation between the carbonate catalyst and diamond.

6.1.1 Methodology

The experiments were performed at the Bayerisches Geoinstitüt, Bayreuth, Germany. They were performed in a 1200-ton multi-anvil press using a 10/5 cell. The furnace was machined from lanthanum chromate and the capsule material used was rhenium foil. The

capsule was packed with a 50:50 by volume mix of graphite and natural New South Wales magnesite. The initial carbon isotopic composition of the graphite was −22.9 ‰ and the initial carbon isotopic composition of the magnesite was −6.4 ‰. Both materials contained blank-level amounts of nitrogen. One experiment was performed at an equivalent pressure of 10 GPa and 1800℃ and a second experiment was performed at 19 GPa and 2000℃.

6.1.2 Results

6.1.2.1 MgC001

This experiment was performed at 10 GPa and 1800℃. The products were analysed using X-ray Diffraction and were found to contain $MgCO_3$ and diamond. The sample was imaged using an SEM. The irregular texture of the carbonate indicates that it has not recrystallised and therefore remained in the solid state throughout the experiment. This means that it did not behave as a typical solvent catalyst for the transformation of graphite to diamond.

The carbon and nitrogen isotopes were analysed using stepwise combustion on the Finesse. The steps below 600℃ are used to remove contamination from the sample and do not need to be considered. The combustion profile (Figure 6.2) shows that a significant amount of nitrogen has been incorporated into both the carbonate and diamond. Interestingly, the carbonate contains more nitrogen than the diamond – 223 ppm and 153 ppm respectively. In both cases, the starting materials contained only blank-level nitrogen once contamination had been removed, meaning that the only source of nitrogen in these experiments was the atmosphere. The δ^{13}C value of the carbonate has reduced from −6.4 ‰ to −21.6 ‰, whereas the δ^{13}C value of the diamond has shown no change (within error) from its original −22.9 ‰ value (as graphite). The δ^{15}N value of the carbonate is 2.8 ‰ and the δ^{15}N value of the diamond is 5.0 ‰.

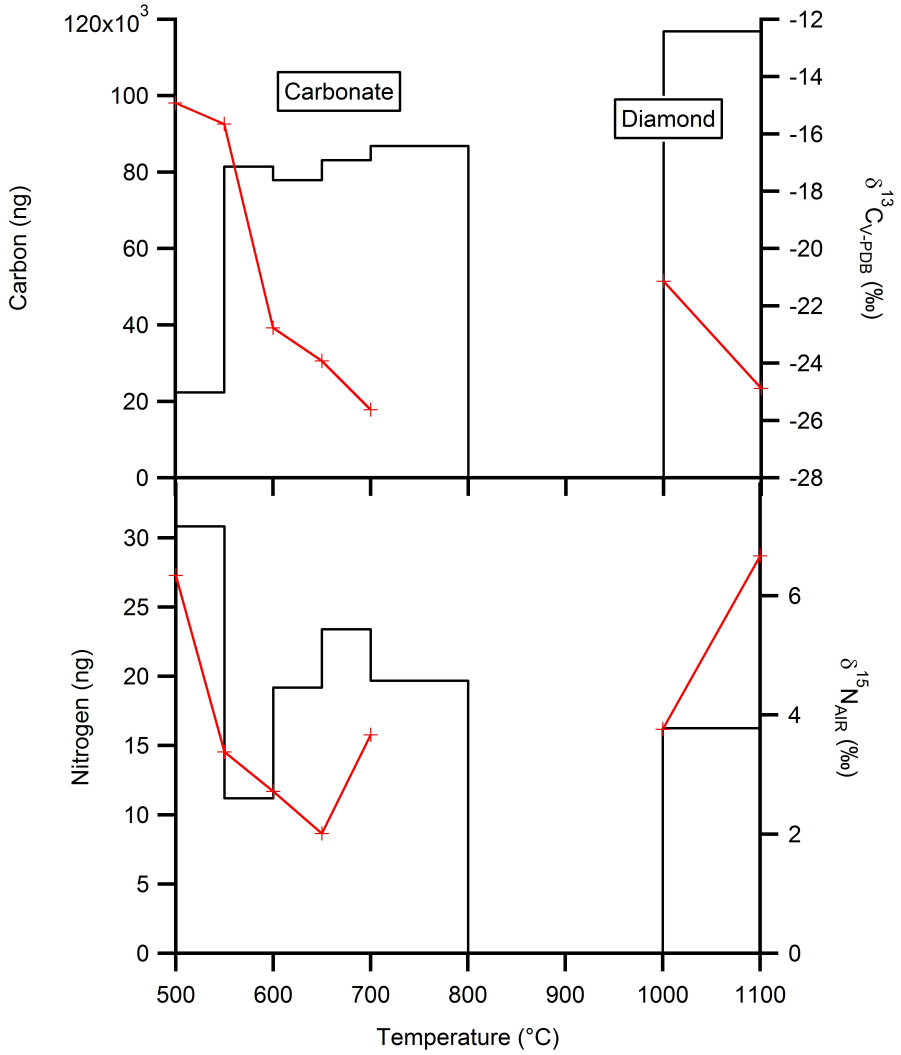

Figure 6.2: Step plots of the combustion of carbon and nitrogen for MgC001. The red line shows the δ^{13}C and δ^{15}N of the sample respectively (right-hand y-axis) and the black line shows carbon/nitrogen abundance (left-hand y-axis).

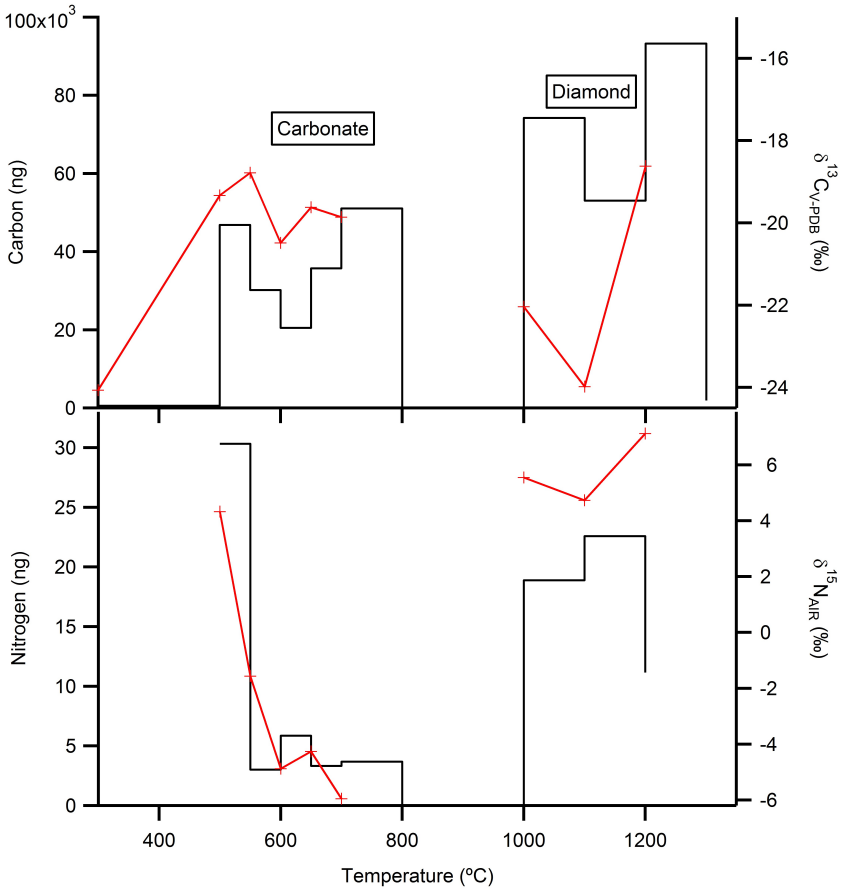

Figure 6.3: Step plots of the combustion of carbon and nitrogen for MgC002. The red line shows the δ^{13}C and δ^{15}N of the sample respectively (right-hand y-axis) and the black line shows carbon/nitrogen abundance (left-hand y-axis).

6.1.2.2 MgC002

This experiment was performed at 19 GPa and 2000°C. The products were analysed using X-ray Diffraction and were found to contain $MgCO_3$ and diamond. The sample was imaged using an SEM. Like MgC001 the irregular texture of the $MgCO_3$, indicates that the carbonate has not recrystallised. Again, this means that the magnesite catalysed the graphite to diamond transformation from the solid state.

The carbon and nitrogen isotopes were analysed using stepwise combustion on the Finesse. The steps below 600 °C are used to remove contamination from the sample and do not need

to be considered. The combustion profile of MgC002 (Figure 6.3) shows that a significant amount of nitrogen has been incorporated into both the carbonate and the graphite. The carbonate contains an average of 20 ppm of nitrogen and the diamond contains an average of 270 ppm of nitrogen. In contrast to MgC001, the diamond conatins the greater amount of nitrogen. In both cases, the starting materials contained only blank-level nitrogen once contamination had been removed. The δ^{13}C value of the carbonate has reduced from −6.4 ‰ to −19.7 ‰, whereas the δ^{13}C value of the diamond has increased from −22.9 ‰ (as graphite) to −21.1 ‰. The δ^{15}N value of the carbonate is −4.4 ‰ and the δ^{15}N value of the diamond is 5.5 ‰.

6.1.3 Discussion

6.1.3.1 Carbon isotope exchange

Both MgC001 and MgC002 show clear evidence for the exchange of carbon isotopes during the growth of the diamond crystals, with former showing almost complete equilibration of the carbon isotopes between the carbonate and the diamond. This shows that there is considerable interaction between the carbonate catalyst and the graphite/diamond during the diamond synthesis.

6.1.3.2 Nitrogen isotope fractionation

Both samples show evidence of fractionation of nitrogen isotopes between carbonate and diamond. In MgC001, the fractionation is small (∼2 ‰), and may be negligible when the error on each measurement is taken into consideration. However, MgC002 shows a large fractionation of ∼10 ‰ between carbonate and diamond.

6.1.3.3 Effects of pressure and temperature

MgC002, the higher PT sample, contains carbonate with considerably less nitrogen than in MgC001, with the nitrogen preferentially partitioning into the diamond. However, in MgC001 the fractionation of nitrogen isotopes is only ∼2 ‰, whereas in MgC002 the fractionation of nitrogen isotopes is ∼10 ‰. This could be due to the effect of the preferential partitioning of nitrogen into diamond at the higher pressure and temperature conditions. However, this may not be the case as the δ^{15}N of the diamond is consistent across both samples, whereas the carbonate is ^{15}N-depleted in MgC002 relative to MgC001. Given that in both experiments, $MgCO_3$ contained a considerable amount of nitrogen, including up to 40 ppm of nitrogen at conditions approaching those of the transition zone, this could be evidence for $MgCO_3$ as an important host for nitrogen in the mantle where carbonate is the stable host of carbon.

6.2 Nitrogen isotope fractionation between graphite and titanium nitride

The results for the experiments involving diamond are interesting, however they do not represent an equilibrium situation. To find the equilibrium fractionation a new approach is needed. The aim of these experiments was to isotopically equilibrate $^{15}N/^{14}N$ between graphite–osbornite (TiN). Graphite was chosen for these experiments instead of diamond because nitrogen diffusion in diamond is too slow to allow experimental studies to obtain isotopic equilibrium (Koga et al., 2003). These experiments may also provide answers to additional problems. The effects that the formation of the Earth's core could have had on the $^{15}N/^{14}N$ composition of the bulk silicate Earth are unclear. Also unclear is the isotopic effect a metal saturated present day mantle could have on the stable isotopes of nitrogen during deep diamond formation. Nitrogen can behave as a siderophile and may have been partitioned into the Earth's core during differentiation. Exploring what effect

Table 6.1: Summary of piston cylinder experiments.

Name	**Starting Materials**	**Pressure (GPa)**	**Temp. (℃)**	**Duration (hrs)**
GTN001	TiN + Graphite	1	1200	1
GTN002	TiN + Graphite	1	1200	75
GTN003	TiN + Graphite	1	1200	24
GTN004	TiN + Graphite	1	1200	48
GTN005	TiN + Graphite	1	1200	6

this may have had on the isotopic ratios may lead to an understanding of the origin of the isotopic inbalance between the Earth's surface reservoirs and the mantle.

6.2.1 Methodology

The starting materials were prepared in a 1:1 molar ratio, therefore 1.2011 g of graphite powder and 6.1887 g of titanium nitride powder were weighed out and mixed in a pestle and mortar under isopropanol for 30 minutes. The mixture was dried, and then packed into the experimental capsule. In these experiments, a double capsule was used. The inner capsule consisted of MgO and the outer capsule was machined from iron metal. During the experiment the Fe and MgO react, keeping the environment within the capsule reducing, and allowing measurement of the oxygen fugacity through the production of FeO. The experiments were performed in two stages. The aim of the first stage was to determine the duration of experiment needed to reach equilibrium. These experiments were performed in the piston cylinder press at UCL at a pressure of 1 GPa and a temperature of 1200℃ for durations of up to 75 hours (Table 6.1).

6.2.2 Results

6.2.2.1 Combustion and isotopic composition of the starting materials

Graphite and TiN were shown to have different combustion temperatures when analysed separately (Figure 6.4a). The main release for graphite is at 850℃ to 900℃, whereas the main release for titanium nitride is at 700℃ to 800℃. The δ^{13}C of the graphite powder is -23.9 ‰ and the δ^{15}N of the titanium nitride is -3.0 ‰. However, when the starting mixture of TiN and graphite is analysed, the main release peaks are shifted towards the same temperature (Figure 6.4b), indicating that there may be some interaction between TiN and graphite during the combustion process. In this case, the main release for TiN is at 750℃, and the main release for graphite is at 800℃, but with a considerable proportion of carbon combusting at 750℃, and therefore overlapping with the nitride release. The isotope ratios of the mixture are comparable with the isotope ratios of the separated starting materials, with a δ^{13}C of -22.7 ‰ for the graphite and a δ^{15}N of -2.2 ‰ for the titanium nitride.

6.2.2.2 Combustion results

The results from the combustion of the experimental products were inconclusive. GTN001 (Figure 6.5a) shows a single release peak for carbon at 800℃, and a double release peak for nitrogen at 800℃ and at 1000–1200℃. GTN003 and GTN004 (Figure 6.5b) produced very similar combustion profiles, with a single release peak for carbon and nitrogen both at 800℃. In all the experiments, there is some variation in the isotope values, but it is impossible to distinguish between the graphite and nitride, to determine whether any transfer of nitrogen or carbon has taken place.

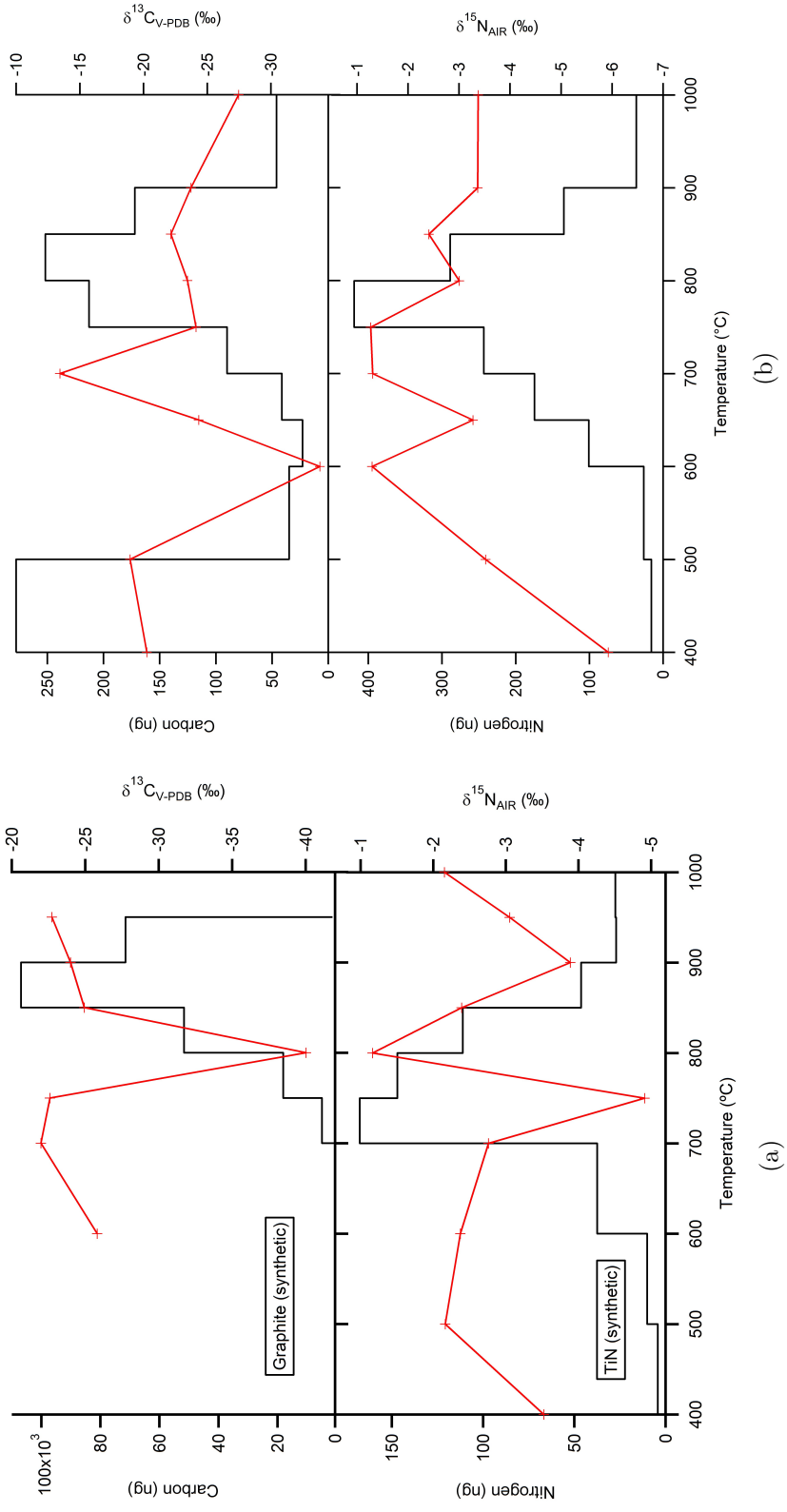

Figure 6.4: Step plots of carbon from graphite and nitrogen from TiN run as (a) separate powders, and (b) a mixture in a 1:1 molar ratio. The red line shows the δ^{13}C and δ^{15}N of the samples respectively (right-hand y-axis) and the black line shows carbon/nitrogen abundance (left-hand y-axis).

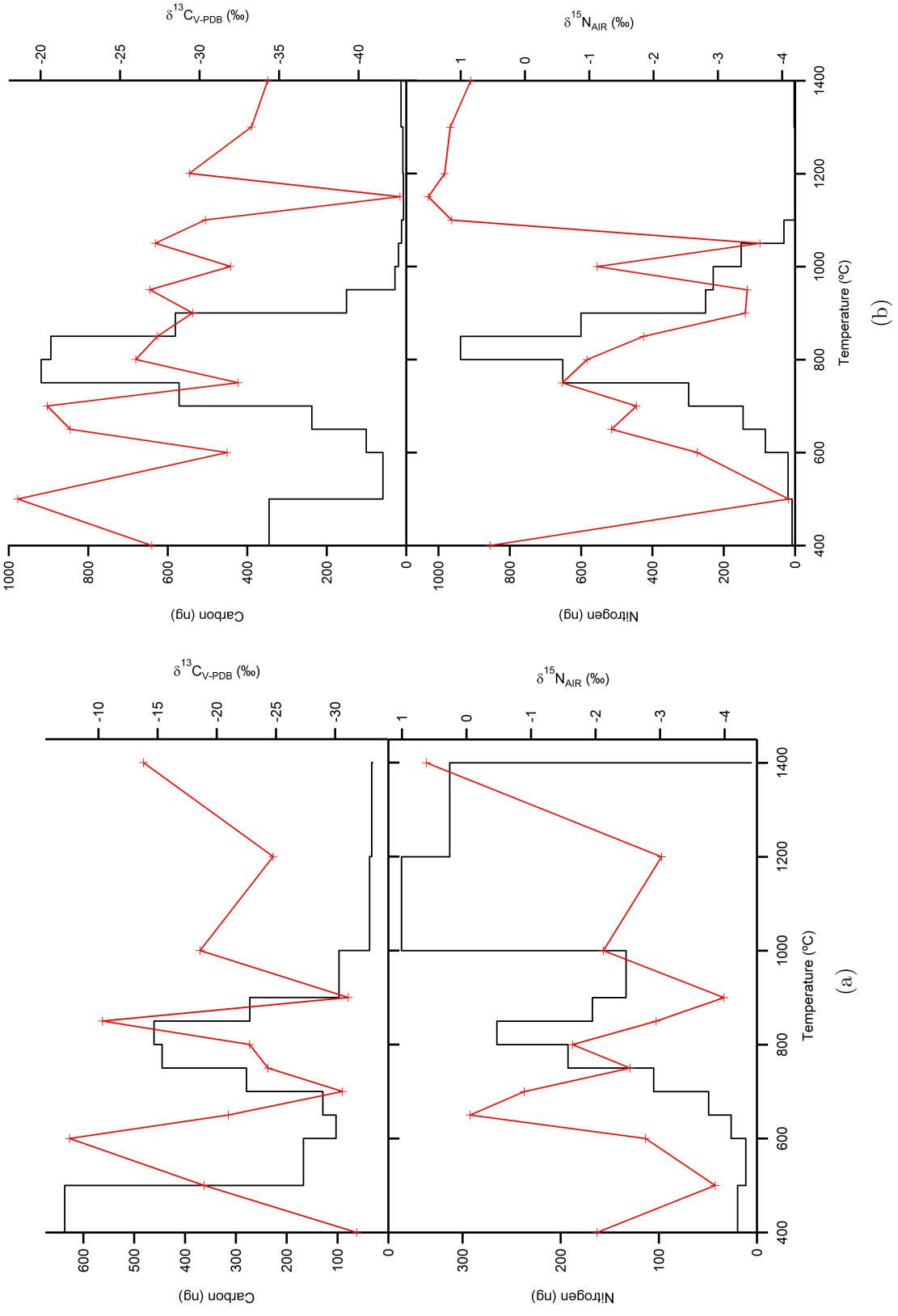

Figure 6.5: Step plots of carbon and nitrogen from (a) GTN001 and (b) GTN004. The red line shows the δ^{13}C and δ^{15}N of the samples respectively (right-hand y-axis) and the black line shows carbon/nitrogen abundance (left-hand y-axis).

6.2.3 Discussion

Previous studies have shown that artificial and natural osbornite combusts at temperatures above 800℃ and often as high as 1200℃ (Grady et al., 1986). However, in this case, the pure TiN starting material combusted at a much lower temperature with the main release at 700℃. This is possibly due to the structure of the TiN, which may be amorphous as opposed to the osbornite structure. The large second release peak for nitrogen at 1000–1200℃ in GTN001 (Figure 6.5a) could represent nitrogen bound in the osbornite structure. However, if the smaller peak were to represent nitrogen bound in graphite, this would require the graphite to contain ∼50% nitrogen, which is unrealistic. It could represent an incomplete phase change, with some of the original TiN remaining, as the experiment was only run for 1 hour. This does not appear to be the case, however, when the longer duration experiments are considered. GTN004 (Figure 6.5b) was run for 48 hours, and there is no evidence of a second, high temperature release of nitrogen to correspond to a phase change to osbornite. XRD analysis of all the run products showed only graphite and TiN, meaning there is no evidence of a reaction forming a third product which could account for the large high temperature nitrogen release seen in GTN001. However, the interaction of the graphite and TiN during combustion seems to have the effect of equalising the combustion temperature of the two phases. Unfortunately, step combustion proved to be the wrong technique to analyse the products.

Chapter 7

Conclusions

7.1 Nitrogen isotope fractionation

The aim of this thesis was to determine the origins of the large variation in nitrogen isotopes seen in mantle-derived diamonds. Whilst equilibrium fractionation could account for only <4 ‰ variation (Petts et al., in press), there was potential for large kinetic fractionations of up to 40 ‰ based on the results of investigations of synthetic diamonds (Boyd et al., 1988; Reutsky et al., 2008b). However, the investigation of natural mixed habit diamonds in Chapter 3 has shown that large kinetic fractionations are unlikley to occur in nature. Therefore, it is necessary to consider an alternate explanation for the large variation in nitrogen isotopes.

7.2 Mantle heterogeneity

If large kinetic fractionations cannot explain the large variations in nitrogen isotopes in mantle-derived diamonds, the variations most likely reflect heterogeneity in the mantle. Evidence in this thesis has shown that this heterogeneity is both primordial , and

subduction-induced. The ^{15}N-depeleted nitrogen in diamonds from Juina (Chapter 5) and heavily ^{15}N-enriched nitrogen in a diamondite from Orapa (Chapter 4) are both reflective of meteoritic values. Whereas, many of the δ^{15}N values in the Juina diamonds are reminiscent of carbonates and organic carbon indicative of a subduction origin. The co-variations in nitrogen and oxygen in diamondites from Orapa also suggest a subducted origin. The large variations in nitrogen isotopes are in contrast to much smaller variations in carbon isotopes, suggesting that carbon in the mantle is well-mixed relative to nitrogen. This means that the carbon and nitrogen systems are largely decoupled in the mantle. However, evidence of co-variation of carbon and nitrogen isotopes, and carbon and oxygen isotopes in diamonds from Orapa, indicates that there is some coupling of the isotope systems when subduction is involved.

7.3 The nitrogen cycle

Currently, as opposed to the deep carbon cycle, there has been little work on a model for the deep nitrogen cycle. Although much more work, particularly on fluxes, is required, based on the evidence from this thesis, I have proposed a preliminary model (Figure 7.1). The flux estimates are taken from Busigny et al. (2011). These estimates include the nitrogen content of altered oceanic crust (AOC). If AOC is not considered in the subducted nitrogen budget, the recycling at the volcanic arc becomes much more efficient with up to 100% of the subducted nitrogen being erupted (Elkins et al., 2006; Fischer et al., 2002; Halama et al., 2010). The proposed nitrogen species in the mantle are based on the studies by Mikhail and Sverjensky (2014) and Li and Keppler (2014), and the species in the volcanic gases have been measured in numerous studies (Oppenheimer et al., 2005; Rinsland et al., 2003). The δ^{15}N values for each of the proposed nitrogen reservoirs are based upon the data from this thesis (Chapters 4 and 5), data from Busigny and Bebout (2013), and the primordial nitrogen values are taken from the model proposed by Javoy (1997) as well as the heavy nitrogen found in diamondites in Orapa (Chapter 4). My

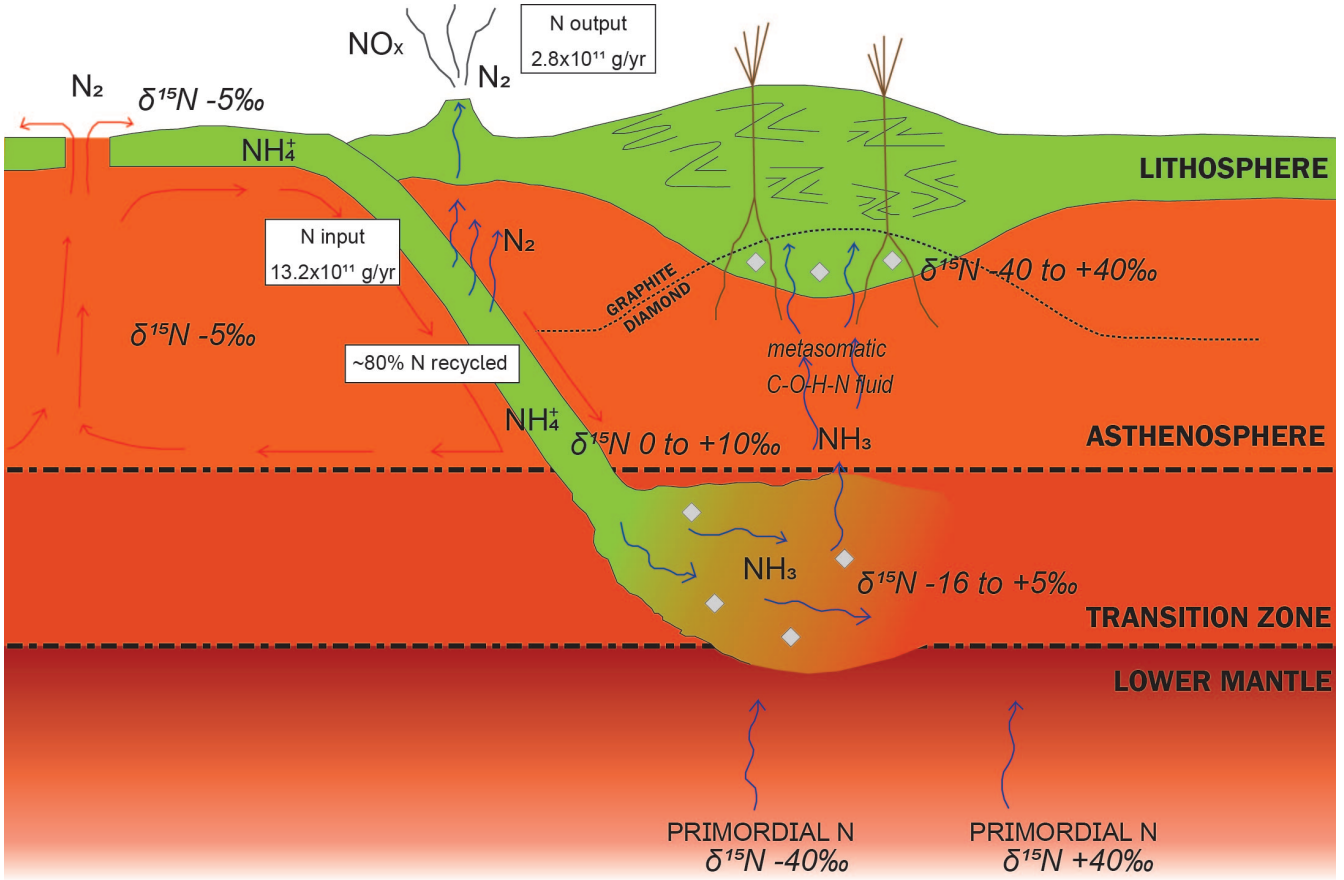

Figure 7.1: A schematic model of the deep nitrogen cycle. Nitrogen flux estimates obtained from Busigny et al. (2011), and N species obtained from Li and Keppler (2014) and Mikhail and Sverjensky (2014).

model for the nitrogen cycle proposes that the majority of subducted nitrogen is carried deep into the upper mantle and transition zone as NH_4^+ within the subducting slab. It is then released into C-O-H-N fluids which metasomatose the surrounding mantle leading the the formation of 'super-deep' diamonds. These fluids also rise through the upper mantle eventually reaching the deep lithospheric roots of the cratons, leading to the formation of lithospheric diamonds. It is likely that diamond formation occurs throughout the upper mantle in the presence of the C-O-H-N fluids (Walter et al., 2011). A further nitrogen source is potentially present in the lower mantle, maintaining the isotopic compositions of the Earth's primordial origins.

7.4 Further work

There are a number of ways the work of this thesis could be expanded upon in the future.

- Continuation of the experimental determination of the equilibrium fractionation factor for nitrogen.
  - Use an ion probe to analyse the samples from the initial experiments between graphite and osbornite to determine whether the experiments succeeded in equilibrating carbon and nitrogen isotopes.
  - If this is proven to be the case, perform the experiments at higher temperatures to determine the effects of temperature on the fractionation and partitioning of nitrogen in graphite and osbornite.
  - Repeat these experiments at different pressures to investigate the effects of pressure on the fractionation and partitioning of nitrogen in graphite and osbornite.
  - These results, if it is shown that nitrogen and carbon isotopes fractionate when equilibrating between graphite and osbornite, may provide some insight into the behaviour of carbon and nitrogen isotopes during core formation – i.e. did heavy or light carbon or nitrogen preferentially partition into the core?

- Perform noble gas measurements on the samples from Orapa (in particular ORF61 and ORF53) to help determine the origin of the heavy nitrogen. If the heavy nitrogen is primordial, there should be a primordial noble gas signature also.
- Determine the paragenesis of the samples from Juina where the paragenesis is currently unknown. This will help to identify more clearly differences and similarities between upper and lower mantle carbon and nitrogen isotopes, and will help towards an understanding of the mixing, or lack thereof, of isotopic systems throughout the mantle as a whole.

Appendix A

Blanks

Table A.1: Stepped combustion data for blanks.

Date	**Run**	**N (ng)**	δ^{15}**N (‰)**	±
04/01/2013	6072	0.38	32.2	5.3
04/07/2013	6085	0.21	4.7	3.0
		0.07	−61.8	14.3
22/01/2014	6429	0.31	−3.2	1.0
		0.26	−5.7	1.0
		0.12	−0.9	1.9
23/01/2014	6432	0.20	−9.8	1.2
		0.07	12.7	2.7
		0.07	3.5	2.7
		0.06	10.5	3.3
24/01/2014	6446	0.06	4.9	3.2
		0.06	21.9	3.3
		0.01	145.1	13.6
09/06/2015	6979	0.41	−6.4	0.9
		0.33	−9.6	1.1
		0.30	−12.1	1.1
22/06/2015	7010	0.46	−10.5	1.6
		0.47	−18.4	1.4
		0.43	−22.3	1.7
		0.41	−18.7	1.8

Appendix B

Combustion data

Table B.1: Stepped combustion data for the mixed-habit diamonds.

	C ng	δ^{13}C (‰)	+/-	N ng	δ^{15}N (‰)	+/-	N ppm
MC01_O	42864	−8.19	0.35	86	−1.21	0.1	1995
MC01_C	71741	−7.22	0.65	112	0.09	0.2	1565
MC02	95030	−7.75	0.57	108	−2.27	1.8	1132
	58182	−7.49	0.19	50	−2.23	0.7	856
MC03	85745	−28.69	0.25	147	−6.30	3.0	1714
MC04	113261	−9.17	0.29	161	−3.22	0.8	1421
MC07_O	53115	−8.17	0.31	89	−0.76	0.1	1681
MC07_C	25554	−9.78	0.95	44	0.70	0.7	1731
	23171	−10.52	5.89	38	1.54	0.8	1638
	17666	−7.74	1.59	26	−1.97	0.7	1449
	5698	−9.86	1.31	5	0.79	0.7	794
MC08_Oa	79958	−10.14	0.39	212	−0.60	0.1	2653
	19434	−7.52	0.20	35	−0.24	0.2	1808
MC08_Ob	79674	−11.11		232	−0.15	0.2	2907
	21951	−8.32	0.40	43	−5.18	2.7	1971
MC08_Oc	37297	−10.98		87	0.28	0.2	2334
MC08_Cb	38191	−10.63		80	−0.68	0.2	2086
	5241	−8.92		6	0.47	0.2	1231
MC08_Cc	87636	−9.47	0.68	157	−3.46	1.8	1795
MC08_Cd	39809	−11.60		90	0.77	0.2	2267
	35765	−12.34		78	−0.23	0.2	2180
	4560	−7.99	0.43	6	−0.78	0.2	1250
MC09_A1	123104	−7.22	1.18	239	0.54	0.3	1945
	30867	−1.34	2.14	39	−2.29	0.4	1263
MC10_O	45196	−7.09	3.80	84	1.51	0.1	1851
MC10_C	42146	−5.61	0.39	50	−2.35	0.2	1192
MC13_O	65982	−7.60	0.35	160	−1.06	0.1	2421
	15768	−8.53	0.74	24	−0.87	0.2	1534
MC13_C	97125	−9.69	1.11	181	−0.21	0.1	1865
	88566	−8.86	0.59	130	−2.42	0.1	1466

Table B.2: Stepped combustion data for the Orapa diamondites. N (ng), δ^{15}N and N ppm values are blank-corrected.

	C ng	δ^{13}C (‰)	+/-	N (ng)	δ^{15}N (‰)	±	%N as blank	N (ppm)
ORF9	151727	−21.6	0.3	1.0	3.6	1.1	29	7
	26463	−19.5	0.4	0.9	−0.6	1.6	31	33
ORF13	33785	−3.5	0.2	0.9	0.6	1.4	31	27
ORF20	137538	−6.1	0.3	5.6	3.4	0.1	7	41
	124439	−7.6	0.4	2.7	4.7	0.2	13	22
ORF78	87249	−12.6	0.2	59.0	0.8	0.0	1	677
	8138	−4.2	0.4	3.4	4.0	0.1	10	423
ORF114	96695	−7.4	0.3	1.3	12.0	0.8	24	13
ORF119	72246	−21.5	0.3	1.7	3.2	0.4	19	24
ORF144	76378	−18.2	0.3	1.4	2.8	0.6	22	18
	27846	−19.6	0.4	0.6	−2.8	3.2	39	23
ORF7	135812	−2.2	0.4	90.9	0.7	0.0	0	669
	56623	−0.5	0.3	19.4	1.8	0.0	2	343
ORF32	148198	−18.4	0.3	2.8	−1.3	0.2	13	19
	47021	−18.8	0.4	2.0	0.7	0.3	17	43
ORF49	109923	−13.0	0.5	4.7	2.1	0.1	8	43
ORF53	129054	−23.3	0.4	2.9	44.4	1.4	12	23
	119550	−17.8	0.4	4.0	38.9	0.9	9	34
	13432	−21.6	0.4	0.1	150.3	147.4	82	7
ORF61	127504	−2.8	0.4	8.2	23.7	0.3	5	64
ORF?	80104	−18.5	0.3	0.6	14.7	2.8	40	7
	40644	−16.2	0.4	0.5	8.0	3.9	44	12

Table B.3: Stepped combustion data for the 10 diamonds from Juina. δ^{15}N and N ppm values are blank-corrected.

	C ng	δ^{13}C (‰)	±	N ng	δ^{15}N (‰)	±	N ppm	Bulk δ^{13}C (‰)	Bulk δ^{15}N (‰)	Bulk N ppm
RS01	64293	−4.43	0.25	38.7	−4.7	0.04	601	−3.93	−5.1	545
	36969	−3.08	0.15	16.5	−6.0	0.08	447			
RS14	36890	−8.59	0.25					−8.57		
	43912	−8.87	0.17							
	42125	−8.22	0.17							
	18087	−8.59	0.13							
RS30	97209	−1.28	2.76	27.8	−3.4	0.07	285	−0.95	−3.5	248
	26734	0.27	2.80	2.9	−3.7	0.38	109			
RS51	77703	−3.89	0.27	12.2	−5.0	0.11	158	−3.54	−4.9	133
	70994	−3.39	0.12	10.5	−5.2	0.13	148			
	54885	−3.24	0.18	4.3	−3.9	0.26	78			
RS55	107246	0.10	0.23	23.0	−3.1	0.07	214	−1.59	−4.4	182
	94195	−3.44	0.35	13.7	−6.4	0.10	145			
	3207	−4.12	0.25	0.5	−7.7	2.71	160			
RS60	95336	−4.45	0.33	4.7	1.7	0.22	50	−4.25	0.4	43
	32821	−3.64	0.28	0.7	−7.6	1.82	22			
RS68	81534	−3.87	0.23	1.6	4.7	0.68	20	−3.85	−2.1	10
	72483	−3.54	0.11	0.4	−13.8	4.30	6			
	69802	−4.67	0.09	0.4	−16.4	4.97	6			
	24526	−2.41	0.22	0.1						
RS101	86920	−2.94	3.37	0.4	−14.8	4.85	5	−3.33	−14.8	2
	72026	−3.74	0.12	0.0						
	21428	−3.58	0.26	0.0						
RS104	82690	−2.66	0.28	41.6	−4.4	0.04	503	−3.80	−1.6	462
	76417	−4.76	0.20	56.0	−1.1	0.04	732			
	59400	−4.17	0.10	3.4	26.1	0.79	58			
RS108	81861	−4.87	0.19	73.0	−6.6	0.04	892	−4.81	−6.1	912
	72142	−5.39	0.09	73.5	−6.2	0.04	1019			
	56583	−3.98	0.15	45.6	−5.3	0.04	806			

Table B.4: Stepped combustion data for the starting materials for the multi-anvil press experiments. Graphite contains no detectable nitrogen, whereas magnesite contains a small amount, which is most likely to be contamination as it is combusted at low temperatures.

	Experiment	**T °C**	**C ng**	δ^{13}**C (‰)**	±	**N ng**	δ^{15}**N (‰)**	±
NSW $MgCO_3$	6449	300	1007	−23.06	0.12	6	−4.1	0.3
		500	28972	−7.67	0.16	8	0.0	0.2
		550	123030	−6.25	0.14	1	3.4	0.3
		600	55401	−6.25	0.15	1	−0.5	0.5
		650	939	−9.41	0.16	0	−8.7	0.6
		700	360	−8.33	0.20	0	−6.5	0.9
		750	215	−9.06	0.12	0	−3.3	0.9
		800	146	−11.74	0.22	0	−7.1	1.1
		1000	252	−10.77	0.23	1	1.9	0.5
		1200	64	−15.21	0.24	0	0.6	0.6
Graphite	6126	500	478	-23.10	0.22	1	−0.8	0.8
		600	2542	−22.14	0.30	0	−11.6	3.1
		700	9461	−23.59	0.29	0	−20.4	2.7
		800	23145	−22.89	0	0	−13.7	2.3
		900	36358	−20.66	0	1	−6.1	1.6
		1000	42825	−24.28	0	0	−4.6	2.0
		1100	20553	−24.07	0	0	−2.3	3.9
		1200	14	−22.76	0	0	13.9	5.1

Table B.5: Stepped combustion data for MgC001.

T (°C)	**C (ng)**	δ^{13}**C (‰)**	±	**N (ng)**	δ^{15}**N (‰)**	±
500	22366	−14.9	0.3	30.8	6.3	0.3
550	81439	−15.7	0.3	11.2	3.4	0.3
600	77891	−22.8	0.3	19.2	2.7	0.3
650	83120	−23.9	0.2	23.4	2.0	0.4
700	86857	−25.6	0.2	19.7	3.7	0.5
1000	116849	−21.1	0.4	16.3	3.8	0.5
1100	68258	−24.9	0.3	11.4	6.7	0.5

Table B.6: Stepped combustion data for MgC002.

T (°C)	**C (ng)**	δ^{13}**C (‰)**	±	**N (ng)**	δ^{15}**N (‰)**	±
500	46862	−19.3	0.1	30.3	4.3	0.3
550	30204	−18.8	0.1	3.0	−1.6	0.4
600	20514	−20.5	0.3	5.9	−4.9	0.5
650	35737	−19.6	0.2	3.3	−4.3	0.3
700	51069	−19.9	0.2	3.7	−6.0	0.3
1000	74223	−22.0	0.3	18.9	5.6	0.2
1100	53084	−24.0	0.2	22.6	4.7	0.3
1200	93278	−18.6	0.2	11.2	7.1	0.2

Table B.7: Stepped combustion data for the starting materials of the piston cylinder experiments when analysed separately. Graphite is shown to contain no nitrogen (blank levels), and TiN is shown to contain small amounts of carbon, but not significantly above blank.

	Experiment	**T'C**	**C ng**	δ^{13}**C (‰)**	±	**N ng**	δ^{15}**N (‰)**	±
Graphite	6714	200	72	−37.73	0.52	1	23.3	0.4
		400	183	−24.42	0.58	3	−4.5	0.5
		600	221	−24.76	0.74	1	14.0	0.5
		700	2074	−33.25	0.54	0	0.3	0.6
		800	19680	−30.94	0.41	1	−1.9	0.6
		900	66995	−21.61	0.21	1	2.6	0.5
		1000	3127	−22.74	0.12	0	−3.9	0.8
		1100	24	−31.07	0.43	1	185.5	0.5
		1200	37	−23.67	0.62	1	167.6	0.5
		1300	14	−28.66	0.28	0	18.2	0.7
Graphite	6722	600	619	−25.81	0.64	7	0.2	0.4
		700	4970	−21.98	0.64	1	−9.1	0.7
		750	18094	−22.59	0.63	2	0.7	0.4
		800	51686	−40.02	0.39	1	−2.5	0.2
		850	106897	−24.93	0.09	2	0.3	0.2
		900	71528	−24.00	0.15	1	0.1	0.2
		950	1350	−22.72	0.10	1	0.9	0.3
TiN	6723	400	667	−27.28	0.59	4	−3.5	0.4
		500	66	−40.44	0.41	10	−2.2	0.2
		600	41	−18.73	0.62	37	−2.4	0.2
		700	22	−35.95	0.37	168	−2.8	0.3
		750	23	−25.64	0.07	147	−4.9	0.3
		800	21	−24.21	0.06	111	−1.2	0.2
		850	20	0	0	46	−2.4	0.2
		900	21	0	0	27	−3.9	0.2
		950	11	0	0	28	−3.1	0.3
		1000	26	0	0	22	−2.2	0.3

Table B.8: Stepped combustion data for the piston cylinder starting mixture of TiN and graphite.

	Experiment	Time T'C	C ng	δ^{13}C (‰)	±	N ng	δ^{15}N (‰)	±
TiN+G	6717	500	74	−24.45	0.59	3	−3.1	0.4
		700	38	−22.86	0.55	84	−1.7	0.3
		800	80	−23.44	0.58	122	−2.4	0.3
		900	35	−34.13	0.43	22	−8.2	0.3
		1000	6	−42.42	0.91	4	−3.7	0.5
		1100	5	−33.92	1.59	1	6.1	0.7
		1200	7	−42.01	0.73	1	−1.8	0.6
		1300	10	−28.64	1.39	1	0.9	0.6
		1400	8	−34.16	1.14	1	10.6	0.3
TiN+G	6724	400	278	−20.26	0.71	16	−5.9	0.3
		500	35	−18.94	0.42	26	−3.5	0.3
		600	23	−33.84	0.38	101	−1.3	0.2
		650	41	−24.33	0.14	175	−3.3	0.4
		700	90	−13.44	0.38	243	−1.3	0.3
		750	213	−24.12	0.34	419	−1.3	0.3
		800	252	−23.45	0.20	289	−3.0	0.3
		850	172	−22.15	1.00	135	−2.4	0.2
		900	46	−23.73	0.36	36	−3.4	0.3
		1000	13	−27.46	0.36	40	−3.4	0.3

Table B.9: Stepped combustion data for GTN001.

T (°C)	**C (ng)**	**δ^{13}C (‰)**	**+/-**	**N (ng)**	**δ^{15}N (‰)**	**+/-**
400	637	-31.8	1.0	19.7	-2.0	0.4
500	167	-18.9	0.7	11.3	-3.9	0.3
600	103	-7.6	0.7	26.4	-2.8	0.3
650	129	-21.0	0.7	49.4	-0.1	0.2
700	279	-30.6	0.5	105.3	-0.9	0.2
750	445	-24.3	0.3	192.6	-2.5	0.3
800	461	-22.8	0.3	265.1	-1.6	0.3
850	273	-10.3	0.6	167.7	-2.9	0.3
900	97	-31.1	0.8	133.4	-4.0	0.4
1000	37	-18.6	0.7	362.4	-2.1	0.2
1200	33	-24.8	1.1	313.2	-3.0	0.3
1400	30	-13.8	0.8	5.3	0.6	0.3

Table B.10: Stepped combustion data for GTN003.

T (°C)	**C (ng)**	δ^{13}**C (‰)**	**+/-**	**N (ng)**	δ^{15}**N (‰)**	**+/-**
400	214	-27.2	0.3	9.0	4.1	0.3
500	43	-37.2	0.6	16.7	-4.3	0.3
600	117	-22.7	0.2	63.4	-3.3	0.3
650	304	-22.6	0.3	137.6	-1.1	0.2
700	617	-33.2	0.9	250.0	-1.7	0.3
750	908	-26.2	0.2	598.1	-1.2	0.2
800	814	-24.8	0.3	895.2	-0.6	0.2
850	448	-21.8	0.3	564.1	-1.7	0.2
900	93	-24.6	0.2	357.1	-3.1	0.2
950	35	-29.8	0.2	401.6	-2.0	0.2
1000	28	-26.5	0.4	294.1	-2.7	0.3
1100	23	-25.7	0.2	159.8	-5.0	0.3
1200	10	-38.5	0.5	4.8	0.0	0.3
1400	60	-24.5	1.1	7.4	-0.5	0.2

Table B.11: Stepped combustion data for GTN004.

T (°C)	**C (ng)**	δ^{13}**C (‰)**	**+/-**	**N (ng)**	δ^{15}**N (‰)**	**+/-**
400	345	-27.0	0.1	8.6	0.5	0.2
500	59	-18.6	1.7	19.9	-4.1	0.3
600	101	-31.7	0.5	83.9	-2.7	0.3
650	238	-21.9	0.7	146.1	-1.3	0.4
700	572	-20.4	1.2	298.6	-1.7	0.3
750	919	-32.4	0.8	651.5	-0.6	0.2
800	894	-26.0	1.8	938.4	-1.0	0.2
850	581	-27.4	0.9	600.4	-1.8	0.2
900	150	-29.6	2.2	251.2	-3.4	0.3
950	29	-26.9	1.2	229.6	-3.5	0.3
1000	20	-31.9	1.1	151.4	-1.1	0.2
1050	12	-27.2	0.5	31.4	-3.7	0.3
1100	7	-30.4	0.5	1.3	1.1	0.3
1150	8	-42.6	0.9	1.4	1.5	0.3
1200	9	-29.3	0.3	1.6	1.3	0.3
1300	13	-33.3	0.6	3.0	1.2	0.4
1400	16	-34.3	0.5	3.6	0.8	0.3

Appendix C

Data from other sources

Table C.1: A summary of the carbon isotope and nitrogen concentration data from Howell et al. (2013b). The full Supplementary Data Table for Howell et al. (2013b) (Deposit AM-13-023; Jan 2013 American Mineralogist) is available at www.minsocam.org

Sample	No. of analyses	Sector	Mean δ^{13}C (‰)	2σ (‰)	N (ppm)
MC01		O			2226
		C			1549
MC07	36	O	-8.76	0.10	2302
	33	C	-8.83	0.10	1679
MC08	9	O	-8.98	0.07	2642
	11	C	-8.90	0.07	1866
MC10		O			2120
		C			1483
MC13		O			2200
		C			1600

Table C.2: A summary of the supplementary data from Howell et al. (2015). Each value listed is the mean of the analyses from a transect made using SIMS.

	Sector	Mean δ^{13}C (‰)	2σ (‰) inter-session	Mean δ^{15}N (‰)	2σ (‰) inter-session	[N] at. ppm
MC08-C	C	-8.91	0.12	-0.42	0.73	2130
MC08-B	O	-8.95	0.12	0.39	0.68	2818
MC08-E	C	-8.90	0.12	-0.42	0.65	1979
MC08-E	O	-8.87	0.12	0.58	0.59	2691
MC10-B	C	-8.70	0.12	-0.05	0.77	1517
MC10-B	O	-8.55	0.12	0.43	0.65	2151
MC10-B	C	-8.63	0.12	0.14	0.79	1536
MC13-A	C	-8.41	0.12			
MC13-A	C	-8.56	0.12	-0.28	0.78	1601
MC13-A	O	-8.34	0.12	0.53	0.65	2258
MC13-A	C	-8.54	0.12	-0.50	0.74	1679
MC13-A	O	-8.48	0.12	0.19	0.63	2290

Table C.3: Carbon and oxygen isotope data for polycrystalline diamonds from Orapa. The letters W, E and P refer to websteritic, eclogitic and peridotitc paragenesis respectively.

Sample	Paragenesis	δ^{13}C (‰)	δ^{18}O (‰)	N ppm	Silicate intergrowths
ORF9	W	-5.3	8.0		garnet
ORF13	W	-9.4	6.0	261	garnet
ORF20	W	-10.7	6.7		garnet
ORF78	W	-14.4	6.9	408	garnet
ORF114	W	-15.7	7.6		garnet
ORF119	W	-22.5	7.3		garnet
ORF144	W	-19.8	7.2		garnet
ORF7	E	-8.2		900	garnet,cpx
ORF32	W	-17.9			garnet
ORF49	W	-16.5			garnet
ORF53	W+P	-21.9			garnet
ORF61	E	-5.6			garnet
ORF145	W	-20.2			garnet
JJG897	W	-19.0			garnet
ORF?	W	-15.6			garnet

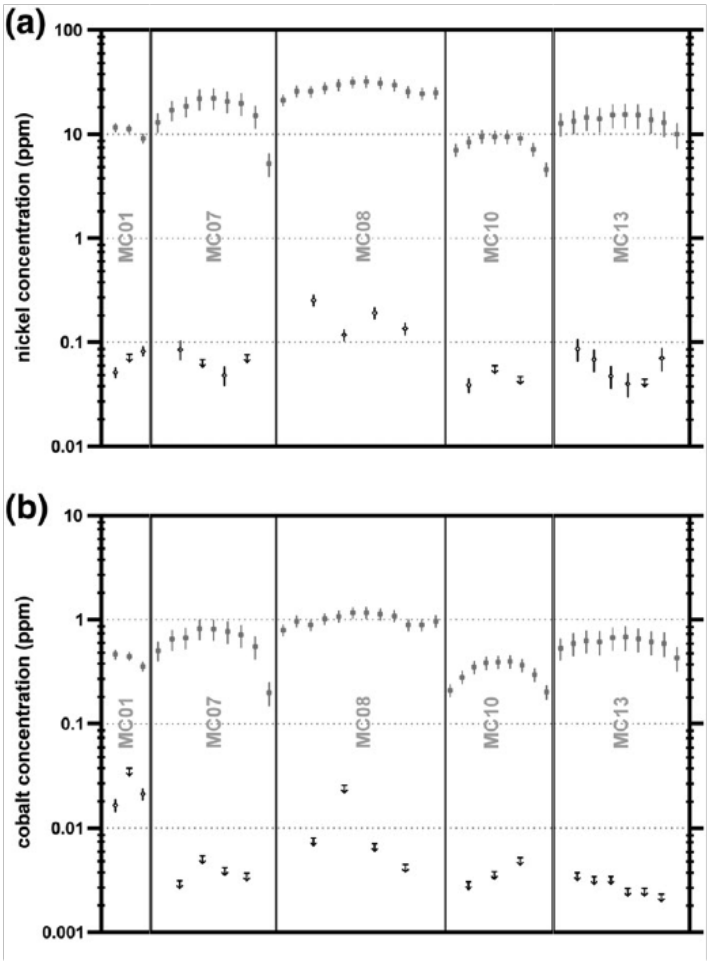

Figure C.1: Partitioning data for nickel and cobalt in mixed habit diamonds. White diamonds and grey squares represent data above the LOQ from the octahedral and cuboid sectors respectively. Error bars represent 1σ uncertainties. Black (octahedral) and grey (cuboid) arrows define the LOQ for the analyses that fall below it. Distances along the x-axis are simply schematic and not to scale. Modified from Howell et al. (2013a).

Table C.4: Stepped carbon and nitrogen isotope data for diamonds from Juina published in the supplementary materials of Mikhail et al. (2014b). The data was collected using the same method as the the data in this thesis - stepwise combustion of the sample by the Finesse machine.

	C mg	δ^{13}C (‰)	δ^{15}N (‰)	+/-	N ppm	Bulk δ^{13}C (‰)	Bulk δ^{15}N (‰)	Bulk N ppm
JUC4	0.16	-6.71	3.26	0.50	13	-6.5	3.4	17
	0.03	-5.12	4.09	0.92	40			
BZ270	0.22	-7.73	4.34	2.52	3	-7.7	4.8	7
	0.22	-7.91	6.18	2.01	4			
	0.03	-6.52	-2.46	0.86	61			
JUC7	0.15	-6.57	-6.83	1.02	12	-6.5	-6.4	12
	0.04	-6.47	-4.62	8.42	10			
J-7	0.16	-5.82	4.00	0.98	33	-5.6	6.1	34
	0.04	-4.81	13.01	3.41	36			
J-17	0.13	-7.72	3.62	0.50	510	-7.6	2.3	463
	0.14	-8.58	4.60	0.50	434			
	0.07	-5.53	-4.75	0.50	435			
J-19	0.12	-19.64	-4.93	0.61	79	-19.9	-2.8	56
	0.08	-20.39	10.87	3.99	20			
J-18	0.13	-24.04	-1.34	0.68	61	-23.8	7.5	48
	0.13	-24.97	19.61	0.80	54			
	0.13	-22.63	0.33	1.65	24			
	0.01	-21.59	12.78	2.00	103			
J-6	0.12	-10.40	10.74	1.03	653	-10.6	12.3	624
	0.12	-11.07	9.05	0.97	592			
	0.13	-10.95	17.91	0.87	686			
	0.12	-10.35	10.98	0.61	600			
	0.04	-9.72	11.37	0.50	517			

Appendix D

High pressure experiments

Table D.1: Heating data for MgC001. The experiment was quenched after 1 hour.

Time	T °C	%P	P(W)	Volts	Amps
14:32	120	3.6	28	24.4	1.4
	208	4.7	50	22.8	2.9
	404	6.9	101	20.6	6.1
	612	8.9	146	20.5	8.8
14:39	840	11	189	20.5	11.5
	1009	12.6	223	20.7	13.5
	1213	14.4	257	21.3	15.3
14:44	1527	17	286	23.0	17.2
	1711	18.4	315	24.2	17.9
14:46	1812	18.9	321	24.7	18.0

Table D.2: Heating data for MgC002. The experiment was quenched after 10 minutes. The thermocouple failed at 1800 °C. The final temperature was estimated using an extrapolation of the power curve (Figure D.1).

Time	T °C	%P	P(W)	Volts	Amps
15:05	112	3.5	34	15.3	2.4
	208	4.9	68	15.5	4.8
	405	7.4	131	15.6	9.1
	601	9.6	183	16.1	12.4
15:13	800	11.7	230	16.6	15.3
	1003	13.8	274	17.4	17.8
	1212	15.9	316	18.4	19.9
15:20	1404	17.7	346	19.4	21.3
15:22	1607	20	380	20.9	22.7
15:33	1803	22.9	418	23	24.0
15:39		26.3	453	25.6	25.0

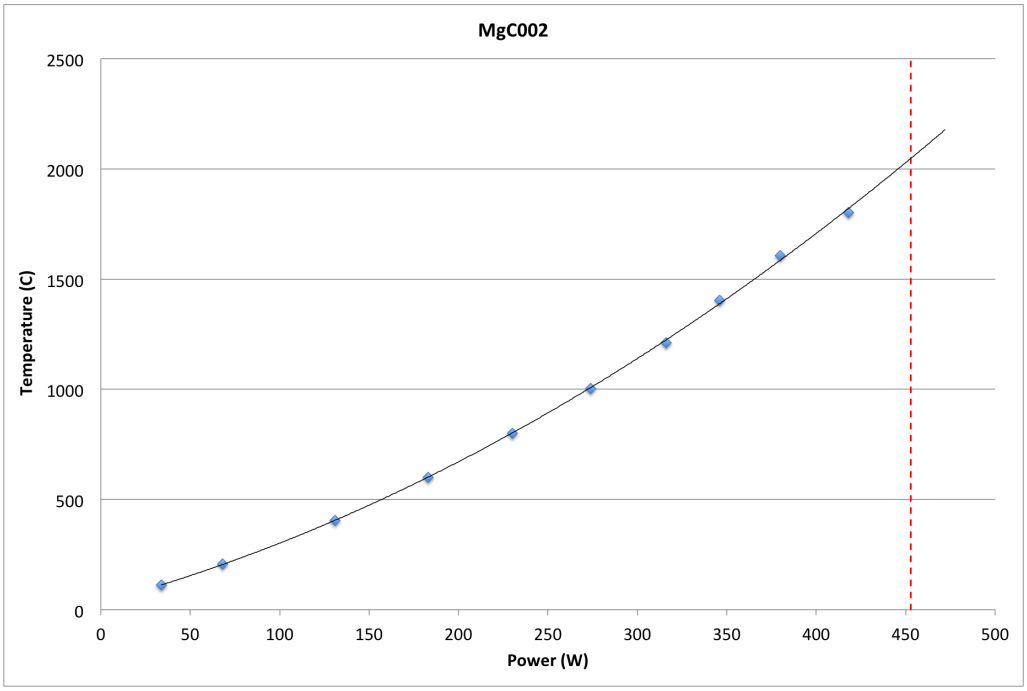

Figure D.1: Power vs. temperature curve for MgC002. Red line shows the maximum power measurement.

Table D.3: Heating data for GTN001. The experiment was quenched gradually starting immediately after the final measurement.

Time	%out	T/C	Amps	Volts	Power (W)	P (kbar)	Comments
15:10							Start heating
15:14	5.8	103	0	32		11.82	
15:17	7.5	200	0	46		11.63	
15:19	9.4	312	5.0	57	285	11.38	
15:21	10.7	419	5.0	64	320	11.19	
15:22	11.6	516	5.5	68	374	10.91	
15:24	12.9	607	6.5	72	468	10.67	
15:26	14.2	712	6.5	75	487.5	10.42	
15:27	15.0	813	7.0	79	553	10.28	
15:29	15.8	912	7.5	81	607.5	10.20	
15:30	16.5	1006	8.0	84	672	10.16	
15:32	17.6	1104	8.5	87	739.5	10.00	
15:34	18.5	1200	9.0	90	810	9.95	Overheated after 1hr

Table D.4: Heating data for GTN002. The ranges shown in the Pressure column indicate where the pressure has fallen on heating and has been manually increased. The experiment was quenched gradually starting immediately after the final measurement.

Date	Time	%Power	Amps	Volts	Power	Resistance	P/bar	T °C
16/5/14	10:30	2.7	19.7	0.54	11	0.0274	390	30.3
		5	53.7	1.30	70	0.0242	390	35.9
		8	77.3	1.72	133	0.0223		165.5
		10	92.0	1.95	179	0.0212	380-400	217.5
		12	108.7	2.19	238	0.0201	384	285.8
		14	127.8	2.43	311	0.0190	375-394	382.7
		16	150.9	2.67	403	0.0177	376-396	505.8
	10:45	18	173.7	2.89	502	0.0166	378-390	661.5
		20	198.8	3.10	616	0.0156	374-390	860.6
		22	224.1	3.27	733	0.0146	380-400	1060.5
	10:55	23.5	246.7	3.39	836	0.0137	392	1208.7
	11:05	23.8	251.4	3.40	855	0.0135	380-404	1216.2
	11:15	24	252.7	3.41	862	0.0135	392	1210.3
	12:00	24	250.9	3.41	856	0.0136	390	1210.1
	13:25	24.3	254.5	3.42	870	0.0134	382-398	1212.7
	15:20	24.5	255.5	3.43	876	0.0134	390	1215.9
	16:25	24.5	256.1	3.43	878	0.0134	390-404	1216.6
19/5/14	10:20	25	272.6	3.43	935	0.0126	374-400	1213.6
	14:10	25	273.0	3.41	931	0.0125	397	1202.5

Table D.5: Heating data for GTN003. The ranges shown in the Pressure column indicate where the pressure has fallen on heating and has been manually increased. The experiment was quenched gradually starting immediately after the final measurement.

Date	Time	%Power	Amps	Volts	Power	Resistance	P/bar	T °C
21/5/14	11:05	2.7	7.8	0.62	5	0.0795	395	25.9
		4	32.6	1.12	37	0.0344	394	50.7
		8	68.2	1.75	119	0.0257	394	134.3
		10	83.1	1.99	165	0.0239	394	183.4
		12	99.6	2.23	222	0.0224	386	244.7
		14	115.5	2.47	285	0.0214	378	314.1
		16	136.6	2.71	370	0.0198	370-398	424.4
		18.4	164.8	2.99	493	0.0181	375-399	597.7
		20	187.9	3.12	586	0.0166	377-396	836.3
		22	231.2	3.24	749	0.0140	372-394	1065.7
	11:30	23.7	256.8	3.39	871	0.0132	385-393	1227.1
	11:45	23.7	258.8	3.36	870	0.0130	371-400	1208.4
	12:00	23.7	260.1	3.36	874	0.0129	390-397	1205.7
	12:05	23.9	262.1	3.38	886	0.0129	396	1215.7
	13:15	24.5	265.8	3.42	909	0.0129	382-398	1228.2
	15:40	24.3	265.6	3.37	895	0.0127	386-397	1213.8
	17:55	24.3	266.4	3.36	895	0.0126	391-400	1218.6
22/5/14	9:55	24.3	264.6	3.34	884	0.0126	394	1208.2
	11:30	24.3	264.5	3.34	883	0.0126	393	1208.1

Table D.6: Heating data for GTN004. The ranges shown in the Pressure column indicate where the pressure has fallen on heating and has been manually increased. The experiment was quenched gradually starting immediately after the final measurement.

Date	Time	%Power	Amps	Volts	Power	Resistance	P/bar	T °C
28/5/14	11:20	2.7	24.2	0.535	13	0.0221	391	40.6
		5	60.4	1.29	78	0.0214	390	106.1
		8	85.2	1.69	144	0.0198	390	180.3
		10	101.5	1.93	196	0.0190	389	239.1
		12	119.4	2.17	259	0.0182	380-398	316.0
		14	141.7	2.39	339	0.0169	380-396	422.9
		16	167.7	2.62	439	0.0156	378-401	557.5
		18	190.2	2.84	540	0.0149	377-400	716.6
		20	220.7	3.04	671	0.0138	377-400	933.4
		22	249.7	3.21	802	0.0129	388-400	1147.2
	11:40	22.8	260.0	3.25	845	0.0125	393	1214.3
	11:50	23.3	266.1	3.29	875	0.0124	384-400	1214.5
	12:05	23.3	265.8	3.28	872	0.0123	396	1215.7
	14:15	23.4	266.2	3.29	876	0.0124	384-399	1212.8
	17:05	23.6	266.7	3.29	877	0.0123	396	1215.7
29/5/14	9:00	23.6	267.3	3.28	877	0.0123	388	1216
	11:50	23.6	266.7	3.28	875	0.0123	386-398	1208.7
	17:45	23.6	266.8	3.27	872	0.0123	395	1211.8
30/5/14	11:40	23.6	267.9	3.30	884	0.0123	373-399	1223.5

Table D.7: Heating data for GTN005. The ranges shown in the Pressure column indicate where the pressure has fallen on heating and has been manually increased. The experiment was quenched gradually starting immediately after the final measurement.

Time	%Power	Amps	Volts	Power	Resistance	P/bar	T °C
11:43	2.7	24.8	0.531	13	0.0214	395	39.3
	5	65.2	1.27	83	0.0195	394	108.4
	8	92.2	1.67	154	0.0181	389-393	185.0
	10	109.9	1.90	209	0.0173	385-404	248.9
	12	129.7	2.12	275	0.0163	384-400	330.4
	14	153.0	2.34	358	0.0153	380-400	441.1
	16	178.5	2.56	457	0.0143	378-401	574.1
	18	202.9	2.78	564	0.0137	375-400	732.4
	20	229.4	2.97	681	0.0129	382-399	926.9
	22	256.6	3.15	808	0.0123	390-398	1135.8
12:03	22.8	269.5	3.21	865	0.0119	392	1212.5
12:10	22.9	273.0	3.21	876	0.0118	378-400	1216.5
12:20	23.0	273.4	3.22	880	0.0118	390-401	1216.9
12:30	23.1	274.2	3.22	883	0.0117	396-400	1218.6
13:15	23.2	274.5	3.22	884	0.0117	394	1214.9
14:40	23.2	274.2	3.22	883	0.0117	391	1209.1
16:30	23.4	275.1	3.24	891	0.0118	388-396	1213.8
18:03	23.4	273.8	3.22	882	0.0118	391	1201.7

Bibliography

J. F. Adler and Q. Williams. A high-pressure X-ray diffraction study of iron nitrides: Implications for Earth's core. *Journal of Geophysical Research*, 110:B011203, 2005.

M. Akaishi, H. Kanda, and S. Yamaoka. Synthesis of diamond from graphite-carbonate system under very high pressure and temperature. *Journal of Crystal Growth*, 104: 578–581, 1990.

M. Akaishi, M. D. Shaji Kumar, H. Kanda, and S. Yamaoka. Reactions between carbon and a reduced C-O-H fluid under diamond-stable HP-HT condition. *Diamond and Related Materials*, 10:2125–2130, 2001.

S. Aulbach, T. Stachel, K. Stephanus Viljoen, G. P. Brey, and J. W. Harris. Eclogitic and websteritic diamond sources beneath the Limpopo Belt - is slab-melting the link? *Contributions to Mineralogy and Petrology*, 143:56–70, 2002.

G. E. Bebout and M. L. Fogel. Nitrogen-isotope compositions of metasedimentary rocks in the Catalina Schist, California: Implications for metamorphic devolatilization history. *Geochimica et Cosmochimica Acta*, 56:2839–2849, 1992.

F. R. Boyd and J. L. England. Apparatus for phase-equilibrium measurements at pressures up to 50 kilobars and temperatures up to 1750 ℃. *Journal of Geophysical Research*, 65: 741–748, 1960.

F. R. Boyd and J. J. Gurney. Diamonds and the African Lithosphere. *Science*, 232: 472–477, 1986.

S. R. Boyd. *A study of carbon and nitrogen isotopes from the Earth's mantle.* PhD thesis, The Open University, 1988.

S. R. Boyd and C. T. Pillinger. A preliminary study of $^{15}N/^{14}N$ in octahedral growth form diamonds. *Chemical Geology*, 116:43–59, 1994.

S. R. Boyd, D. P. Mattey, C. T. Pillinger, H. J. Milledge, M. J. Mendelssohn, and M. Seal. Multiple growth events during diamond genesis: an integrated study of carbon and nitrogen isotopes and nitrogen aggregation state in coated stones. *Earth and Planetary Science Letters*, 86:341–353, 1987.

S. R. Boyd, C. T. Pillinger, H. J. Milledge, M. J. Mendelssohn, and M. Seal. Fractionation of nitrogen isotopes in a synthetic diamond of mixed crystal habit. *Nature*, 331:604–607, 1988.

S. R. Boyd, C. T. Pillinger, H. J. Milledge, M. J. Mendelssohn, and M. Seal. C and N isotopic composition and the infrared absorption spectra of coated diamonds evidence for the regional uniformity of CO_2-H_2O rich fluids in lithospheric mantle. *Earth and Planetary Science Letters*, 109:633–644, 1992.

F. E. Brenker, C. Vollmer, L. Vincze, B. Vekemans, A. Szymanski, K. Janssens, I. Szaloki, L. Nasdala, W. Joswig, and F. Kaminsky. Carbonates from the lower part of transition zone or even the lower mantle. *Earth and Planetary Science Letters*, 260(1-2):1–9, 2007.

G. P. Bulanova. The formation of diamond. *Journal of Geochemical Exploration*, 53:1–23, 1995.

G. P. Bulanova, D. G. Pearson, E. H. Hauri, and B. J. Griffin. Carbon and nitrogen isotope systematics within a sector-growth diamond from the Mir kimberlite, Yakutia. *Chemical Geology*, 188:105–123, 2002.

G. P. Bulanova, M. J. Walter, C. B. Smith, S. C. Kohn, L. S. Armstrong, J. Blundy, and L. Gobbo. Mineral inclusions in sublithospheric diamonds from Collier 4 kimberlite

pipe, Juina, Brazil: subducted protoliths, carbonated melts and primary kimberlite magmatism. *Contributions to Mineralogy and Petrology*, 160(4):489–510, 2010.

F. P. Bundy. The P, T Phase and Reaction Diagram for Elemental Carbon, 1979. *Journal of Geophysical Research*, 85(B12):6930–6936, 1980.

H. Bureau, F. Langenhorst, A.-L. Auzende, D. J. Frost, I. Estève, and J. Siebert. The growth of fibrous, cloudy and polycrystalline diamonds. *Geochimica et Cosmochimica Acta*, 77:202–214, 2012.

R. Burgess, E. Layzelle, G. Turner, and J. W. Harris. Constrains on the age and halogen composition of mantle fluids in siberian coated diamonds. *Earth and Planetary Science Letters*, 197:193–203, 2002.

R. C. Burns, V. Cvetkovic, C. N. Dodge, D. J. F. Evans, M.-L. T. Rooney, P. M. Spear, and C. M. Welbourn. Growth sector dependence of optical features in large synthetic diamonds. *Journal of Crystal Growth*, 104:257–279, 1990.

V. Busigny and G. E. Bebout. Nitrogen in the Silicate Earth: Speciation and Isotopic Behaviour during Mineral-Fluid Interactions. *Elements*, 9:353–358, 2013.

V. Busigny, P. Cartigny, P. Philippot, M. Ader, and M. Javoy. Massive recycling of nitrogen and other fluid-mobile elements (K, Rb, Cs, H) in a cold slab environment: evidence from HP to UHP oceanic metasediments of the Schistes Lustrés nappe (western Alps, Europe). *Earth and Planetary Science Letters*, 215(1-2):27–42, 2003.

V. Busigny, P. Cartigny, and P. Philippot. Nitrogen isotopes in ophiolitic metagabbros: A re-evaluation of modern nitrogen fluxes in subduction zones and implication for the early Earth atmosphere. *Geochimica et Cosmochimica Acta*, 75(23):7502–7521, 2011.

P. Cartigny. Stable Isotopes and the Origin of Diamond. *Elements*, 1:79–84, 2005.

P. Cartigny and B. Marty. Nitrogen Isotopes and Mantle Geodynamics: The Emergence of Life and the Atmosphere-Crust-Mantle Connection. *Elements*, 9:359–366, 2013.

P. Cartigny, S. R. Boyd, J. Harris, and M. Javoy. Nitrogen isotopes in peridotitic diamonds from Fuxian, China: the mantle signature. *Terra Nova*, 9:175–179, 1997.

P. Cartigny, J. W. Harris, and M. Javoy. Eclogitic Diamond Formation at Jwaneng: No Room for a Recycled Component. *Science*, 280(5368):1421–1424, 1998a.

P. Cartigny, J. W. Harris, D. Phillips, M. Girard, and M. Javoy. Subduction related diamonds? -the evidence for a mantle-derived origin from coupled δ^{13}C-δ^{15}N determinations. *Chemical Geology*, 147:147–159, 1998b.

P. Cartigny, J. Harriws, and M. Javoy. *Eclogitic, Peridotitic and Metamorphic diamonds and the problems of carbon recycling - the case of Orapa (Botswana)*, pages 117–124. 1, Red Roof Design, 1999.

P. Cartigny, J. W. Harris, and M. Javoy. Diamond genesis, mantle fractionations and mantle nitrogen content: a study of δ^{13}C-N concentrations in diamonds. *Earth and Planetary Science Letters*, 185:85–98, 2001.

P. Cartigny, J. W. Harris, A. Taylor, R. Davies, and M. Javoy. On the possibility of a kinetic fractionation of nitrogen stable isotopes during natural diamond growth. *Geochimica et Cosmochimica Acta*, 67(8):1571–1576, 2003.

P. Cartigny, J. Farquhar, E. Thomassot, J. W. Harris, B. Wing, A. Masterson, K. McKeegan, and T. Stachel. A mantle origin for Paleoarchean peridotitic diamonds from the Panda kimberlite, Slave Craton: Evidence from ^{13}C-, ^{15}N- and ^{33,34}S-stable isotope systematics. *Lithos*, 112:852–864, 2009.

P. Cartigny, M. Palot, E. Thomassot, and J. W. Harris. Diamond Formation: A Stable Isotope Perspective. *Annual Review of Earth and Planetary Sciences*, 42(1):699–732, 2014.

T. Chacko, R. Cole, and J. Horita. Equilibrium oxygen, hydrogen, and carbon isotope fractionation factors applicable to geologic systems. *Reviews in Mineralogy and Geochemistry*, 43:1–81, 2001.

H. Chen, Z. Qiu, T. Lu, R. Stern, T. Stachel, Y. Sun, J. Zhang, J. Ke, S. Peng, and S. Qin. Variations in carbon isotopic composition in the subcontinental lithospheric mantle beneath the Yangtze and North China Cratons: Evidence from in-situ analysis of diamonds using SIMS. *Chinese Science Bulletin*, 58(1):99–107, 2012.

R. M. Chrenko. Boron, Dominant Acceptor in Semiconducting Diamond. *Physical Review B*, 7:4560–4567, 1973.

H. Craig. The geochemistry of the stable carbon isotopes. *Geochimica et Cosmochimica Acta*, 3:53–92, 1953.

N. Dauphas and B. Marty. Heavy Nitrogen in Carbonatites of the Kola Peninsula: A Possible Signature of the Deep Mantle. *Science*, 286(5449):2488–2490, 1999.

P. Deines. The carbon isotopic composition of diamonds: relationship to diamond shape, color, occurrence and vapor composition. *Geochimica et Cosmochimica Acta*, 44:943–961, 1980.

P. Deines. The role of mantle fluids in the growth of diamonds. In *Advanced materials '96*, pages 61–64, 1996.

P. Deines, J. J. Gurney, and J. W. Harris. Associated chemical and carbon isotopic variations in diamonds from Finsch and Premier kimberlite, South Africa. *Geochimica et Cosmochimica Acta*, 48:325–342, 1984.

P. Deines, J. W. Harris, P. M. Spear, and J. J. Gurney. Nitrogen and ^{13}C content of Finsch and Premier diamonds and their implications. *Geochimica et Cosmochimica Acta*, 53: 1367–1378, 1989.

P. Deines, J. W. Harris, and J. J. Gurney. Depth-related carbon isotope and nitrogen concentration variability in the mantle below the Orapa kimberlite, Botswana, Africa. *Geochimica et Cosmochimica Acta*, 57:2781–2796, 1993.

G. Dobosi and G. Kurat. Trace element abundances in garnets and clinopyroxenes from diamondites - a signature of carbonatitic fluids. *Mineralogy and Petrology*, 76:21–38, 2002.

L. F. Dobrzhinetskaya, R. Wirth, J. Yang, I. D. Hutcheon, P. K. Weber, and H. W. Green II. High-pressure highly reduced nitrides and oxides from chromitite of a tibetan ophiolite. *PNAS*, 106:19233–19238, 2009.

D. P. Dobson, P. G. Meredith, and S. A. Boon. Detection and analysis of microseismicity in multi anvil experiments. *Physics of the Earth and Planetary Interiors*, 143-144:337–346, 2004.

ElementSix. Diamond crystallography, 2015. URL http://www.e6cvd.com/cvd/page.jsp?pageid=361.

L. Elkins, T. Fischer, D. Hilton, Z. Sharp, S. McKnight, and J. Walker. Tracing nitrogen in volcanic and geothermal volatiles from the Nicaraguan volcanic front. *Geochimica et Cosmochimica Acta*, 70(20):5215–5235, 2006.

T. P. Fischer, D. R. Hilton, M. M. Zimmer, A. M. Shaw, Z. D. Sharp, and J. A. Walker. Subduction and recycling of nitrogen along the Central American margin. *Science*, 297 (5584):1154–7, 2002.

T. P. Fischer, N. Takahata, Y. Sano, H. Sumino, and D. R. Hilton. Nitrogen isotopes of the mantle: Insights from mineral separates. *Geophysical Research Letters*, 32(11), 2005.

I. C. W. Fitzsimons, B. Harte, I. L. Chinn, J. J. Gurney, and W. R. Taylor. Extrreme chemical variation in complex diamonds from George Creek, Colorado: a SIMS study of carbon isotope composition and nitrogen abundance. *Mineralogical Magazine*, 63: 87–878, 1999.

F. C. Frank. Defects in diamond. In J. Burls, editor, *Science and Technology of Industrial Diamonds, vol. 1*. Industrial Diamond Information Bureau, London, 1967.

D. J. Frost. Introduction to oxygen fugacity and its petrologic importance. In D. Lindsley, editor, *Oxide Minerals: Petrologic and Magnetic Significance*, volume 25 of *Reviews in Mineralogy*. Mineralogical Society of America, Washington, DC, 1991.

D. J. Frost and C. A. McCammon. The Redox State of Earth's Mantle. *Annual Review of Earth and Planetary Sciences*, 36(1):389–420, 2008.

E. M. Galimov. Isotope fractionation related to kimberlite magmatism and diamond formation. *Geochimica et Cosmochimica Acta*, 55:1697–1708, 1991.

C. Gautheron, P. Cartigny, M. Moreira, J. Harris, and C. Allegre. Evidence for a mantle component shown by rare gases, C and N isotopes in polycrystalline diamonds from Orapa (Botswana). *Earth and Planetary Science Letters*, 240(3-4):559–572, 2005.

M. Grady, I. Wright, L. Carr, and C. Pillinger. Compositional differences in enstatite chondrites based on carbon and nitrogen stable isotope measurements. *Geochimica et Cosmochimica Acta*, 50:2799–2813, 1986.

J. J. Gurney, J. W. Harris, and R. S. Rickard. Silicate and oxide inclusions in diamonds from the Orapa Mine, Botswana. In J. Kornprobst, editor, *Kimberlites II: the mantle and crustmantle relationships.* Elsevier, Amsterdam, 1984.

J. J. Gurney, H. H. Helmstaedt, S. H. Richardson, and S. B. Shirey. Diamonds through time. *Economic Geology*, 105:689–712, 2010.

D. Haendel, K. Muhle, H.-M. Nitzsche, G. Stiehl, and U. Wand. Isotopic variations of the fixed nitrogen in metamorphic rocks. *Geochimica et Cosmochimica Acta*, 50:759–758, 1986.

S. E. Haggerty. Diamond genesis in a multiply constrained model. *Nature*, 320:34–38, 1986.

R. Halama, G. E. Bebout, T. John, and V. Schenk. Nitrogen recycling in subducted oceanic lithosphere: The record in high- and ultrahigh-pressure metabasaltic rocks. *Geochimica et Cosmochimica Acta*, 74(5):1636–1652, 2010.

R. Halama, G. E. Bebout, T. John, and M. Scambelluri. Nitrogen recycling in subducted mantle rocks and implications for the global nitrogen cycle. *International Journal of Earth Sciences*, 2012.

G. E. Harlow and R. M. Davies. Diamonds. *Elements*, 1:67–70, 2005.

J. W. Harris. Diamond Geology. In J. Field, editor, *The Properties of Natural and Synthetic Diamond*. Academic Press Limited, London, 1992.

B. Harte, J. J. Gurney, and J. W. Harris. The Formation of Peridotitic Suite Inclusions in Diamonds. *Contributions to Mineralogy and Petrology*, 72:181–190, 1980.

B. Harte, I. C. W. Fitzsimons, J. W. Harris, and M. L. Otter. Carbon isotope ratios and nitrogen abundances in relation to cathodoluminescence characteristics for some diamonds from the Kaapvaal Province, S. Africa. *Mineralogical Magazine*, 63:829–856, 1999.

P. C. Hayman, M. G. Kopylova, and F. V. Kaminsky. Lower mantle diamonds from Rio Soriso (Juina area, Mato Grosso, Brazil). *Contributions to Mineralogy and Petrology*, 149:430–445, 2005.

R. M. Hazen and C. M. Schiffries. Why Deep Carbon? *Reviews in Mineralogy and Geochemistry*, 75:1–6, 2013.

P. J. Heaney, E. P. Vicenzi, and S. De. Strange Diamonds: The Mysterious Origins of Carbonado and Framesite. *Elements*, 1:85–89, 2005.

R. C. Hin. *Stable isotope behaviour during planetary differentiation*. PhD thesis, ETH Zurich, 2012.

J. Hoefs. *Stable Isotope Geochemistry*. Springer, sixth edition, 2009.

H. Honma and Y. Itihara. Distribution of ammonium in minerals of metamorphic and granitic rocks. *Geochimica et Cosmochimica Acta*, 45:983–988, 1981.

D. Howell, W. L. Griffin, N. J. Pearson, W. Powell, P. Wieland, and S. Y. O'Reilly. Trace element partitioning in mixed habit diamonds. *Chemical Geology*, 355:134–143, 2013a.

D. Howell, W. L. Griffin, S. Piazolo, J. M. Say, R. A. Stern, T. Stachel, L. Nasdala, J. R. Rabeau, N. J. Pearson, and S. Y. O'Reilly. A spectroscopic and carbon-isotope study of mixed-habit diamonds: Impurity characteristics and growth environment. *American Mineralogist*, 98(1):66–77, 2013b.

D. Howell, R. A. Stern, W. L. Griffin, R. Southworth, S. Mikhail, and T. Stachel. Nitrogen isotope systematics and origins of mixed-habit diamonds. *Geochimica et Cosmochimica Acta*, 157:1–12, 2015.

E. S. Izraeli, J. W. Harris, and O. Navon. Brine inclusions in diamonds: a new upper mantle fluid. *Earth and Planetary Science Letters*, 187:323–332, 2001.

D. E. Jacob. Nature and origin of eclogite xenoliths from kimberlites. *Lithos*, 77:295–316, 2004.

M. Javoy. The integral enstatite chondrite model of the earth. *Geophysical Research Letters*, 22:2219–2222, 1995.

M. Javoy. The major volatile elements of the Earth: Their origin, behavior, and fate. *Geophysical Research Letters*, 24:177–180, 1997.

M. Javoy and F. Pineau. The volatiles record of a popping rock from the Mid-Atlantic Ridge at ^{14}N chemical and isotopic composition of gas trapped in the vesicles. *Earth and Planetary Science Letters*, 107:598–611, 1991.

M. Javoy, F. Pineau, and D. Demaiffe. Nitrogen and carbon isotopic composition in the diamonds of Mbuji Mayi (Zaire). *Earth and Planetary Science Letters*, 68:399–412, 1984.

W. Kaiser and W. Bond. Nitrogen, A Major Impurity in Common Type I Diamond. *Physical Review*, 115(4):857–863, 1959.

F. V. Kaminsky and R. Wirth. Iron Carbide Inclusions in Lower-Mantle Diamond from Juina, Brazil. *The Canadian Mineralogist*, 49(2):555–572, 2011.

F. V. Kaminsky, O. Zakharchenko, R. Davies, W. L. Griffin, G. Khachatryan-Blinova, and A. Shiryaev. Superdeep diamonds from the Juina area, Mato Grosso state, Brazil. *Contributions to Mineralogy and Petrology*, 140:734–753, 2001.

N. Kawai, S. Endho, and K. Itho. Split sphere high pressure vessel and phase equilibrium relation in the system Mg_2SiO_4-Fe_2SiO_4. *Physics of Earth and Planetary Interiors*, 3: 182–185, 1970.

C. S. Kennedy and G. C. Kennedy. The Equilibrium Boundary Between Graphite and Diamond. *Journal of Geophysical Research*, 81:2467–2470, 1976.

O. Klein-BenDavid, A. M. Logvinova, M. Schrauder, Z. V. Spetius, Y. Weiss, E. H. Hauri, F. V. Kaminsky, N. V. Sobolev, and O. Navon. High-Mg carbonatitic micro inclusions in some Yakutian diamonds - a new type of diamond-forming fluid. *Lithos*, 1125:648–659, 2009.

O. Klein-BenDavid, D. G. Pearson, G. M. Nowell, C. Ottley, J. C. R. McNeill, and P. Cartigny. Mixed fluid sources involved in diamond growth constrained by Sr-Nd-Pb-C-N isotopes and trace elements. *Earth and Planetary Science Letters*, 289(1-2):123–133, 2010.

K. T. Koga, J. A. Van Orman, and M. J. Walter. Diffusive relaxation of carbon and nitrogen isotope heterogeneity in diamond: a new thermochronometer. *Physics of the Earth and Planetary Interiors*, 139(1-2):35–43, 2003.

M. Kopylova, O. Navon, L. Dubrovinsky, and G. Khachatryan. Carbonatitic mineralogy of natural diamond-forming fluids. *Earth and Planetary Science Letters*, 291:126–137, 2010.

C. Kung and R. Clayton. Nitrogen abundances and isotopic compositions in stony meteorites. *Earth and Planetary Science Letters*, 38:421–435, 1978.

G. Kurat and G. Dobosi. Garnet and diopside-bearing diamondites (framesites). *Mineralogy and Petrology*, 69:143–159, 2000.

A. R. Lang. On the growth-sectorial dependence of defects in natural diamonds. *Proceedings of the Royal Society of London A*, 340:233–248, 1974.

A. R. Lang, A. P. Yelisseyev, N. P. Pokhilenko, J. W. Steeds, and A. Wotherspoon. Is dispersed nickel in natural diamonds associated with cuboid growth sectors in diamonds that exhibit a history of mixed-habit growth? *Journal of Crystal Growth*, 263:575–589, 2004.

L. Li, G. Bebout, and B. Idleman. Nitrogen concentration and δ^{15}N of altered oceanic crust obtained on ODP Legs 129 and 185: Insights into alteration-related nitrogen enrichment and the nitrogen subduction budget. *Geochimica et Cosmochimica Acta*, 71 (9):2344–2360, 2007.

Y. Li and H. Keppler. Nitrogen speciation in mantle and crustal fluids. *Geochimica et Cosmochimica Acta*, 129:13–32, 2014.

G. Libourel, B. Marty, and F. Humbert. Nitrogen solubility in basaltic melt. Part I. Effect of oxygen fugacity. *Geochimica et Cosmochimica Acta*, 67(21):4123–4135, 2003.

R. W. Luth. Diamonds, eclogites, and the oxidation state of the Earth's mantle. *Science*, 261:66–68, 1993.

I. Martinez and M. Javoy. The stability of nitrides in meteorites and in the Earth's mantle: a thermodynamic and experimental study. *Mineralogical Magazine*, 62A:955–956, 1998.

B. Marty. Nitrogen content of the mantle inferred from N_2-Ar correlation in oceanic basalts. *Nature*, 377:326–329, 1995.

B. Marty and N. Dauphas. The nitrogen record of crust-mantle interaction and mantle convection from Archean to Present. *Earth and Planetary Science Letters*, 206(3-4): 397–410, 2003.

B. Marty and F. Humbert. Nitrogen and argon isotopes in oceanic basalts. *Earth and Planetary Science Letters*, 152:101–112, 1997.

D. Mattey, D. Lowry, and C. Macpherson. Oxygen-isotope composition of mantle peridotite. *Earth and Planetary Science Letters*, 128:231–240, 1994.

S. Mikhail. *Stable isotope fractionation during diamond growth and the Earth's deep carbon cycle*. PhD thesis, University College London, 2011.

S. Mikhail and D. A. Sverjensky. Nitrogen speciation in upper mantle fluids and the origin of Earth's nitrogen-rich atmosphere. *Nature Geoscience*, 7:816–819, 2014.

S. Mikhail, C. Guillermier, I. A. Franchi, A. D. Beard, K. Crispin, A. B. Verchovsky, A. P. Jones, and H. J. Milledge. Empirical evidence for the fractionation of carbon isotopes between diamond and iron carbide from the Earth's mantle. *Geochemistry Geophysics Geosystems*, 15:855–866, 2014a.

S. Mikhail, A. B. Verchovsky, D. Howell, M. T. Hutchison, R. Southworth, A. R. Thomson, P. Warburton, A. P. Jones, and H. J. Milledge. Constraining the internal variability of the stable isotopes of carbon and nitrogen within mantle diamonds. *Chemical Geology*, 366:14–23, 2014b.

S. Mikhail, F. M. McCubbin, F. E. Jenner, R. Bowden, D. Rumble, S. B. Shirey, and J. J. Gurney. Diamondite vs. monocrystalline diamond: petrological and stable isotope evidence for depth dependent diamond growth in the sub-continental mantle beneath Orapa, Botswana. in review.

A. Miyazaki, H. Hiyagon, N. Sugiura, K. Hirose, and E. Takahashi. Solubilities of nitrogen and noble gases in silicate melts under various oxygen fugacities: implications for the origin and degassing history of nitrogen and noble gases in the earth. *Geochimica et Cosmochimica Acta*, 68(2):387–401, 2004.

R. K. Mohapatra, D. Harrison, U. Ott, J. D. Gilmour, and M. Trieloff. Noble gas and

nitrogen isotopic components in Oceanic Island Basalts. *Chemical Geology*, 266(1-2): 29–37, 2009.

M. Moore and A. R. Lang. On the internal structure of natural diamonds of cubic habit. *Philosophical Magazine*, 26:1313–1325, 1972.

P. H. Nixon. *Mantle Xenoliths*. Wiley, Chichester, 1987.

C. Oppenheimer, P. R. Kyle, V. I. Tsanev, A. J. S. McGonigle, T. A. Mather, and D. Sweeney. Mt. Erebus, the largest point source of NO_2 in Antarctica. *Atmospheric Environment*, 39(32):6000–6006, 2005.

M. Palot, P. Cartigny, and F. Viljoen. Diamond origin and genesis: A C and N stable isotope study on diamonds from a single eclogitic xenolith (Kaalvallei, South Africa). *Lithos*, 112:758–766, 2009.

M. Palot, P. Cartigny, J. W. Harris, F. V. Kaminsky, and T. Stachel. Evidence for deep mantle convection and primordial heterogeneity from nitrogen and carbon stable isotopes in diamond. *Earth and Planetary Science Letters*, 357-358:179–193, 2012.

M. Palot, D. G. Pearson, R. A. Stern, T. Stachel, and J. W. Harris. Multiple growth events, processes and fluid sources involved in diamond genesis: A micro-analytical study of sulphide-bearing diamonds from Finsch mine, RSA. *Geochimica et Cosmochimica Acta*, 106:51–70, 2013.

M. Palot, D. G. Pearson, R. A. Stern, T. Stachel, and J. W. Harris. Isotopic constraints on the nature and circulation of deep mantle C-H-O-N fluids: Carbon and nitrogen systematics within ultra-deep diamonds from Kankan (Guinea). *Geochimica et Cosmochimica Acta*, 139:26–46, 2014.

Y. N. Pal'yanov, A. G. Sokol, Y. M. Borzdov, A. F. Khokhryakov, A. F. Shatsky, and N. V. Sobolev. The diamond growth from Li_2CO_3, Na_2CO_3, K_2CO_3 and Cs_2CO_3 solvent-catalysts at P=7 GPa and T=1700 ℃. *Diamond and Related Materials*, 8:1118–1124, 1999.

Y. N. Pal'yanov, A. G. Sokol, Y. M. Borzdov, A. F. Khokhryakov, and N. V. Sobolev. Diamond formation through carbonate-silicate interaction. *American Mineralogist*, 87: 1009–1013, 2002.

D. G. Pearson, F. E. Brenker, F. Nestola, J. McNeill, L. Nasdala, M. T. Hutchison, S. Matveev, K. Mather, G. Silversmit, S. Schmitz, B. Vekemans, and L. Vincze. Hydrous mantle transition zone indicated by ringwoodite included within diamond. *Nature*, 507 (7491):221–4, 2014.

D. Petts, T. Chacko, T. Stachel, R. Stern, and L. Heaman. A nitrogen isotope fractionation factor between diamond and its parental fluid derived from a detailed SIMS analysis of a gem diamond and theoretical calculations. in press.

I. Pitcairn, D. Teagle, R. Kerrich, D. Craw, and T. Brewer. The behavior of nitrogen and nitrogen isotopes during metamorphism and mineralization: Evidence from the Otago and Alpine Schists, New Zealand. *Earth and Planetary Science Letters*, 233(1-2): 229–246, 2005.

V. N. Reutsky, Y. M. Borzdov, and Y. N. Palyanov. Carbon isotope fractionation associated with HPHT crystallization of diamond. *Diamond and Related Materials*, 17(11): 1986–1989, 2008a.

V. N. Reutsky, B. Harte, Y. M. Borzdov, and Y. N. Palyanov. Monitoring diamond crystal growth, a combined experimental and SIMS study. *European Journal of Mineralogy*, 20 (3):365–374, 2008b.

P. Richet, Y. Bottinga, and M. Javoy. A review of hydrogen, carbon, nitrogen, oxygen, sulphur, and chlorine stable isotope fractionation among gaseous molecules. *Annual Review of Earth and Planetary Sciences*, 5:65–110, 1977.

A. E. Ringwood. Phase transformations and their bearing on the constitution and the dynamics of the mantle. *Geochimica et Cosmochimica Acta*, 55:2083–2110, 1991.

C. Rinsland, D. Weisenstein, M. Ko, L. Chiou, E. Mahieu, R. Zander, and P. Demoulin. Post-Mount Pinatubo eruption ground-based infrared stratospheric column measurements of HNO_3, NO, and NO_2 and their comparison with model calculations. *Journal of Geophysical Research*, 108(D15), 2003.

M. Roskosz, B. Mysen, and G. Cody. Dual speciation of nitrogen in silicate melts at high pressure and temperature: An experimental study. *Geochimica et Cosmochimica Acta*, 70(11):2902–2918, 2006.

M. Roskosz, M. A. Bouhifd, A. P. Jephcoat, B. Marty, and B. O. Mysen. Nitrogen solubility in molten metal and silicate at high pressure and temperature: a first experimental approach. In *43rd Lunar and Planetary Science Conference*, 2012.

D. C. Rubie. Characterising the sample environment in multianvil high-pressure experiments. *Phase Transitions*, 68:431–451, 2006.

J. F. Rudge, B. C. Reynolds, and B. Bourdon. The double spike toolbox. *Chemical Geology*, 265:420–431, 2009.

S. J. Sadofsky and G. Bebout. Nitrogen geochemistry of subducting sediments: New results from the Izu-Bonin-Mariana margin and insights regarding global nitrogen subduction. *Geochemistry Geophysics Geosystems*, 5(3), 2004.

K. Sato, M. Akaishi, and S. Yamaoka. Spontaneous nucleation of diamond in the system $MgCO_3$-$CaCO_3$-C at 7.7 GPa. *Diamond and Related Materials*, 8:1900–1905, 1999.

S. Satoh, H. Sumiya, K. Tsuji, and S. Yazu. Difference in nitrogen concentration and aggregation among (111) and (100) growth sectors of large synthetic diamonds. In S. Saito, O. Fukunaga, and M. Yoshikawa, editors, *Science and Technology of New Diamond*. KTK Scientific Publishers / Terra Scientific Publishing Company, 1990.

E. A. Schauble. Applying stable isotope fractionation theory to new systems. *Reviews in Mineralogy and Geochemistry*, 55:65–111, 2004.

E. A. Schauble. Role of nuclear volume in driving equilibrium stable isotope fractionation of mercury, thallium, and other very heavy elements. *Geochimica et Cosmochimica Acta*, 71:2170–2189, 2007.

B. H. Scott Smith, R. V. Danchin, J. W. Harris, and K. J. Stracke. Kimberlites near Orroroo, South Australia. In J. Kornprobst, editor, *Kimberlites I: kimberlites and related rocks.* Elsevier, Amsterdam, 1984.

M. Sephton, A. Verchovsky, P. Bland, I. Gilmour, M. Grady, and I. Wright. Investigating the variations in carbon and nitrogen isotopes in carbonaceous chondrites. *Geochimica et Cosmochimica Acta*, 67:2093–2108, 2003.

Z. Sharp. *Principles of stable isotope geochemistry.* Pearson Education, Inc., New Jersey, 2007.

D. Shelkov, A. B. Verchovsky, H. J. Milledge, and C. T. Pillinger. Carbonado: A comparison between Brazilian and Ubangui sources with other forms of microcrystalline diamond based on carbon and nitrogen isotopes. *Geologiya i Geofizika*, 38:315–322, 1997.

D. A. Shelkov. *N and C isotopic composition of different varieties of terrestrial diamond and carbonado.* PhD thesis, The Open University, 1997.

S. B. Shirey, P. Cartigny, D. J. Frost, S. Keshav, F. Nestola, P. Nimis, D. G. Pearson, N. V. Sobolev, and M. J. Walter. Diamonds and the Geology of Mantle Carbon. *Reviews in Mineralogy and Geochemistry*, 75(1):355–421, 2013.

A. A. Shiryaev, E. S. Izraeli, E. H. Hauri, O. D. Zakharchenko, and O. Navon. Chemical, optical and isotopic investigations of fibrous diamonds from brazil. *Geologiya i Geofizika*, 46:1207–1222, 2005.

K. A. Smart, T. Chacko, T. Stachel, K. Muehlenbachs, R. A. Stern, and L. M. Heaman. Diamond growth from oxidized carbon sources beneath the Northern Slave Cra-

ton, Canada: A $\delta^{13}C$-N study of eclogite-hosted diamonds from the Jericho kimberlite. *Geochimica et Cosmochimica Acta*, 75(20):6027–6047, 2011.

E. M. Smith, M. G. Kopylova, M. L. Frezzoti, and V. P. Afanasiev. N-rich fluid inclusions in octahedrally-grown diamond. *Earth and Planetary Science Letters*, 393:39–48, 2014.

N. V. Sobolev, V. N. Sobolev, G. A. Snyder, E. S. Yefimova, and L. A. Taylor. Significance of Eclogitic and Related Parageneses of Natural Diamonds. *International Geology Review*, 41(2):129–140, 1999.

A. G. Sokol and Y. N. Pal'yanov. Diamond formation in the system MgO-SiO_2-H_2O-C at 7.5 GPa and 1,600 ℃. *Contributions to Mineralogy and Petrology*, 155(1):33–43, 2008.

T. Stachel and J. W. Harris. Formation of diamond in the Earth's mantle. *Journal of Physics: Condensed Matter*, 21(36):364206, 2009.

T. Stachel, J. W. Harris, G. P. Brey, and W. Joswig. Kankan diamonds (Guinea) II: lower mantle inclusion parageneses. *Contributions to Mineralogy and Petrology*, 140:16–27, 2000.

T. Stachel, G. P. Brey, and J. W. Harris. Inclusions in Sublithospheric Diamonds: Glimpses of the Deep Earth. *Elements*, 1:73–78, 2005.

T. Stachel, J. W. Harris, and K. Muehlenbachs. Sources of carbon in inclusion bearing diamonds. *Lithos*, 112:625–637, 2009.

V. Stagno and D. J. Frost. Carbon speciation in the asthenosphere: Experimental measurements of the redox conditions at which carbonate-bearing melts coexist with graphite or diamond in peridotite assemblages. *Earth and Planetary Science Letters*, 300(1-2): 72–84, 2010.

V. Stagno, D. O. Ojwang, C. A. McCammon, and D. J. Frost. The oxidation state of the mantle and the extraction of carbon from Earth's interior. *Nature*, 493(7430):84–8, 2013.

R. A. Stern, M. Palot, D. Howell, T. Stachel, D. G. Pearson, P. Cartigny, and A. Oh. Methods and reference materials for SIMS diamond C- and N-isotope analysis (2014). Canadian Centre for Isotopic Microanalysis Technical Report 14-01. Technical report, Education and Research Archive, University of Alberta permalink: http://hdl.handle.net/10402/era.38738, 2014.

I. Sunagawa. *Crystals - Growth, Morphology and Perfection*. Cambridge University Press, Cambridge, 2005.

S. Suzuki and A. R. Lang. Occurrences of facetted re-entrants on rounded growth surfaces of natural diamonds. *Journal of Crystal Growth*, 34:29–37, 1976.

T. Taniguchi, D. Dobson, A. P. Jones, R. Rabe, and H. J. Milledge. Synthesis of cubic diamond in the graphite-magnesium carbonate and graphite-$K_2Mg(CO_3)_2$ systems at high pressure of 9-10 GPa region. *Journal of Materials Research*, 11:2622–2632, 1996.

W. R. Taylor, D. Canil, and H. J. Milledge. Kinetics of Ib to IaA nitrogen aggregation in diamond. *Geochimica et Cosmochimica Acta*, 60:4725–4733, 1996.

E. Thomassot, P. Cartigny, J. Harris, and K. Fanusviljoen. Methane-related diamond crystallization in the Earth's mantle: Stable isotope evidences from a single diamond-bearing xenolith. *Earth and Planetary Science Letters*, 257(3-4):362–371, 2007.

E. Thomassot, P. Cartigny, J. W. Harris, J. P. Lorand, C. Rollion-Bard, and M. Chaussidon. Metasomatic diamond growth: A multi-isotope study (^{13}C, ^{15}N, ^{33}S, ^{34}S) of sulphide inclusions and their host diamonds from Jwaneng (Botswana). *Earth and Planetary Science Letters*, 282(1-4):79–90, 2009.

C. Thomazo, D. L. Pinti, V. Busigny, M. Ader, K. Hashizume, and P. Philippot. Biological activity and the Earth's surface evolution: Insights from carbon, sulfur, nitrogen and iron stable isotopes in the rock record. *Comptes Rendus Palevol*, 8(7):665–678, 2009.

E. L. Tomlinson, A. P. Jones, and J. W. Harris. Co-existing fluid and silicate inclusions in mantle diamond. *Earth and Planetary Science Letters*, 250(3-4):581–595, 2006.

E. L. Tomlinson, D. Howell, A. P. Jones, and D. J. Frost. Characteristics of HPHT diamond grown at sub-lithosphere conditions (10-20GPa). *Diamond and Related Materials*, 20 (1):11–17, 2011.

W. Utsumi, T. Okada, T. Taniguchi, K.-i. Funakoshi, T. Kikegawa, N. Hamaya, and O. Shimomura. In situ x-ray diffraction of graphite-diamond transformation using various catalysts under high pressures and high temperatures. *Journal of Physics: Condensed Matter*, 16(14):S1017–S1026, 2004.

A. B. Verchovsky, A. V. Fisenko, L. F. Semjonova, I. P. Wright, M. R. Lee, and C. T. Pillinger. C, N, and Noble Gas Isotopes in Grain Size Separates of Presolar Diamonds from Efremovka. *Science*, 281(5380):1165–1168, 1998.

D. Walker, M. A. Carpenter, and C. M. Hitch. Some simplifications to multianvil devices for high pressure experiments. *American Mineralogist*, 75:1020–1028, 1990.

M. J. Walter, G. P. Bulanova, L. S. Armstrong, S. Keshav, J. D. Blundy, G. Gudfinnsson, O. T. Lord, A. R. Lennie, S. M. Clark, C. B. Smith, and L. Gobbo. Primary carbonatite melt from deeply subducted oceanic crust. *Nature*, 454(7204):622–5, 2008.

M. J. Walter, S. C. Kohn, D. Araujo, G. P. Bulanova, C. B. Smith, E. Gaillou, J. Wang, A. Steele, and S. B. Shirey. Deep mantle cycling of oceanic crust: evidence from diamonds and their mineral inclusions. *Science*, 334(6052):54–7, 2011.

A. Watenphul, B. Wunder, R. Wirth, and W. Heinrich. Ammonium-bearing clinopyroxene: A potential nitrogen reservoir in the Earth's mantle. *Chemical Geology*, 270(1-4):240–248, 2010.

Y. Weiss, I. Kiflawi, N. Davies, and O. Navon. High-density fluids and the growth of monocrystalline diamonds. *Geochimica et Cosmochimica Acta*, 141:145–159, 2014.

C. M. Welbourn, M.-L. T. Rooney, and D. J. F. Evans. A study of diamond of cube and cube-related shape from the Jwaneng mine. *Journal of Crystal Growth*, 94:229–252, 1989.

K. Westerlund and J. Gurney. Silicate and oxide inclusion characteristics and infra-red absorption analysis of diamonds from the Kilpspringer kimberlites, South Africa. *South African Journal of Geology*, 107:131–146, 2004.

D. F. Wiggers de Vries, G. P. Bulanova, K. De Corte, D. G. Pearson, J. A. Craven, and G. R. Davies. Micron-scale coupled carbon isotope and nitrogen abundance variations in diamonds: Evidence for episodic diamond formation beneath the Siberian Craton. *Geochimica et Cosmochimica Acta*, 100:176–199, 2013.

R. Yokochi, B. Marty, G. Chazot, and P. Burnard. Nitrogen in peridotite xenoliths: Lithophile behavior and magmatic isotope fractionation. *Geochimica et Cosmochimica Acta*, 73(16):4843–4861, 2009.

D. A. Zedgenizov and B. Harte. Microscale variations of δ^{13}C and N content within a natural diamond with mixed-habit growth. *Chemical Geology*, 205(1-2):169–175, 2004.

D. A. Zedgenizov, H. Kagi, V. S. Shatsky, and A. L. Ragozin. Local variations of carbon isotope composition in diamonds from São-Luis (Brazil): Evidence for heterogenous carbon reservoir in sublithospheric mantle. *Chemical Geology*, 363:114–124, 2014.